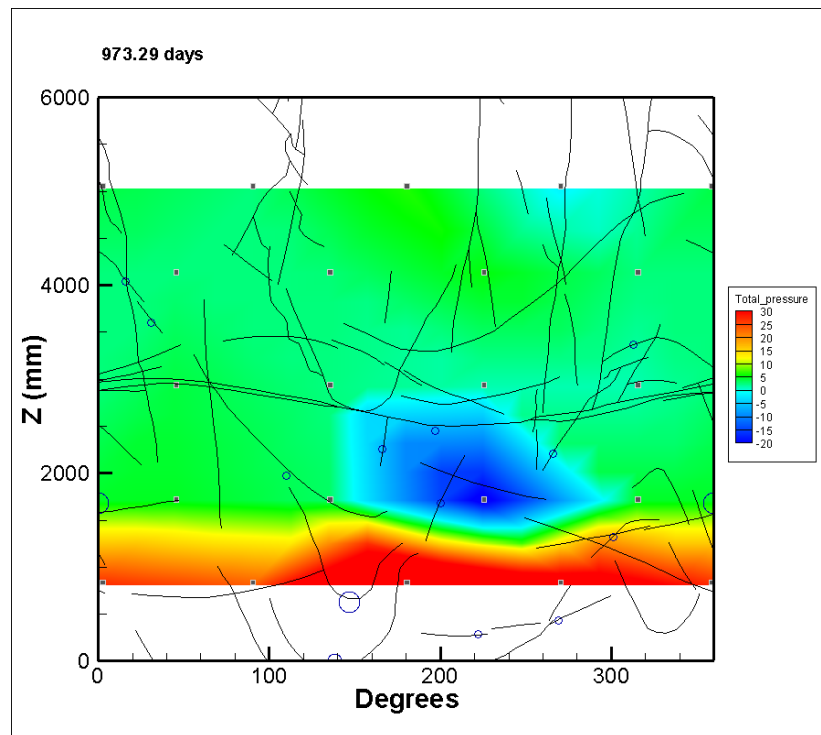




Large scale gas injection test (Lasgit) performed at the Äspö Hard Rock Laboratory: Summary report 2007

Chemical and Biological Hazards Programme

Commissioned Report CR/07/211 ^N



BRITISH GEOLOGICAL SURVEY

CHEMICAL AND BIOLOGICAL HAZARDS PROGRAMME

COMMISSIONED REPORT CR/07/211^N

Large scale gas injection test (Lasgit) performed at the Äspö Hard Rock Laboratory: Summary report 2007

J.F. Harrington, D.J. Birchall, D.J. Noy and R.J. Cuss

Keywords

Lasgit, gas injection, bentonite, modelling, hydration, hydraulic, storage, gas entry pressure.

Front cover

Intensity plot showing the disturbance in (normalised) radial stresses caused by the injection of gas.

Bibliographical reference

HARRINGTON, J.F., BIRCHALL, D.J., NOY, D.J. AND CUSS, R.J.. 2008. Large scale gas injection test (Lasgit) performed at the Äspö Hard Rock Laboratory: Summary report 2007. *British Geological Survey Commissioned Report*, CR/07/211. 87pp.

Copyright in materials derived from the British Geological Survey's work is owned by the Natural Environment Research Council (NERC) and/or the authority that commissioned the work. You may not copy or adapt this publication without first obtaining permission. Contact the BGS Intellectual Property Rights Section, British Geological Survey, Keyworth, e-mail ipr@bgs.ac.uk. You may quote extracts of a reasonable length without prior permission, provided a full acknowledgement is given of the source of the extract.

BRITISH GEOLOGICAL SURVEY

The full range of our publications is available from BGS shops at Nottingham, Edinburgh, London and Cardiff (Welsh publications only) see contact details below or shop online at www.geologyshop.com

The London Information Office also maintains a reference collection of BGS publications, including maps, for consultation.

We publish an annual catalogue of our maps and other publications; this catalogue is available online or from any of the BGS shops.

The British Geological Survey carries out the geological survey of Great Britain and Northern Ireland (the latter as an agency service for the government of Northern Ireland), and of the surrounding continental shelf, as well as basic research projects. It also undertakes programmes of technical aid in geology in developing countries.

The British Geological Survey is a component body of the Natural Environment Research Council.

British Geological Survey offices

BGS Central Enquiries Desk

Tel 0115 936 3143 Fax 0115 936 3276
email enquires@bgs.ac.uk

Kingsley Dunham Centre, Keyworth, Nottingham NG12 5GG

Tel 0115 936 3241 Fax 0115 936 3488
email sales@bgs.ac.uk

Murchison House, West Mains Road, Edinburgh EH9 3LA

Tel 0131 667 1000 Fax 0131 668 2683
email scotsales@bgs.ac.uk

London Information Office at the Natural History Museum (Earth Galleries), Exhibition Road, South Kensington, London SW7 2DE

Tel 020 7589 4090 Fax 020 7584 8270
Tel 020 7942 5344/45 email bgs_london@bgs.ac.uk

Columbus House, Greenmeadow Springs, Tongwynlais, Cardiff CF15 7NE

Tel 029 2052 1962 Fax 029 2052 1963

Forde House, Park Five Business Centre, Harrier Way, Sowton EX2 7HU

Tel 01392 445271 Fax 01392 445371

Maclean Building, Crowmarsh Gifford, Wallingford OX10 8BB

Tel 01491 838800 Fax 01491 692345

Geological Survey of Northern Ireland, Colby House, Stranmillis Court, Belfast BT9 5BF

Tel 028 9038 8462 Fax 028 9038 8461

www.bgs.ac.uk/gsni/

Parent Body

Natural Environment Research Council, Polaris House, North Star Avenue, Swindon SN2 1EU

Tel 01793 411500 Fax 01793 411501
www.nerc.ac.uk

Website www.bgs.ac.uk

Shop online at www.geologyshop.com

Acknowledgements

This study was undertaken by staff of the Chemical and Biological Hazards Programme of the BGS. Funding for the study was provided by SKB (Stockholm), the British Geological Survey and the European Commission through the NF-PRO project (Understanding and physical and numerical modelling of the key processes in the near-field, and their coupling, for different host rocks and repository strategies) undertaken within the auspices of the EURATOM 6th framework programme.

The authors would also like to thank Patrik Sellin for his support of the research area, SKB colleagues at the Äspö Hard Rock Laboratory for their help in the set-up, maintenance and operation of the Lasgit experiment, colleagues at Clay Technology AB who were responsible for the installation of the Geokon instrumentation and buffer clay and Marcus Sen for the derivation of the flow equation described in Section 2.8.

The authors would also like to acknowledge the important contribution made by Dr Steve Horseman during the earlier stages of the project before his untimely death in 2004. Steve pioneered work on the movement of gas in clays and mudrocks and remains a much respected scientist whose encyclopaedic knowledge, enthusiasm and energy for his science continues to be greatly missed by all those who knew and worked with him.

Contents

Acknowledgements	i
Contents	i
Executive summary	vii
1 Introduction	1
2 Experimental geometry and data reduction	1
2.1 Gas laboratory	2
2.2 Apparatus and instrumentation	3
2.3 Data acquisition and control system	12
2.4 Calibration	12
2.5 Alarm systems	13
2.6 Error checking of Lasgit data	13
2.7 Methodology for incrementally raising water pressure in the artificial hydration system	14
2.8 Calculation of gas flow into the clay	15
3 Hydration phase: Predictive modelling	16
3.1 Model setup	16
3.2 Homogeneous bentonite models.....	18
3.3 Heterogeneous bentonite models.....	20
4 Hydration Phase 1: Experimental results	27

4.1	Evolution of porewater pressure	27
4.2	Evolution of total stress	42
4.3	Evolution of water content in the bentonite buffer	48
4.4	Axial force acting on the steel lid	49
4.5	Displacement of lid and canister.....	50
4.6	Discharge rates from Lasgit deposition hole	51
4.7	Volumetric flow rate into artificial hydration system.....	52
4.8	Laboratory utilities.....	54
5	Hydraulic and gas injection tests	55
5.1	Basline hydraulic test results	56
5.2	Gas injection test results	61
5.3	Hydraulic test post gas injection.....	69
6	Summary.....	69
	References	74

FIGURES

Figure 2-1	Large-scale gas injection test (Lasgit) 420m below ground at the Äspö Hard Rock Laboratory in Sweden. A BGS scientist works next to the large steel lid anchored over the deposition hole.	2
Figure 2-2	Schematic layout of Gas Laboratory showing the main experimental components and office furniture	4
Figure 2-3	Schematic diagram showing a 100mm filter housing in cross-section.....	5
Figure 2-4	Schematic side view of canister and visible filters (shown in green). The second graphic is a 2D representation showing the relative positions of the 12 radial injection filters.	7
Figure 2-5	Schematic showing the filter assembly located in the base of the canister.....	7
Figure 2-6	The photograph on the left-hand side shows a view looking into the Lasgit deposition hole showing tube work containing the electrical connections from total stress and porewater pressure sensors mounted on rock face. The photographs on the upper and lower right-hand show a total stress and a pore water pressure sensor respectively.	8
Figure 2-7	Photograph showing the lid (coloured grey), the anchor cables and linear displacement sensors. The Gas Laboratory (coloured blue) with its air-conditioning system mounted on the roof can be seen in the background.	11
Figure 2-8	Screen shots taken from the data acquisition software.	13
Figure 3-1	Components of the bentonite buffer model used for resaturation calculations.....	17
Figure 3-2	Gas saturations after 1yr of water injection for a model with a low permeability host rock (10^{-22} m^2) and a homogeneous bentonite buffer.....	19
Figure 3-3	Gas saturations after 1yr of water injection for a model with a higher permeability host rock (10^{-19} m^2) and a homogeneous bentonite buffer.....	19
Figure 3-4	The effect of a fracture on gas saturations after 180 days of water injection.	20

Figure 3-5	Gas saturations after 1yr of water injection for a model with a low permeability host rock (10^{-22} m^2) and a heterogeneous bentonite buffer.....	22
Figure 3-6	Gas saturations after 1yr of water injection for a model with a higher permeability host rock (10^{-19} m^2) and a heterogeneous bentonite buffer.....	22
Figure 3-7	Gas saturations after 3yr of water injection for a model with a higher permeability host rock (10^{-19} m^2) and a heterogeneous bentonite buffer.....	23
Figure 3-8	Gas saturations after 1yr of water injection for a model with a low permeability host rock (10^{-22} m^2) and a lower α (0.098).....	24
Figure 3-9	Gas saturations after 1yr of water injection for a model with a higher permeability host rock (10^{-19} m^2) and a higher injection pressure (10MPa).....	24
Figure 3-10	Gas saturations after 1yr of water injection for a model with a low host rock permeability (10^{-22} m^2) and an inner fill permeability of 10^{-18} m^2	25
Figure 3-11	Gas saturations after 1yr of water injection for a model with a high host rock permeability (10^{-19} m^2) and an inner fill permeability of 10^{-18} m^2	26
Figure 3-12	Gas saturations after 3yr of water injection for a model with a low host rock permeability (10^{-22} m^2) and an inner fill permeability of 10^{-18} m^2	26
Figure 4-1	Schematic representation of borehole infrastructure taken from the R4 Report by Sandén (2003). Cartesian coordinates and a description of each sensor is included in the R4 report (“P” signifies a total pressure cell, “U” a pore pressure cell, “W” a relative humidity sensor, “PC” a total pressure on canister, “FM” a filter mat and “IF” an injection filter). The dark and light blue lines respectively highlight the position of filter mats bolted to the rock surface and those located between bentonite blocks. The red lines show the planes along which the canister filters are positioned.....	28
Figure 4-2	Evolution of water pressure within the canister filters.	34
Figure 4-3	Evolution of water pressure at the borehole wall due to hydraulically induced piping during artificial hydration activities. The series of images start at 167 days and finish at 172 days.	35
Figure 4-4	Evolution of water pressure in the filter mats located on the borehole wall and within the bentonite blocks. Filter mat FR901 is in direct communication with the drain holes and was therefore allowed to evolve independently from the other filter mats.	36
Figure 4-5	Variation in porewater within the bentonite at the 6 monitoring points. The large spikes in the data correspond with attempts to increase porewater pressure within the artificial hydration system early in the test history.	37
Figure 4-6	Variation in porewater pressure with time measured at the rock face. The spikes in the data from 141 days to 203 days correlate with attempts to increase porewater pressure in the artificial hydration system. The rapid increase in pressure from around 415 days relate to changes in the boundary condition during the installation of packers in PRH1 and 2 and their subsequent closure.	38
Figure 4-7	Evolution in porewater pressure measured at the interface between the rock wall and the bentonite from 132 to 275 days. The series of images show a general increase in porewater pressure. The high pressure zones in images (3) and (5) relate to piping events during artificial hydration activities.	39
Figure 4-8	Evolution of pore pressure at the deposition hole wall from 400 to 840 days.....	40

Figure 4-9	Porewater pressures measured in the packered sections of the pressure relief boreholes.	41
Figure 4-10	Evolution of pressure in packered intervals within PRH1 and PRH2.	41
Figure 4-11	Variation in radial stress with time. In the absence of preferential flow (piping), the rate at which total stress increases is insensitive to the absolute value of porewater pressure applied to the filters.	42
Figure 4-12	Evolution in radial stress around the deposition hole wall from 75 to 272 days. From image [5] onwards a narrow zone of high pressure can be seen propagating upwards.	43
Figure 4-13	Evolution of radial stress around the deposition hole wall from 400 to 840 days.	44
Figure 4-14	Depth averaged radial stresses represented as vectors in the horizontal plane.	45
Figure 4-15	Evolution of the magnitude of the net horizontal stress with time during the hydration phase.	45
Figure 4-16	Evolution of the locus of the net horizontal stress with time during the hydration phase.	45
Figure 4-17	Development of axial and radial pressure on the side and base of canister.	46
Figure 4-18	Development of axial stress measured at 12 locations within the buffer.	47
Figure 4-19	Intensity plots showing the distribution of axial stress across the borehole from day 200 to 847. The range of colour variations has been adjusted to the range of stress values in each plot to highlight the variation over the section.	48
Figure 4-20	Suction pressures recorded at sensors WB901 to WB907 for the entire test.	49
Figure 4-21	Axial force acting on steel lid measured by 3 load cells attached to separate rock anchors.	50
Figure 4-22	Linear displacement of the steel lid and copper canister. Movements of the lid are measured relative to both the gallery floor and ceiling. Movements of the canister are measured relative to the steel lid.	51
Figure 4-23	Discharge rates from the Lasgit deposition hole.	52
Figure 4-24	Volumetric flow rate into the artificial hydration systems. From 485 days onwards, control of the separate hydration systems alternated between individual pumps or pumpsets while repairs (due to corrosion and scoring of the barrels) were afforded to decommissioned systems.	53
Figure 4-25	Temperatures recorded in the Gas Laboratory, office, canister, and HRL.	54
Figure 4-26	Plot showing the variation in pressure for both the compressed air lines and the water inlet feed from a near-by borehole. From 707 days onwards, the water inlet feed was switched to a fresh water supply.	55
Figure 5-1	Pressures observed at the lower canister filters FL901 to FL904 during the hydraulic test.	57
Figure 5-2	Flow rate observed at lower canister filter FL903 during the constant pressure phases of the hydraulic test.	57
Figure 5-3	Porewater pressures observed at deposition hole wall sensors UR907 to UR910 during the hydraulic test.	58

Figure 5-4	Pressure heads in a finite element model of single phase variably saturated flow around filter FL901 after 840 days of hydration. Dark blue bands indicate remaining zones of partially saturated material.	59
Figure 5-5	Comparison of model simulations to shut-in pressure data for the injection filters FL901 to FL904 during the hydraulic test.	59
Figure 5-6	Comparison of model simulations with flow rates at FL903 during the constant pressure test steps.	60
Figure 5-7	Simulated pressure heads around each filter at 840 days, the end of the hydration phase.	61
Figure 5-8	Comparison of predicted and observed gas pressures at FL903 during the gas injection test.	62
Figure 5-9	Estimated rate of gas flow into the system and the clay compared to the predicted and observed gas pressures during the first phase of the gas injection test.	62
Figure 5-10	Estimated rate of gas flow into the clay compared to the predicted and observed gas pressures during the second phase of the gas injection test.	63
Figure 5-11	Unsmoothed flow rate and pressure responses around peak gas pressure. Gas flow into the clay rapidly increases following the peak which is followed by a small spontaneous negative transient.	63
Figure 5-12	Shut-in response for filter FL903. The inflections in the pressure decay response are suggestive of dynamic gas flow and pathway closure.	64
Figure 5-13	Radial stresses observed in a selection of sensors close to FL903 at the end of the second gas pressurisation phase.	65
Figure 5-14	Pore pressures observed in a selection of sensors close to FL903 at the end of the second gas pressurisation phase.	65
Figure 5-15	Evolution in normalised radial stress around the deposition hole wall prior to and after the peak in gas pressure (days 972.2 to 979.99). The intensity plots indicate a general increase in radial stress around the base of the deposition hole. Adjacent to the filter radial stresses appears to decline momentarily.	66
Figure 5-16	Evolution in normalised porewater pressure around the deposition hole wall prior to and after the peak in gas pressure (days 972.2 to 979.99). The intensity plots indicate a general increase in porewater pressure around the base of the deposition hole focussed in the vertical plane of the source filter (FL903). Adjacent to the filter porewater pressure appears to decline momentarily.	67
Figure 5-17	Selected axial stress data during the second phase of gas injection. The strongest response is observed by PB902, which, located below the canister, exhibits signs of time depended pathway flow.	68
Figure 5-18	Evolution in flow rate for hydraulic tests performed before and after gas injection.	69

TABLES

Table 2-1	Dimensions of hydration mats and canister filters.	5
Table 2-2	List of logged parameters from the ISCO 500 Series D syringe pumps.	6

Table 2-3	List of pressure transducers attached to the canister filters and large hydration mats showing sensor name, location, unit of measurement and a description of the monitored parameter.	8
Table 2-4	List of total stress sensors showing name, location, unit of measurement and a description of the monitored parameter.	9
Table 2-5	List of porewater pressure sensors showing name, location, unit of measurement and a description of the monitored parameter.	10
Table 2-6	List of psychrometers sensors showing name, location, unit of measurement and a description of the monitored parameter.....	10
Table 2-7	List of linear displacement sensors showing name, location, unit of measurement and a description of the monitored parameter.	10
Table 2-8	List of Glotzl load cells showing name, location, unit of measurement and a description of the monitored parameter.	11
Table 2-9	List of ancillary systems contained in or connected to the Gas Laboratory.	12
Table 3-1	Porosities and initial saturations for individual bentonite blocks. The blocks are approximately 0.5 m tall and have been ordered in this table from bottom (C1) to top (C5). See Johannesson (2003) for details.	18
Table 3-2	Variation of pressure with time at the model injection points.	21
Table 4-1	Log of dates and events in the Lasgit test history to June 2007. Where stated calibrated values refer to scaled outputs prior to error checking (Section 2.6.1). .	32
Table 4-2	Timeline of key hydration events.	33
Table 4-3	Sequence of events during the installation of packers into the pressure relief boreholes PRH1 and PRH2.....	33
Table 4-4	Volumetric flow rate into the canister filters and artificial hydration systems (flux values in the table have been rounded to 2 decimal places and have been time averaged approximately 0.25 days either side of the quoted time).....	53
Table 5-1	Hydraulic parameters obtained from fits to shut-in pressure curves for injection filters FL901 to FL904.....	60

Executive summary

The deposition hole was closed on the 1st February 2005 signifying the start of the hydration phase. Groundwater inflow through a number of conductive discrete fractures resulted in elevated porewater pressures leading to the formation of conductive channels (piping), the extrusion of bentonite from the hole and the discharge of groundwater to the gallery floor. This problem was addressed by drilling two pressure-relief holes in the surrounding rock mass.

Artificial hydration began on the 18th May 2005 after 106 days of testing. Initial attempts to raise porewater pressure in the artificial hydration arrays often resulted in the formation of preferential pathways. These pressure dependent features were not focused in one location but occurred at multiple sites at different times in the test history. These pathways appear to be relatively short lived, closing when water pressure is reduced.

It was determined that both pressure relief holes should remain open until the bentonite had generated sufficient swelling pressure to withstand the high water pressure in the system when these holes are closed. Packers were installed into the pressure relief holes on 23rd March 2006 and sections in them closed off over the period to 5th July 2006. There was no repeat of the formation of piping through discrete channels so, on 20th November 2006, pressures to the artificial hydration filters on the canister were increased to 2350 kPa.

Pressure data from a number of sensors including FR901, RW901 and most of the porewater pressure sensors mounted on the borehole surface, seem to suggest some form of time dependent (temporal) evolution in the hydraulic characteristics of the rock mass adjacent to the Lasgit deposition hole. Monitored discharge rates from the pressure relief holes show a slow progressive reduction in value with time. These effects could be caused by a number of reasons from clogging and permeability reduction along conductive fractures near the Lasgit deposition hole, to operational activities performed at different locations within the site.

Monitored porewater pressures within the bentonite remain low, ranging from 230 kPa to 635 kPa. This is in contrast to the water pressure measured at the face of the deposition hole which ranges from 1055 kPa to 2510 kPa. Suction pressures recorded at psychrometers embedded within the bentonite show that suction is declining, confirming that resaturation is progressing, although the rate of hydration does appear to be slowing.

Monitored radial stress around the clay continues to increase steadily ranging in value from 1685 kPa to 5515 kPa, with an average value of 4230 kPa. In the absence of hydraulic piping the rate at which radial stress increases appears insensitive to the absolute value of porewater pressure applied to the filter assemblies, confirming the modelling work described in this report. Analysis of the distribution in radial stress shows a narrow expanding zone of elevated stress propagating vertically upwards to around 3.5m.

Stress measurements on the canister surface indicate radial stresses in the range 4800 kPa and 5030 kPa, which is comparable with the average value of radial stress monitored on the rock face. Axial stress is significantly lower at 4380 kPa.

Axial stress within the clay ranges from 4910 kPa to 6230 kPa (excluding sensor PB901). Axial stress is non-uniformly distributed across the major axis of the emplacement hole and generally exhibits only minor sensitivity to changes in porewater pressure.

The axial force acting on the steel lid initially reduced after the deposition hole was closed but has risen again following the closure of the pressure relief holes. The continuum axial swelling pressure within the bentonite is now greater than the initial pre-stress applied by the lid. The slight reduction in force prior to the closure of the pressure relief hole packers can be explained by convex deformation of the steel lid in response to the uneven distribution in axial stress.

Displacement sensors indicate a fairly uniform drop in lid height relative to the gallery floor during the early part of the test history, mirroring the relaxation in the initial pre-stressing applied to the lid. Analysis of the subsequent displacement data suggests a slight distortion of the lid may have occurred as it deforms to accommodate the uneven distribution in axial stress. Since the installation and closure of packers into the pressure relief holes the lid has moved significantly upwards with an increasing disparity in displacements at different locations, indicating an increased distortion, probably linked to the uneven distribution of the axial force across the deposition hole.

Analysis of the volumetric flow rate data indicates a disproportionately large flux into the bentonite around the canister, indicating a higher permeability value in this region of the system. Volumetric flow rate through the artificial hydration filters is not particularly sensitive to the modest pressures applied to the filters.

Analysis of the volumetric flow rate data indicates that in general the proportion of flux into the clay from the various hydration sources (i.e. mats and canister filters) remains fairly constant with time, suggesting a general reduction in clay permeability as the clay hydrates.

The resaturation phase of the Lasgit experiment has been examined using numerical models developed with the TOUGH2 code and the EOS3 equation of state module. Model runs found that the impact of a single flowing fracture on the overall resaturation process was likely to be limited. In contrast, flow through the general rock mass and associated minor fractures could have a significant effect on the resaturation process depending on the permeability value selected.

A second group of models incorporating explicit representation of the individual bentonite rings and cylinders found that the rings around the canister were the most difficult to resaturate fully within the timescale of the experiment. In particular, if the gap between canister and bentonite rings seals quickly and effectively then full resaturation could take many years.

The effectiveness of the seal between canister and bentonite appears to be a critical parameter in determining the overall time taken to resaturate the facility.

A preliminary set of hydraulic and gas injection tests were started on the 25th May 2007 with the isolation of the lower canister filters FL901 to FL904 while artificial hydration continued through all other canister filters and filter mats. After a period of 27 days a constant head test was initiated on filter FL903, raising its pressure to 4.3 MPa for 28 days and then reducing it to 560 kPa for a further 19 days. Gas injection to FL903 was then begun with an initial volume of gas being compressed at a steady rate for 13 days, a period of 22 days with gas pressure held constant and then a further period of 22 days during which pressures were raised again. Compression of the gas was then halted and the pressure monitored as it decayed for a further 4 weeks.

Preliminary modelling of the hydraulic test has been carried out using a 2D axisymmetric variably saturated finite element porewater flow model. Fits were obtained to the initial pressure decay data for the four filters that were isolated using values for hydraulic conductivity ranging from 9×10^{-14} to $1.6 \times 10^{-13} \text{ ms}^{-1}$ and specific storage values ranging from 5.5×10^{-5} to $4.4 \times 10^{-4} \text{ m}^{-1}$. The constant pressure test on filter FL903 was fitted with a hydraulic conductivity of $7.5 \times 10^{-14} \text{ ms}^{-1}$ and a specific storage of $2.5 \times 10^{-5} \text{ m}^{-1}$. The modelling done to set the initial conditions also shows that a significant zone around each of the canister filters remains unsaturated.

Analysis of the gas injection data suggest that gas starts to flow into the buffer at a pressure of about 775 kPa, which is much lower than the expected gas entry pressure for intact bentonite. It therefore seems likely that gas is flowing between the bentonite and the canister and possibly between bentonite blocks. The sudden reduction in gas flow when injection pressure was held constant is strongly indicative of pathway rather than visco-capillary flow within the original porosity of the clay.

Upon restarting gas injection pathway propagation continues at the outset. Gas flux into the clay gradually increases as the pressure in the system rises. At a gas pressure marginally greater than the local total stress measured on the rock wall (but a little smaller than the radial and axial stresses measured on and near the canister surface respectively), flux into the clay rapidly increases. Gas pressure continues to rise reaching a peak pressure of 5.66 MPa, which is marginally greater than the axial stress measured at PB902. This is followed by a small spontaneous negative transient leading to a quasi steady state. The post peak gas flux exhibits dynamic behaviour (over and undershooting flux into the system) suggestive of unstable gas flow. This general behaviour is reminiscent of the responses observed in laboratory scale tests reported by Horseman et al. (1999) and Harrington and Horseman (2003).

Following the cessation of injection, the pressure initially drops rapidly but then decays very slowly towards an asymptotic capillary threshold pressure, which is estimated to be about 4900 kPa, close to the average radial stress measured on the canister surface of 4900 kPa.

Following peak gas pressure a well pronounced increase in radial stress occurs around the entire base of the deposition hole, with the highest increase noted in the vertical plane below the point of injection. Porewater pressure data from the deposition hole wall exhibit similar behaviour, though initial results suggest that the pulse in porewater pressure dissipates at a faster rate than that of the radial stress.

Porewater pressure sensors located within the buffer show no obvious sensitivity to the injection of gas. In contrast, axial stress sensors located beneath and above the canister appear to register the passage of gas providing evidence for the time dependent propagation of gas pathways.

While it is difficult to make definitive statements regarding the exact direction and number of gas flow paths, it seems highly probable that the gas moved generally downwards away from the injection filter and then along the interface between blocks C1 and R1 and/or R1 and R2. This is logical as there is a clear axial stress gradient running from high to low from the top of the deposition hole to the lowest stress sensor. Under most conditions gas would propagate along such a stress vector. The fact that the gas pressure asymptotes at a value close to the local total stress, may suggest that the small amount of gas injected during the test remained resident in the buffer/deposition hole.

However, the general coupling between gas, stress and porewater pressure at the repository scale is extremely important and can readily be explained through concepts of pathway dilatancy. The reduction in flux when gas pressure was held constant supports this hypothesis. These observations are qualitatively similar to those reported by Horseman et al. (2004).

During the hydration phase, Lasgit has yielded high quality data relating to the hydration of the bentonite and the evolution in hydrogeological properties adjacent to the deposition hole. The limited preliminary hydraulic and gas injection tests confirm the correct working of all control and data acquisition systems. Lasgit has been in successful operation for in excess of 1000 days. The decreasing rate of change in sensor outputs demonstrates that significant progress in the hydration of the bentonite has been made.

1 Introduction

In the Swedish KBS-3 repository concept for spent nuclear fuel, copper/steel canisters containing spent fuel will be placed in large diameter boreholes drilled into the floor of the repository tunnels. The space around each canister will be filled with pre-compacted bentonite blocks, which over time, will draw in the surrounding groundwater and swell, closing up any construction gaps. While the copper/steel canisters are expected to have a very substantial life, from a performance assessment perspective, it is important to consider the possible impact of groundwater penetrating one of the canisters. Under certain conditions corrosion of the steel inner of each canister will lead to the formation of hydrogen. Radioactive decay of the waste and the radiolysis of water will produce some additional gas. Depending on the gas production rate and the rate of diffusion of gas molecules in the pores of the bentonite, it is possible that gas will accumulate in the void-space of each canister.

Current knowledge pertaining to the movement of gas in initially saturated buffer bentonite is based on small-scale laboratory studies [Donohew et al. (2000); Harrington and Horseman (1999); Horseman et al. (1999; 1997); Hume (1999); Pusch et al. (1987; 1985); Tanai et al. (1997)]. Recent laboratory tests have demonstrated the importance of the boundary condition on gas migration [Harrington and Horseman (2003); Horseman et al. (2004)]. Gas penetration and subsequent flow is accompanied by local dilation of the buffer clay. Porewater pressure and total stress acting within the clay are strongly affected by the passage of gas. The maximum gas pressure attainable during a discharge event, in part, relates to the geometry and spatial distribution of both the gas pathways within the buffer and the characteristics of the fractures distributed along the walls of the emplacement borehole. The transmissivity and hydrostatic pressure of these features will affect the maximum gas pressure that can be generated within the buffer.

While significant improvements in our understanding of the gas-buffer system have taken place [Harrington and Horseman, 2003], recent laboratory work has highlighted a number of uncertainties, notably the sensitivity of the gas migration process to experimental boundary conditions and possible scale-dependency of the measured responses. These issues were best addressed by undertaking a large-scale gas injection test or "Lasgit".

Lasgit is a full-scale demonstration experiment operated by SKB at the Äspö Hard Rock Laboratory at a depth of 420m. The objective of Lasgit is to provide quantitative data to improve process understanding and test/validate modelling approaches which might be used in performance assessment.

2 Experimental geometry and data reduction

The Lasgit experiment has been commissioned in deposition hole No. DA3147G01 - the first emplacement borehole to be drilled at the Äspö URL. The deposition hole has a length of 8.5 m and a diameter of around 1.8 m. A full scale KBS-3 canister has been modified for the Lasgit experiment with twelve circular filters of varying dimensions located on its surface to provide point sources for gas injection, mimicking potential canister defects. These filters can also be used to inject water during the hydration phase.

The deposition hole, buffer and canister are equipped with instrumentation to measure the total stress, porewater pressure and relative humidity in 32, 26 and 7 positions respectively. Additional instrumentation continually monitors variations in temperature, relative displacement of the lid and the restraining forces on the rock anchors. The emplacement hole has been capped

by a conical concrete plug retained by a reinforced steel lid capable of withstanding over 5000 tonnes of force. Figure 2-1 shows a photograph of the test site following the installation phase.

The state-of-the-art experimental monitoring and control systems for Lasgit are housed in the "Gas Laboratory" which is a self-contained unit designed and assembled by BGS within a modified shipping container. A customised graphical interface based on National Instruments LabVIEW™ software enables remote control and monitoring to be undertaken by project staff from any Internet connected PC around the world.



Figure 2-1 Large-scale gas injection test (Lasgit) 420m below ground at the Äspö Hard Rock Laboratory in Sweden. A BGS scientist works next to the large steel lid anchored over the deposition hole.

2.1 GAS LABORATORY

The Gas Laboratory is housed in a fully insulated pre-fabricated shipping container. This facility houses all experimental circuits (hydration, hydraulic and gas injection) as well as data acquisition and telemetry systems.

Figure 2-2 shows a schematic outlining the general layout of the main Gas Laboratory infrastructure. The shipping container has been partitioned into two sections. The first comprises the office area and contains the workstation plus general office furniture, telemetry system and main electrical consumer unit. The second area contains all of the experimental apparatus, test circuits and data acquisition systems.

Temperature in both the office and laboratory sections is controlled by two independent air conditioning systems. The temperature of the office area is maintained at around 18-19°C, while the temperature in the Laboratory section is somewhat lower at around 15.5°C (similar to the ambient conditions within the Lasgit borehole). To maintain a flow-through of air and help to minimise condensation, the air is continuously replaced and its humidity controlled to prevent damage to test systems. Temperature sensors located in both compartments of the Gas Laboratory are continuously monitored by the data acquisition software and by the Alpha Alarm system, the latter providing 24hr support in the event of a system failure.

To prevent asphyxiation due to an unforeseen leakage of helium - an oxygen detector has been installed in the main laboratory area. This is connected to a waterproof display terminal located next to the external door of the Gas Laboratory and to an audible alarm which will alert any individuals who may be working in the vicinity of the laboratory if there is a problem.

2.2 APPARATUS AND INSTRUMENTATION

The following sections describe the key components of the Lasgit system.

2.2.1 Canister filters

The design of the filter assemblies had to accommodate a number of engineering and experimental considerations. To help maintain structural integrity and strength of the canister, the diameter of the filter assemblies were minimised, in order to retain as much of the original canister material as possible (Figure 2-3). The rigidity of the canister was enhanced by securing each filter assembly with 8 Monel cap-screws, tensioned uniformly to apply an even load.

To minimise leakage of test fluids around each filter assembly into the main body of the canister, a dual O-ring sealing mechanism was developed. All pressure connections were made using standard 1/8" BSP stainless steel male connectors. An advantage of using this type of fitting was that it ensured engaged thread lengths are constant for each pressure connection, which means that each fitting could be tightened to a similar torque, reducing the chance of leakage and accidental shearing of the copper threads.

Each filter array has been design with dual ports to facilitate the removal of test permeants and "sweeping" of the sintered filter. The size of the filter discs installed in each housing have been varied to examine the effect of gas pressure gradient on the gas entry pressure (Table 2-1). The filter housings were also profiled with respect to the major axis of the cylinder to help reduce the potential for voids or "bridging", caused by the flat face of the housing protruding from the curved surface of the canister.

The maximum fluid pressure generated within each filter assembly is continuously monitored and controlled by reciprocating ISCO syringe pumps (Section 2.2.2). Alarm functions embedded in each pump controller provide a facility for controlling the maximum fluid pressure generated by the pump system. Force gauges, mounted on a number of the rock anchors holding the lid in position, continually monitor the pressure applied to the lid by the bentonite so that pumping can be stopped if the force exceeds a pre-determined value. In addition to these monitoring points, a number of linear displacement transducers have also been installed on the lid and Monel tube to provide axial strain data for both the lid and canister movement.

2.2.1.1 SINTERED DISCS

To minimise corrosion and galvanic responses between the porous filter and the main body of the filter assembly (manufactured from C103 copper), a number of alternative sinter materials were examined. After consultation with SKB, it was decided to use sintered bronze as the filter material. This copper-alloy is mechanically robust, can be readily machined, and because of its copper content, should exhibit low corrosion and galvanic responses when in communication with the canister infrastructure and test permeants. To prevent intrusion of bentonite during the testing, a relatively small mean pore size distribution for the sintered bronze discs was selected (i.e. 4 to 8 microns). This range in pore size equates to an air entry pressure of between 0.02 and 0.04 MPa, assuming circular pores and an interfacial tension coefficient between the gas and porewater of $7.275 \times 10^{-2} \text{ Nm}^{-1}$ at 20 °C. This air-entry value is well below the expected gas entry pressure for saturated buffer bentonite.

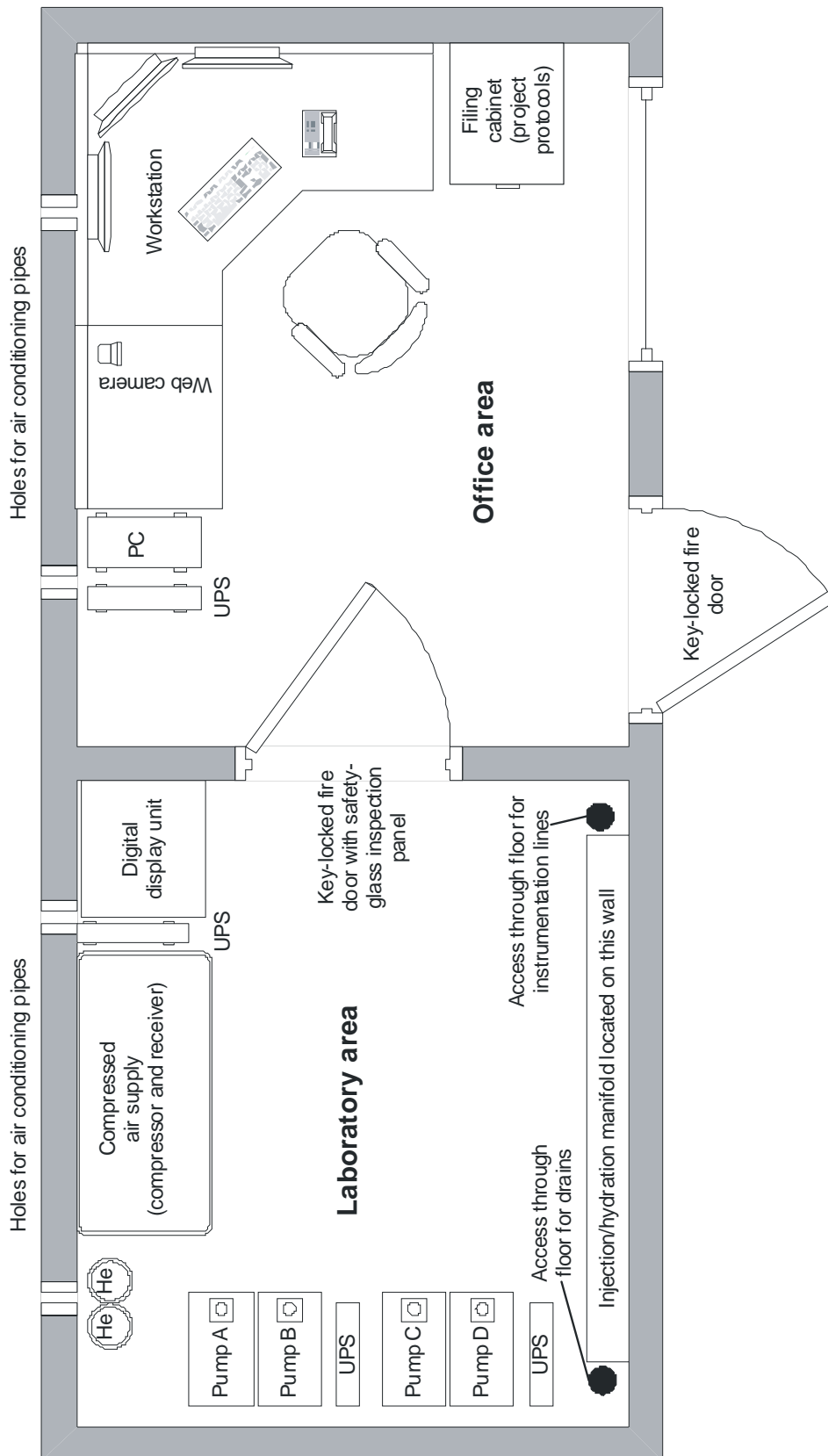


Figure 2-2 Schematic layout of Gas Laboratory showing the main experimental components and office furniture

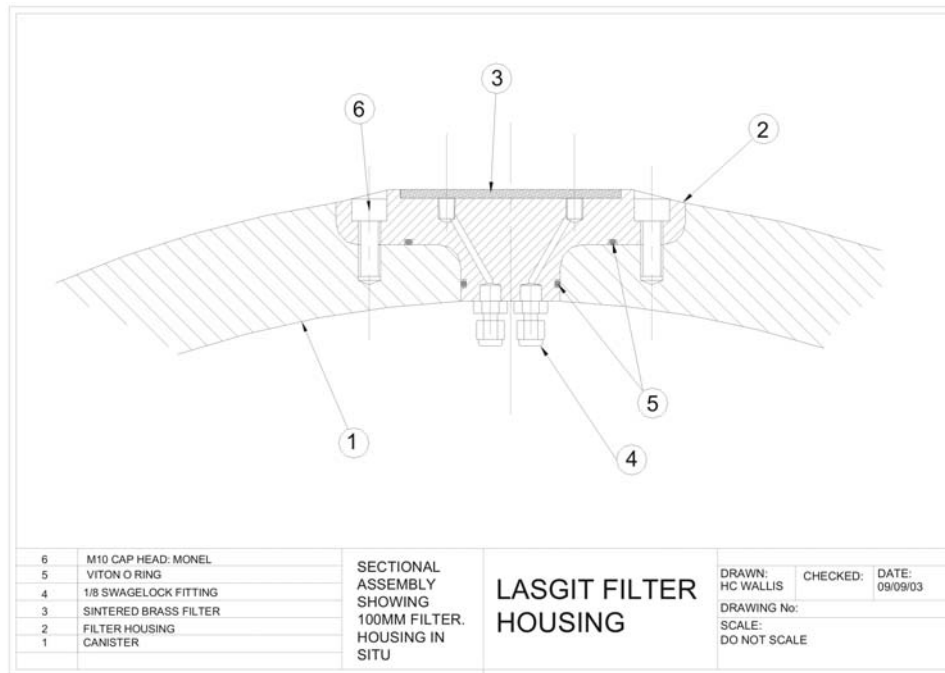


Figure 2-3 Schematic diagram showing a 100mm filter housing in cross-section.

Device name	Location	Units	Description	Dimensions (mm)		
				Height	Width	Radius
AXG0FR901	Rock wall	kPa	Pressure in filter mat 1	350	5500	
AXG0FR902	Rock wall	kPa	Pressure in filter mat 2	750	5500	
AXG0FB903	Bentonite	kPa	Pressure in filter mat 3	-	-	400
AXG0FB904	Bentonite	kPa	Pressure in filter mat 4	-	-	400
PXG0FL901	Cannister	kPa	Pressure in injection filter	-	-	50
PXG0FL902	Cannister	kPa	Pressure in injection filter	-	-	5
PXG0FL903	Cannister	kPa	Pressure in injection filter	-	-	50
PXG0FL904	Cannister	kPa	Pressure in injection filter	-	-	25
PXG0FM905	Cannister	kPa	Pressure in injection filter	-	-	50
PXG0FM906	Cannister	kPa	Pressure in injection filter	-	-	50
PXG0FM907	Cannister	kPa	Pressure in injection filter	-	-	50
PXG0FM908	Cannister	kPa	Pressure in injection filter	-	-	50
PXG0FU909	Cannister	kPa	Pressure in injection filter	-	-	50
PXG0FU910	Cannister	kPa	Pressure in injection filter	-	-	25
PXG0FU911	Cannister	kPa	Pressure in injection filter	-	-	50
PXG0FU912	Cannister	kPa	Pressure in injection filter	-	-	5
PXG0FC901	Cannister	kPa	Pressure in injection filter	-	-	-

Table 2-1 Dimensions of hydration mats and canister filters.

2.2.1.2 LOCATION OF INJECTION FILTERS

Given the relatively low cost of manufacture it was decided to place 13 filter assemblies at specific locations on the canister surface. In order to provide adequate contingency and provide additional points of porewater pressure measurement, a decision was made to place four filter assemblies at 90° intervals around the circumference of the canister at each selected elevation (Figure 2-4). To improve the spatial coverage of porewater pressure measurements, the upper and lower filter arrays were rotated 45° with respect to the mid-plane array. This results in a triangular mesh of porewater pressure measurements. An additional filter assembly was also

placed in the base of the canister (Figure 2-5), in communication through a gas-actuated valve with the internal void space of the canister.

2.2.2 Reciprocating syringe pumps

The volumetric flow rate of the injected fluid and the pressure within the Lasgit filters are controlled using two pairs of reciprocating ISCO 500 Series D syringe pumps operated by two digital control units. A pressure transducer mounted in the head of each pump monitors the outgoing pressure and provides a feedback signal to the microprocessor when the pump is set in constant pressure mode. Piston motion gives a direct measure of the volumetric flow rate. When set in constant flow rate mode the piston advances at a constant velocity. The pump controller is connected and controlled by the data acquisition system through an RS232 connection. Table 2-2 gives a list of the parameters logged from both ISCO pump controllers.

2.2.3 Pressure transducers

Individual pressure transducers connected to each canister filter and hydration mat provide a continuous measure of up-hole pressure for each system component (Table 2-3). Each transducer is rated to 25 MPa and is accurate to 0.25% full scale. Output signals from the pressure transducers (4-20 mA) are logged by the data acquisition system. Prior to the commencement of testing each transducer was calibrated on site to a known pressure standard (Section 2.4).

Device	Location	Units	Description
PXG0PP901	Gas Laboratory	kPa	Pressure in pump A1
PXG0PP902	Gas Laboratory	kPa	Pressure in Pump A2
PXG0PP903	Gas Laboratory	kPa	Pressure in pump B1
PXG0PP904	Gas Laboratory	kPa	Pressure in pump B2
PXG0QP901	Gas Laboratory	variable	Flowrate of pump A1
PXG0QP902	Gas Laboratory	variable	Flowrate of pump A2
PXG0QP903	Gas Laboratory	variable	Flowrate of pump B1
PXG0QP904	Gas Laboratory	variable	Flowrate of pump B2
PXG0VP901	Gas Laboratory	ml	Volume in pump A1
PXG0VP902	Gas Laboratory	ml	Volume in pump A2
PXG0VP903	Gas Laboratory	ml	Volume in pump B1
PXG0VP904	Gas Laboratory	ml	Volume in pump B2
PXG0VD901	Gas Laboratory	litres	Total cumulative volume pumped by pumps A1 and A2
PXG0VD902	Gas Laboratory	litres	Total cumulative volume pumped by pumps B1 and B2

Table 2-2 List of logged parameters from the ISCO 500 Series D syringe pumps.

2.2.4 Total stress sensors

Total stress in the Lasgit deposition hole is monitored at 32 separate locations (Table 2-4). Of these devices, 20 Geokon sensors are mounted on the rock wall (Figure 2-6), 9 Geokon sensors are located within the buffer material itself and 3 Sensotec sensors are positioned at specific locations on the canister surface. Each Geokon sensor incorporates an integrated thermocouple which is used to correct the output signal from each device for fluctuations in background temperature. Factory calibrations are used to process the Geokon data into a stress value. An additional offset is then applied to the data to compensate for “drift” during the installation process. Each device outputs a resistance measurement which is collected by a custom built multilogger and then relayed to the data acquisition system (DAQ) within the laboratory. The three stress sensors located on the canister output a current directly into the data acquisition system. These devices were calibrated prior to installation.

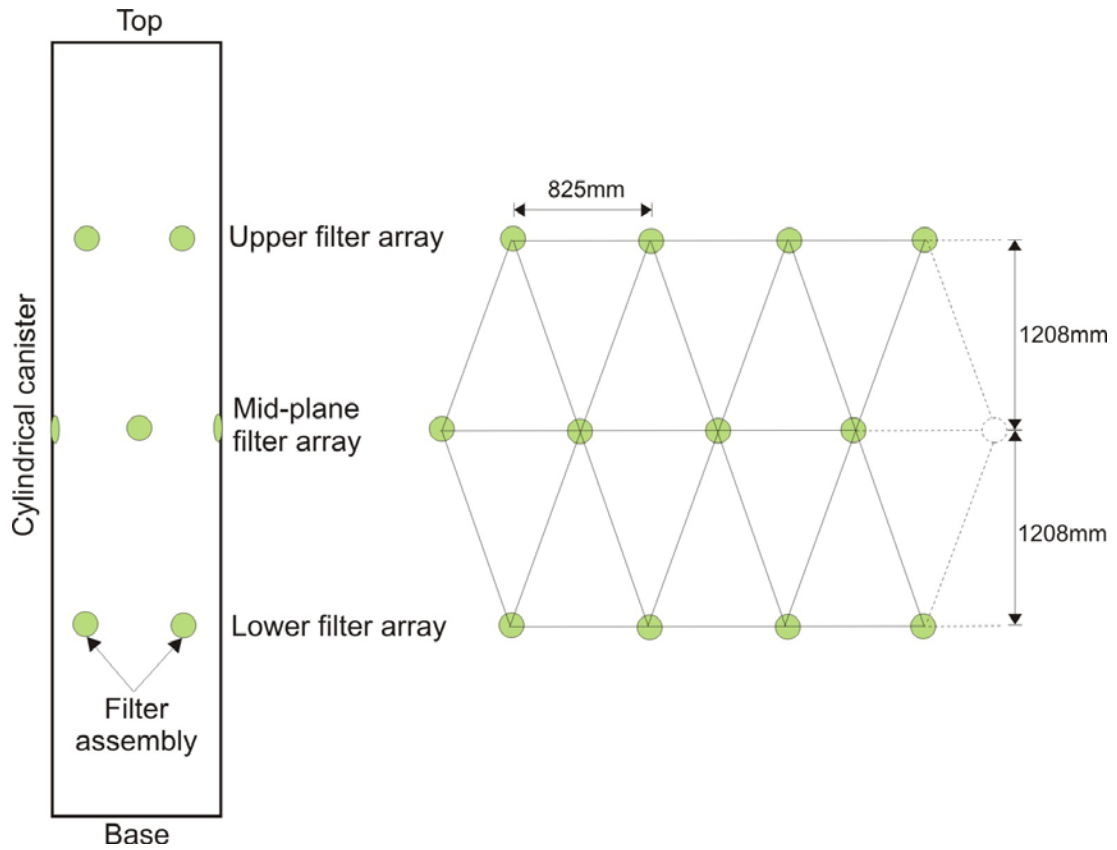


Figure 2-4 Schematic side view of canister and visible filters (shown in green). The second graphic is a 2D representation showing the relative positions of the 12 radial injection filters.

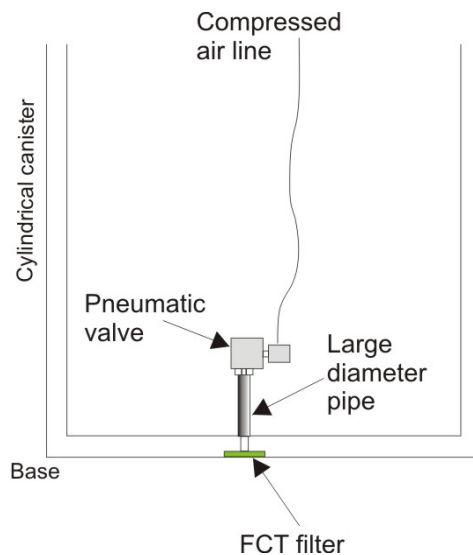


Figure 2-5 Schematic showing the filter assembly located in the base of the canister.

Device	Location	Units	Description
AXG0FR901	Rock wall	kPa	Pressure in filter mat 1
AXG0FR902	Rock wall	kPa	Pressure in filter mat 2
AXG0FB903	Bentonite	kPa	Pressure in filter mat 3
AXG0FB904	Bentonite	kPa	Pressure in filter mat 4
PXG0FL901	Cannister	kPa	Pressure in injection filter
PXG0FL902	Cannister	kPa	Pressure in injection filter
PXG0FL903	Cannister	kPa	Pressure in injection filter
PXG0FL904	Cannister	kPa	Pressure in injection filter
PXG0FM905	Cannister	kPa	Pressure in injection filter
PXG0FM906	Cannister	kPa	Pressure in injection filter
PXG0FM907	Cannister	kPa	Pressure in injection filter
PXG0FM908	Cannister	kPa </td <td>Pressure in injection filter</td>	Pressure in injection filter
PXG0FU909	Cannister	kPa	Pressure in injection filter
PXG0FU910	Cannister	kPa	Pressure in injection filter
PXG0FU911	Cannister	kPa	Pressure in injection filter
PXG0FU912	Cannister	kPa	Pressure in injection filter
PXG0FC901	Cannister	kPa	Pressure in injection filter

Table 2-3 List of pressure transducers attached to the canister filters and large hydration mats showing sensor name, location, unit of measurement and a description of the monitored parameter.

2.2.5 Porewater pressure sensors

The Lasgit experiment also uses Geokon porewater pressure sensors to monitor water pressure inside the buffer material and at the bentonite/diorite interface (Figure 2-6). A total of 26 sensors are used in the Lasgit hole, of which 20 are located on the rock face at the bentonite/diorite interface and 6 are positioned inside the buffer mass (Table 2-5). As with the total stress instruments described in Section 2.2.4, each device uses an integrated thermocouple to correct the output signal for thermal fluctuations in background temperature. This data is logged through the multilogger, which in turn passes on the raw outputs to the Lasgit DAQ system for scaling into calibrated figures.



Figure 2-6 The photograph on the left-hand side shows a view looking into the Lasgit deposition hole showing tube work containing the electrical connections from total stress and porewater pressure sensors mounted on rock face. The photographs on the upper and lower right-hand show a total stress and a pore water pressure sensor respectively.

Device	Location	Units	Description
PXG0PC901	Cannister	kPa	Pressure on outside of cannister
PXG0PC902	Cannister	kPa	Pressure on outside of cannister
PXG0PC903	Cannister	kPa	Pressure on outside of cannister
PXG0PB901	Rockwall	kPa	Pressure in bentonite
PXG0PB902	Rockwall	kPa	Pressure in bentonite
PXG0PR903	Rockwall	kPa	Pressure at bentonite/rock interface
PXG0PR904	Rockwall	kPa	Pressure at bentonite/rock interface
PXG0PR905	Rockwall	kPa	Pressure at bentonite/rock interface
PXG0PR906	Rockwall	kPa	Pressure at bentonite/rock interface
PXG0PR907	Rockwall	kPa	Pressure at bentonite/rock interface
PXG0PR908	Rockwall	kPa	Pressure at bentonite/rock interface
PXG0PR909	Rockwall	kPa	Pressure at bentonite/rock interface
PXG0PR910	Rockwall	kPa	Pressure at bentonite/rock interface
PXG0PR911	Rockwall	kPa	Pressure at bentonite/rock interface
PXG0PR912	Rockwall	kPa	Pressure at bentonite/rock interface
PXG0PR913	Rockwall	kPa	Pressure at bentonite/rock interface
PXG0PR914	Rockwall	kPa	Pressure at bentonite/rock interface
PXG0PR915	Rockwall	kPa	Pressure at bentonite/rock interface
PXG0PR916	Rockwall	kPa	Pressure at bentonite/rock interface
PXG0PR917	Rockwall	kPa	Pressure at bentonite/rock interface
PXG0PR918	Rockwall	kPa	Pressure at bentonite/rock interface
PXG0PR919	Rockwall	kPa	Pressure at bentonite/rock interface
PXG0PR920	Rockwall	kPa	Pressure at bentonite/rock interface
PXG0PR921	Rockwall	kPa	Pressure at bentonite/rock interface
PXG0PR922	Rockwall	kPa	Pressure at bentonite/rock interface
PXG0PB923	Rockwall	kPa	Pressure in bentonite
PXG0PB924	Rockwall	kPa	Pressure in bentonite
PXG0PB925	Rockwall	kPa	Pressure in bentonite
PXG0PB926	Rockwall	kPa	Pressure in bentonite
PXG0PB927	Rockwall	kPa	Pressure in bentonite
PXG0PB928	Rockwall	kPa	Pressure in bentonite
PXG0PB929	Rockwall	kPa	Pressure in bentonite

Table 2-4 List of total stress sensors showing name, location, unit of measurement and a description of the monitored parameter.

2.2.6 Psychrometers

To monitor the state of suction within the bentonite seven Wescor psychrometric microvolt meters have been installed at various locations within the buffer mass (Table 2-6). These devices give an output between 10 and 300 microvolts and are factory calibrated with an effective operating range of 95 to 100% relative humidity. The outputs from these devices are recorded by a Campbell multilogger and downloaded to a separate stand alone PC attached to another experiment.

2.2.7 Linear displacement sensors

Four linear displacement sensors (LDS) are used to continuously monitor the movement of the lid in relation to both the gallery floor and ceiling (Table 2-7). A fifth sensor is used to monitor the movement of the canister in relation to the lid. Each LDS is fixed into position by a retaining clamp bolted to either the gallery floor, lid or monel pipe (connected to the canister), with the measuring armature resting against the lid providing a continuous measure of linear displacement.

Device	Location	Units	Description
PXG0UB901	AP TD F122-03-024	kPa	Porewater pressure in bentonite
PXG0UB902	AP TD F122-03-024	kPa	Porewater pressure in bentonite
PXG0UR903	AP TD F122-03-024	kPa	Porewater pressure at bentonite/rock interface
PXG0UR904	AP TD F122-03-024	kPa	Porewater pressure at bentonite/rock interface
PXG0UR905	AP TD F122-03-024	kPa	Porewater pressure at bentonite/rock interface
PXG0UR906	AP TD F122-03-024	kPa	Porewater pressure at bentonite/rock interface
PXG0UR907	AP TD F122-03-024	kPa	Porewater pressure at bentonite/rock interface
PXG0UR908	AP TD F122-03-024	kPa	Porewater pressure at bentonite/rock interface
PXG0UR909	AP TD F122-03-024	kPa	Porewater pressure at bentonite/rock interface
PXG0UR910	AP TD F122-03-024	kPa	Porewater pressure at bentonite/rock interface
PXG0UR911	AP TD F122-03-024	kPa	Porewater pressure at bentonite/rock interface
PXG0UR912	AP TD F122-03-024	kPa	Porewater pressure at bentonite/rock interface
PXG0UR913	AP TD F122-03-024	kPa	Porewater pressure at bentonite/rock interface
PXG0UR914	AP TD F122-03-024	kPa	Porewater pressure at bentonite/rock interface
PXG0UR915	AP TD F122-03-024	kPa	Porewater pressure at bentonite/rock interface
PXG0UR916	AP TD F122-03-024	kPa	Porewater pressure at bentonite/rock interface
PXG0UR917	AP TD F122-03-024	kPa	Porewater pressure at bentonite/rock interface
PXG0UR918	AP TD F122-03-024	kPa	Porewater pressure at bentonite/rock interface
PXG0UR919	AP TD F122-03-024	kPa	Porewater pressure at bentonite/rock interface
PXG0UR920	AP TD F122-03-024	kPa	Porewater pressure at bentonite/rock interface
PXG0UR921	AP TD F122-03-024	kPa	Porewater pressure at bentonite/rock interface
PXG0UR922	AP TD F122-03-024	kPa	Porewater pressure at bentonite/rock interface
PXG0UB923	AP TD F122-03-024	kPa	Porewater pressure in bentonite
PXG0UB924	AP TD F122-03-024	kPa	Porewater pressure in bentonite
PXG0UB925	AP TD F122-03-024	kPa	Porewater pressure in bentonite
PXG0UB926	AP TD F122-03-024	kPa	Porewater pressure in bentonite

Table 2-5 List of porewater pressure sensors showing name, location, unit of measurement and a description of the monitored parameter.

Device	Location	Units	Description
WB001	AP TD F122-03-024	%	RH in section 2
WB002	AP TD F122-03-024	%	RH in section 2
WB003	AP TD F122-03-024	%	RH in section 11
WB004	AP TD F122-03-024	%	RH in section 11
WB005	AP TD F122-03-024	%	RH in section 14
WB006	AP TD F122-03-024	%	RH in section 14
WB007	AP TD F122-03-024	%	RH in section 16

Table 2-6 List of psychrometers sensors showing name, location, unit of measurement and a description of the monitored parameter.

Device	Location	Units	Description
PXG0DP901	Monel to Lid	mm	Movement of monel pipe to lid
PXG0DP902	Lid to Floor	mm	Movement of lid to gallery floor
PXG0DP903	Lid to Floor	mm	Movement of lid to gallery floor
PXG0DP904	Lid to Floor	mm	Movement of lid to gallery floor
PXG0DP905	Lid to Ceiling	mm	Movement of lid to gallery ceiling

Table 2-7 List of linear displacement sensors showing name, location, unit of measurement and a description of the monitored parameter.

To monitor the movement of the lid with respect to the gallery ceiling, an invar wire has been run from the roof to an LDS mounted on the lid. This provides a mechanism for monitoring the true vertical displacement of the steel retaining lid. The output from each device (-3.6 to +3.6) is logged directly by the DAQ system.

2.2.8 Load sensors

Axial movement of the lid is limited by 10 rock anchors equally spaced around the circumference of the hole - initially pre-tensioned to 1300 kN. Glotzl load cells (Figure 2-7) have been positioned on three of the anchor cables at approximately 120° to each other (Table 2-8). These devices provide a continuous measure of the force acting on the lid. Output signals (0-10 volts) from these devices are logged by the DAQ system. To prevent possible damage to either the rock anchors or the retaining systems during gas testing, the output from each device is alarmed (section 2.5).

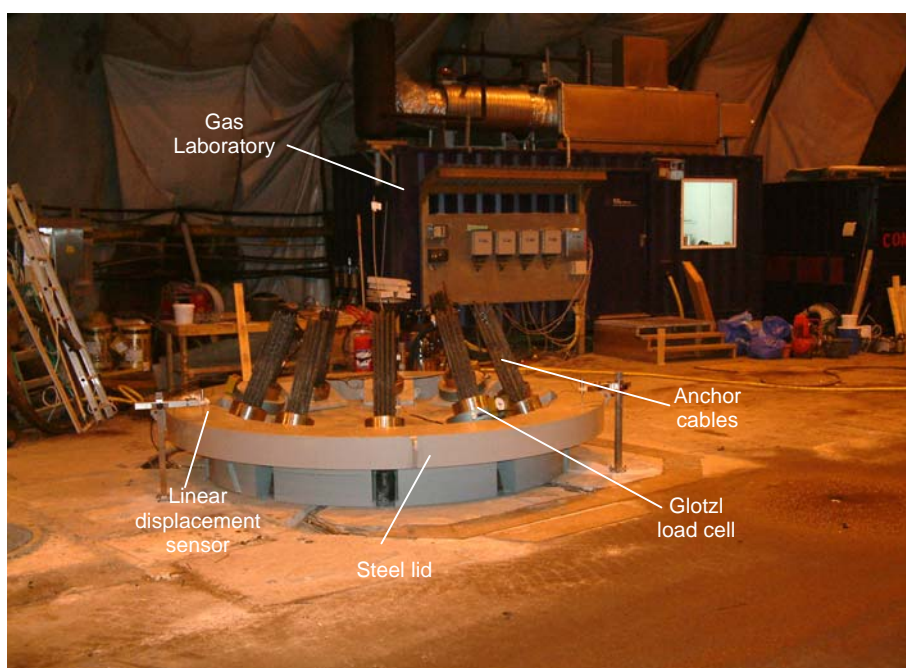


Figure 2-7 Photograph showing the lid (coloured grey), the anchor cables and linear displacement sensors. The Gas Laboratory (coloured blue) with its air-conditioning system mounted on the roof can be seen in the background.

Device	Location	Units	Description
PXG0LP901	Lid	kN	Force on anchor cables
PXG0LP902	Lid	kN	Force on anchor cables
PXG0LP903	Lid	kN	Force on anchor cables

Table 2-8 List of Glotzl load cells showing name, location, unit of measurement and a description of the monitored parameter.

2.2.9 Ancillary systems

A number of ancillary systems are routinely monitored by the DAQ (Table 2-9). These include: water pressure from a nearby borehole piped into the Gas Laboratory; helium pressure in the gas supply lines running around the laboratory section; compressed air pressure in the receiver (used to actuate servo-controlled valvework) and Geokon battery voltage (used to initiate the logging sequence).

Device	Location	Units	Description
PXG0TC901	Cannister	°C	Temperature inside the cannister
PXG0TL902	Lab	°C	Temperature near the ceiling in the lab
PXG0TL903	Lab	°C	Temperature near the floor in the lab
PXG0TO904	Office	°C	Temperature in the office
PXG0TA905	HRL	°C	Temperature outside the lab
PXG0FC901	Cannister	kPa	Pressure in injection filter
PXG0RW901	Lab	kPa	Pressure of water used to refill pumps A1, A2, B1, B2
PXG0RH902	Lab	kPa	Pressure of Helium Gas inside lab
PXG0RA903	Lab	kPa	Pressure of Compressed air in lab
PXG0OL901	Lab	%	Oxygen level in lab
PXG0VG901	Geokon	Volts	Geokon Battery level

Table 2-9 List of ancillary systems contained in or connected to the Gas Laboratory.

2.3 DATA ACQUISITION AND CONTROL SYSTEM

In total, over 150 instrument outputs are monitored and recorded by a customised data acquisition (DAQ) graphical interface based on National Instruments LabVIEW™ software. The data acquisition system, located in the office area of the Gas Laboratory, operates on a personal computer that is connected to the SKB local area network (LAN) providing real-time data acquisition and control. Key experimental circuits and down-hole instrumentation are represented by a schematic display spread across a number of screens (Figure 2-8) located in the office section of the Gas Laboratory.

The LabVIEW software performs two primary functions. The first is to log all device outputs from both the depositional hole and the experimental apparatus (excluding the RH sensors which are monitored by existing equipment attached to another experiment at the HRL). Data is written to a hierarchical file structure that can be accessed through a secure user interface. Project participants can download experimental data from a members website. The second function of the system is to provide remote control of key experimental systems such as the ISCO syringe pumps and automated servo-controlled valve work. Proximity sensors mounted on each valve provide continuous feedback to the control system identifying the current status of a particular valve. This facility enables staff at BGS Headquarters in Keyworth to change pump settings and/or open/close any of the 68 actuated valves housed within the gas laboratory, remotely in real-time in order to initiate test sequences.

Automated alarm systems embedded in the Lasgit software (Section 2.5) can be configured to provide both e-mail notification and, under certain circumstances shutdown the ISCO pump systems if required.

2.4 CALIBRATION

All measurement devices used in the Lasgit experiment which record pressure or displacement outputs are calibrated against known standards to ensure accurate and comparable outputs during the course of the experimental programme. This is achieved through factory calibration settings (e.g. Geokon, displacement and Glotzl instruments) or by manual calibration using a Fluke calibration unit (all transducers, thermocouples and pumps). Where calibration has been undertaken in the field, least-squares linear regression of the data is used to provide the slopes and intercepts necessary for data processing.

Data reduction during gas testing also requires an accurate determination of the total system volume during any particular test stage. Where possible the total volume of each test circuit from the syringe pump to injection filter was measured prior to the start of testing.

To minimise possible errors introduced into the data from instrumentation drift caused by the extended test duration of the Lasgit project, recalibration of laboratory pressure transducers and thermocouples is performed every 6 months, the exact date of which, is based on convenience to the test programme. As such, Lasgit data are processed in six monthly blocks as described in Section 2.6

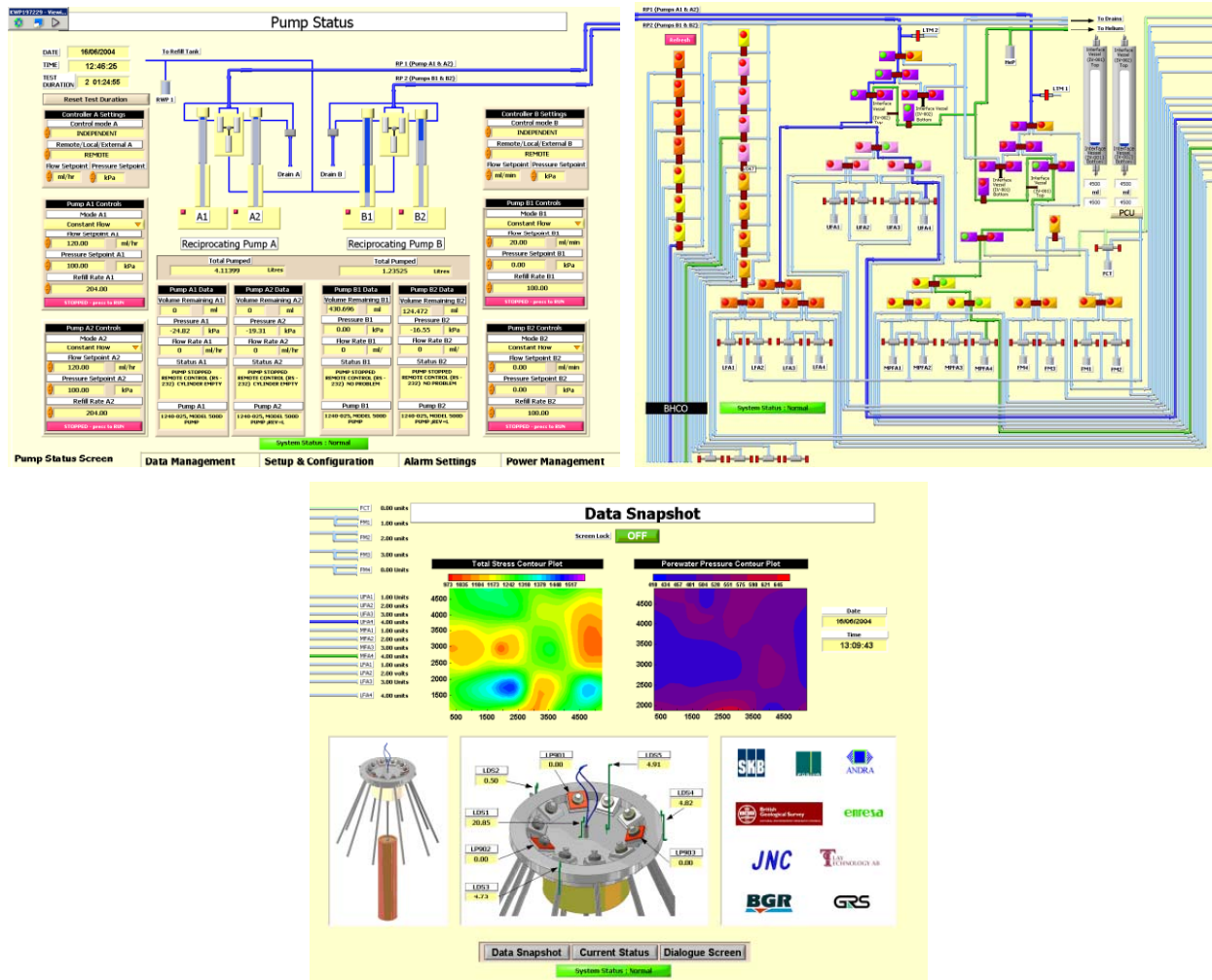


Figure 2-8 Screen shots taken from the data acquisition software.

2.5 ALARM SYSTEMS

Instrumentation outputs are monitored by an alarm system incorporated into the data acquisition software. This allows the end-user to preset minimum and maximum values for each device output. If any instrument over or under ranges then an e-mail message is sent to a predefined list of project staff alerting them to the problem. When safety critical instruments such as the Glotzl cells or pumps over-range, the alarm system also automatically stops all of the ISCO pumps, preventing any risk of over pressurising the experiment or downhole infrastructure.

2.6 ERROR CHECKING OF LASGIT DATA

To date, over 1000 days of logging have occurred, resulting in over 37,000 data records. This means that over 15 million cells of data exist, all of which require error checking, synchronisation, analysis and distribution to partners.

Data are generally transferred on a daily basis from Äspö Hard Rock Laboratory to BGS Keyworth using the remote Citrix server link. Once the data has been transferred to the UK, it is opened using a text editor program to ensure that the data are not corrupt. A check is made that data are not missing by comparing the time stamp of the new data with that from the previous data transfer. Once these initial checks have been conducted the data is copied to an Excel spreadsheet that contains all of the unprocessed (raw) legacy data.

All data are processed in a second spreadsheet, which is linked to the raw data sheet. Here, data are converted from raw to scaled units ready for graphing and interpretation. Graphs of all parameters of interest are available for viewing and allow on-going quality control (QC) of the data.

2.6.1 Data processing and traceability

There are a number of issues that arise in the recorded data. These include data synchronisation, erroneous values, loss of data during servicing or interruptions to logging system and transducer drift. However, a number of QC methodologies are routinely employed to ensure both the quality and traceability of the Lasgit data. On a three-monthly basis, all data are thoroughly QC checked. This is performed using a series of conditional formatted Excel spreadsheets. Data are thoroughly checked for erroneous values or “outliers”, with every anomaly examined and a decision made whether to or not to remove, edit or retain the data point in question. To ensure a coherent and traceable process a log is made of each change to the data sheet. No changes are ever made to the raw data files.

For such a long-term experiment it is necessary to re-calibrate certain devices on a regular basis; for Lasgit this occurs bi-annually. The change in calibration alters data values in the Excel spreadsheet, which can manifest themselves as an instantaneous jump in value. In order to minimise for this, a time dependent correct is applied to the calibration coefficients. Linear drift of each instrument is assumed between the two calibrations, resulting in a steady variation over a six month period; this provides a clean, smooth data set.

2.7 METHODOLOGY FOR INCREMENTALLY RAISING WATER PRESSURE IN THE ARTIFICIAL HYDRATION SYSTEM

In an attempt to minimise the time taken to hydrate the bentonite, a decision was made at the start of the project to actively hydrate the clay through the canister filters and the large hydration mats installed at key locations within the system. Water pressure, controlled by the reciprocating syringe pumps (Section 2.2.2), is simultaneously applied to all of the filter arrays except FR901, which is in hydraulic communication with the fracture system of the host rock (Section 4.1.2).

Before an increase in porewater pressure is applied to the system, all canister filters and filter mats are isolated from each other using the automated valvework situated within the Gas Laboratory. The pressure in each filter is continuously monitored during this time by the appropriate transducer (Table 2-3). A note is then made for each pumpset (RP1 and RP2) recording the total volume of fluid pumped into the system. Pressure is then increased to the desired value. The total volumes are recorded again and the isolating valve to the first canister filter then opened. Each filter is pressurised in turn when the volumetric flow rate into the system drops below $1 \text{ mL}\cdot\text{min}^{-1}$, starting at the base of the canister with FL901 and then proceeding vertically upwards until the pressure in FU912 reaches the target value. The total volumes pumped into the system by each pumpset are recorded before each new valve is opened. In this way, the pressures in all 12 canister filters is increased to the target value and are thereafter in direct communication with their respective pumpsets.

2.8 CALCULATION OF GAS FLOW INTO THE CLAY

The mass flux of gas per unit time into the bentonite buffer at any point during the gas injection history, can be simply derived using a data reduction algorithm based on the ideal gas law. At any point in time, the total volume of the injection system V_s is:

$$V_s = V_w + V_g \quad 2-1$$

where V_w and V_g are the volume of water and gas respectively. It should be noted that it is possible to correct for compressibility of the test apparatus and compression of the water. However, in previous laboratory tests these corrections have been extremely small and in the absence of representative data, it was felt inappropriate to apply such a correction.

As the injection pump advances (i.e. water is injected into the interface vessel), the volume of gas reduces by an equal amount as compression of the gas occurs i.e.

$$(V_g)_t = V_s - (V_w)_t \quad 2-2$$

The ideal gas law states that:

$$PV_g = nRT \quad 2-3$$

where P is the gas pressure (Pa), n is the number of moles of gas in the system, R is the universal gas constant (taken as $8.3 \text{ JK}^{-1} \text{ mol}^{-1}$) and T is ambient temperature (K). Thus the number of moles of gas injected into the clay can be calculated from:

$$n_{t=0} - n_t = \frac{P_{t=0}(V_g)_{t=0} - P_t(V_g)_t}{RT} \quad 2-4$$

By multiplying Equation (2-3) by the molar volume of gas (taken as $0.02241 \text{ m}^3 \text{ mol}^{-1}$) defined at STP conditions¹, the equivalent volumetric flow rate of gas (at STP conditions) injected into the buffer clay can be obtained.

It should be noted that the calculation procedure outlined above is extremely sensitive to the start volume of gas. Minor errors in this parameter can have a very significant effects on the calculation of gas flows and the subsequent interpretation of the data.

¹ Defined as 273.15 K and 101.325 kPa.

3 Hydration phase: Predictive modelling

Numerical modelling of the resaturation phase of the experiment was performed in advance of the experimental work using the TOUGH2 code (Preuss et al., 1999) with the EOS3 equation of state module. This module assumes that classic porous medium two-phase flow concepts are applicable with gas moving by displacing water within an essentially fixed porous medium framework. The applicability of these physical assumptions to gas flow in bentonite is open to debate since laboratory scale experiments such as those reported in Harrington and Horseman (2003) and Horseman et al. (2004) indicate that gas flow may occur along discrete flow paths opened-up by the pressure of the gas itself. Thus it is suggested that the gas flows by displacing the bentonite matrix rather than the water contained within it. Modelling codes that embody such flow mechanisms are not currently available, so the modelling reported here may be seen as a benchmark against which the experimental data may be tested for the appearance of alternative physical processes.

Some initial calculations were made assuming that the bentonite buffer was homogeneous. These calculations provided a simplified test bed of the model's performance with various values for material properties and also gave initial indications of the likely relative importance of the host rock as a source of water compared to the experimental injection points.

Further calculations were then made with initial saturations defined separately for each of the bentonite cylinders and rings that make up the full buffer. These values vary as a result of the manufacturing process and the revised models showed how they could affect the progress of resaturation. The importance of the effective permeability of the 'inner gap' between canister and buffer material was also highlighted by these calculations.

3.1 MODEL SETUP

The calculations described in this report were done using a mesh defined over a quarter cylinder approximation of the experimental facility. This allowed some compromise between the need for detailed representation of the experiment and the computational burden. This arrangement implies a high degree of cylindrical symmetry in the host rock flow system but preserves most of the details of the locations of injection points and sensors. Figure 3-1 shows the components that were incorporated into the model. It will be seen that, in addition to the bentonite buffer immediately surrounding the canister, the model includes a portion of the host rock extending out radially for a further 1m. In the absence of more extensive regional modelling of the flow field around the facility it is recognised that this choice is arbitrary and provides only a first approximation to the possible influence of the host environment on the performance of the experiment.

The main boundary conditions required by these models are those imposed on the outer surface of the host rock component of the model. These were specified by assuming that the water pressure increases linearly with depth below the Assembly Hall floor from atmospheric to an excess pressure of 1MPa at 10m depth, based loosely on the observations in test boreholes reported in Hardenby and Lundin (2003).

The main material properties required by the model are (i) the intrinsic permeabilities of the bentonite and host rock plus the 'fill' zones at the inner and outer boundaries of the buffer and of the concrete plug, (ii) the relative permeabilities of water and gas in each material as a function of saturation, and (iii) the capillary pressure in each material as a function of saturation. Little information was available on suitable values for these various parameters, so it is necessary to view the results obtained with some caution.

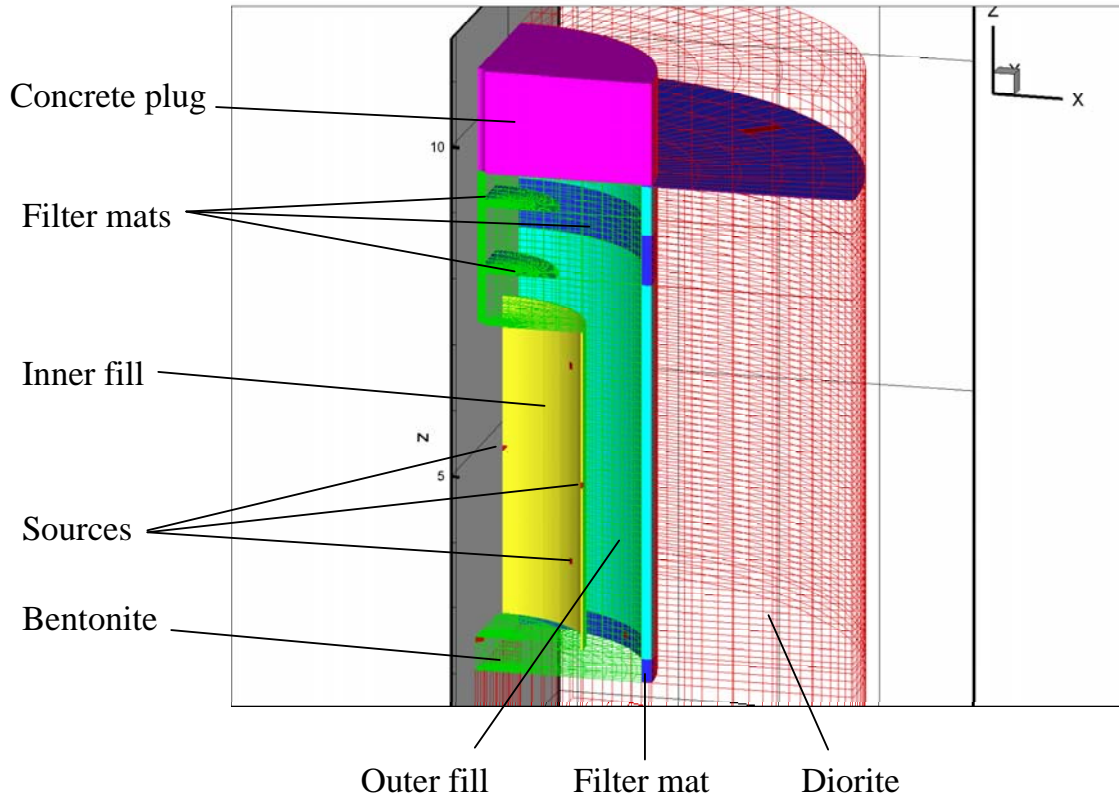


Figure 3-1 Components of the bentonite buffer model used for resaturation calculations.

For most calculations, the saturated permeability of the bentonite has been taken to be 10^{-20} m^2 , with a few variations run at 10^{-21} m^2 . The saturated permeability of the diorite host rock was assumed to take one of two values. For runs in which it was required that the host rock make very little contribution, the value was set at 10^{-22} m^2 . For runs in which a more significant contribution was required, the value of 10^{-19} m^2 was adopted, based upon the experimental observations of Nowak et al. (2003). The permeability of the ‘fill’ between buffer and host rock was assumed to be 10^{-19} m^2 . The ‘fill’ between canister and buffer, which represents an initial gap that becomes filled by the swelling of the bentonite, was set at 10^{-16} m^2 in early calculations and reduced to 10^{-18} or 10^{-19} m^2 in later calculations. The cement plug was given a permeability of 10^{-18} m^2 . Filter mats, that are placed near the bottom of the emplacement hole and between some of the bentonite slabs in the upper part of the assembly, were given permeabilities of 10^{-16} m^2 , which is sufficiently high to ensure that pressures rapidly equalize over the surfaces of the mats.

The capillary pressure and relative permeability functions of van Genuchten (1980) were used for all materials in the model. These are written as

$$P_{\text{cap}} = -\frac{\rho g}{\alpha} \left[\left(\frac{S - S_{\text{res}}}{S_{\text{max}} - S_{\text{res}}} \right)^{-1/m} - 1 \right]^{1-m} \quad (3-1)$$

for the capillary pressure and

$$k_{\text{rw}} = \left(\frac{S - S_{\text{res}}}{S_{\text{max}} - S_{\text{res}}} \right)^{0.5} \left[1 - \left\{ 1 - \left(\frac{S - S_{\text{res}}}{S_{\text{max}} - S_{\text{res}}} \right)^{1/m} \right\}^m \right]^2 \quad (3-2)$$

for the relative permeability of water with that for gas given by

$$k_{rg} = 1 - k_{rw} \quad (3-3)$$

For all materials, these models used $S_{\max} = 1$ and $m = 0.557$. For numerical reasons, TOUGH2 requires that S_{res} is less for the capillary pressure function than for the relative permeability function, so values of 0.1 and 0.15 respectively were used for these. The final parameter required for these equations is α . This was set to a value of 0.981 m^{-1} for all materials in most of these calculations. It is recognised that a much smaller value would normally be considered appropriate for the bentonite in particular, but it was found that reducing it significantly caused severe convergence problems for the TOUGH2 code, resulting in the use of very small timesteps or the code stopping altogether.

The final parameters required by the model are the porosity of each material and their initial saturations. The calculations fall into two groups. For the first, the bentonite was considered homogeneous, so the porosity of all materials except the diorite host rock was set to 40%, with the host rock being set to 1%. For these calculations it was also assumed that the bentonite was uniformly 95% saturated initially, with other materials fully saturated. For the second group of calculations the porosity and initial saturation were set separately for each of the bentonite rings and cylinders as shown in Table 3-1.

Block No.	Porosity	Initial saturation
C1	0.426	0.986
R1	0.400	0.958
R2	0.397	0.953
R3	0.396	0.962
R4	0.399	0.970
R5	0.396	0.964
R6	0.399	0.974
R7	0.399	0.953
R8	0.398	0.957
R9	0.396	0.964
R10	0.396	0.964
C2	0.424	0.989
C3	0.425	0.984
C4	0.427	0.997
C5	0.423	0.986

Table 3-1 Porosities and initial saturations for individual bentonite blocks. The blocks are approximately 0.5 m tall and have been ordered in this table from bottom (C1) to top (C5). See Johannesson (2003) for details.

3.2 HOMOGENEOUS BENTONITE MODELS

As indicated above, some initial calculations were carried out with no variation in the bentonite properties and a uniform initial saturation state. These calculations were also made with a relatively high assumed value for the ‘inner fill’ zone (10^{-16} m^2) based on the fact that this is initially an air gap that becomes closed only as the bentonite swells. The TOUGH2 code is not able to predict the timing of this swelling.

3.2.1 The effect of host rock permeability

The first calculations show the potential importance of the host rock permeability to the progress of the resaturation process. Figure 3-2 shows the variation of gas saturation after resaturation has been taking place for 1yr with a very low value for the diorite permeability (10^{-22} m^2). It can be seen that gas content remains significant both above and below the canister and also adjacent to the emplacement wall alongside the canister.

Figure 3-3 shows the same plot for a model in which the diorite permeability has been increased to 10^{-19} m^2 , the value that has been measured for an un-fractured section of the emplacement hole wall (Nowak, 2003). Comparison with Figure 3-2 shows that the gas saturations are significantly reduced around the emplacement hole wall, the effect being particularly noticeable alongside the canister.

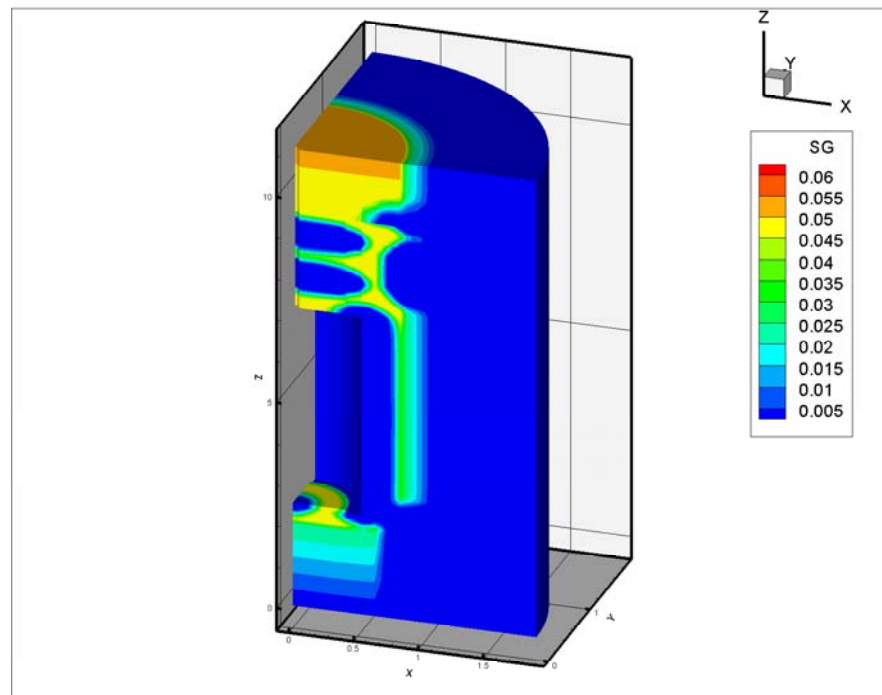


Figure 3-2 Gas saturations after 1yr of water injection for a model with a low permeability host rock (10^{-22} m^2) and a homogeneous bentonite buffer.

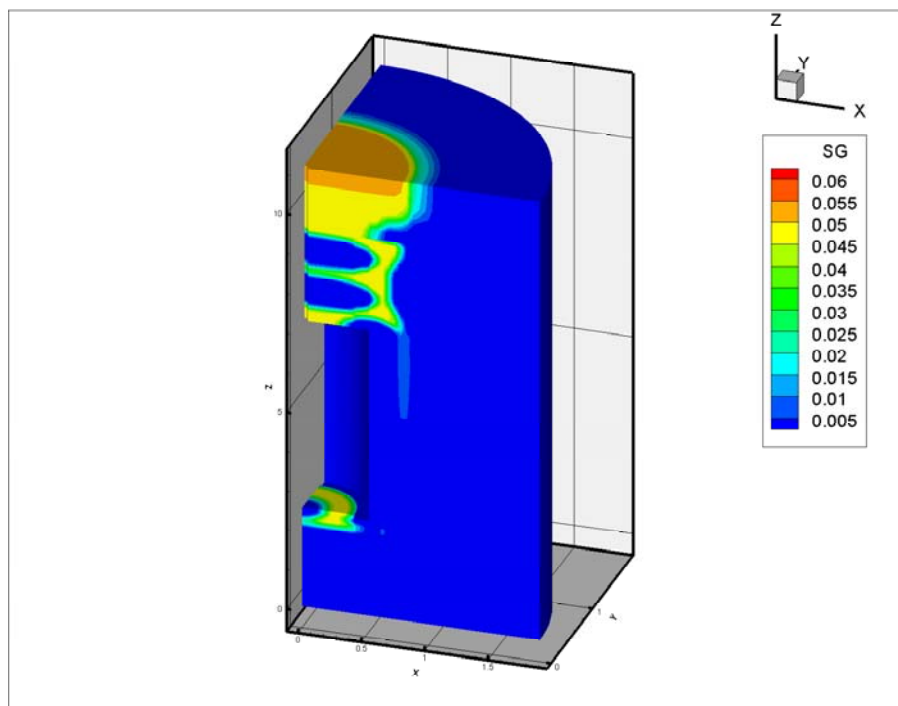


Figure 3-3 Gas saturations after 1yr of water injection for a model with a higher permeability host rock (10^{-19} m^2) and a homogeneous bentonite buffer.

3.2.2 The effect of fractures

The deposition hole wall was mapped for fractures by Hardenby and Lundin (2003) who found that although fracture traces were widespread over the surface, there are relatively few places where water seepage was observed. Of these, only three are described as ‘flowing’ and these are all located towards the bottom of the hole.

In order to help assess the potential impact of such water inflow points a model was created that included a single fracture ‘channel’. This channel was created by using a line of high permeability (10^{-15} m^2) elements running radially from the specified pressure outer boundary of the model to the deposition hole wall at a height of 1m above the floor of the hole.

Figure 3-4 shows gas saturations on sections cut through models with and without the fracture channel. The influence of the channel’s presence is quite small and has been highlighted with a red circle. In these models the main bulk of the diorite host rock has been given the low permeability of 10^{-22} m^2 to emphasise the fracture’s effect. Even with this, the plot has had to be generated at a simulated time of 180 days instead of 1yr because by that later time it becomes difficult to find the difference.

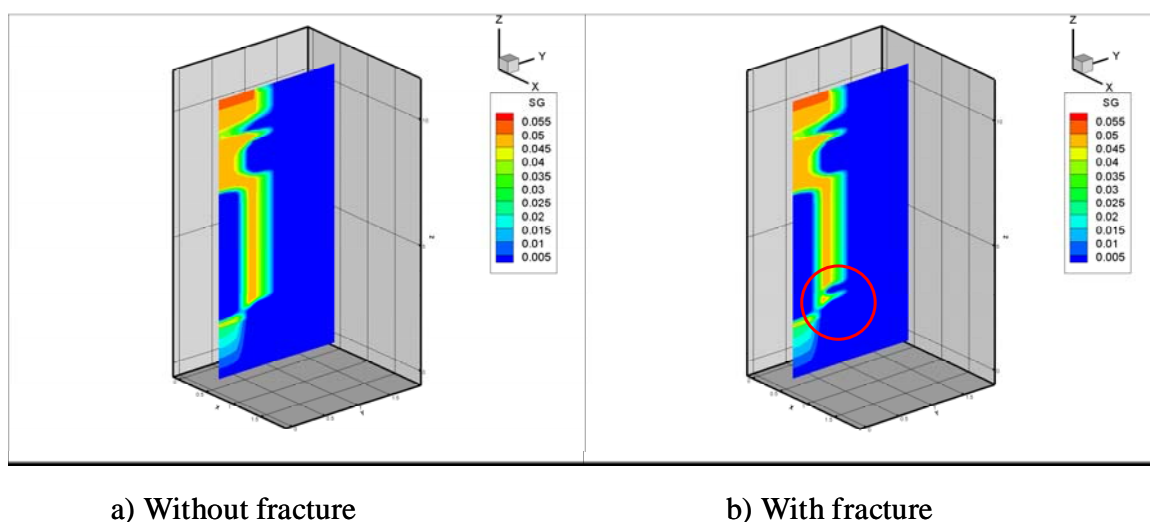


Figure 3-4 The effect of a fracture on gas saturations after 180 days of water injection.

3.3 HETEROGENEOUS BENTONITE MODELS

The treatment of the bentonite buffer as a single homogenous mass provides a relatively simple system on which to test the sensitivity to parameters. However, the process of manufacturing the individual bentonite rings and cylinders which fill in the void around the canister gives rise to small variations in void ratio and degree of water saturation. Because of the extremely low permeability of this material these variations will give rise to significant variations in the time taken to resaturate and may persist into the gas injection phase of the experiment. To help to assess the impact of this, additional models have been constructed which treat each of the bentonite blocks as a separate material type with porosities and initial saturation states as indicated in Table 3-1.

Additionally, it was felt that setting the inner fill permeability as high as was done for the above calculations might be unduly overestimating the rate of resaturation. The second group of calculations were therefore performed with the inner fill permeability reduced to a more conservative value of 10^{-19} m^2 .

Finally, the first group of calculations were performed with the pressure at the injection points on the canister surface and attached to the filter disks stepped instantly at $t=0$ to their final long term

values (5MPa) and then held constant throughout the calculation. For this second group of models, the pressures of these source points were raised in a series of increments as the model progressed, in line with the intended experimental procedure. Thus, the pressures applied to the injection points on the canister surface and filter disks are given as a function of time in Table 3-2.

Time (days)	Pressure (MPa)
0	0.0
4.42	0.0
5.58	0.25
49.42	0.25
50.58	1.00
99.42	1.00
100.58	2.50
149.42	2.50
150.58	5.00
1095.0	5.00

Table 3-2 Variation of pressure with time at the model injection points.

3.3.1 The effect of host rock permeability

As for the homogeneous bentonite group, the first calculations carried out in this group examine the effect of the host rock permeability on the resaturation of the bentonite. Figure 3-5 and Figure 3-6 show plots of gas saturation after 1 yr of resaturation with low and high host rock permeability respectively. These plots again show that the inflow of water from the surrounding host rock could make a significant difference to the progress of the system.

However, comparing Figure 3-5 and Figure 3-6 with Figure 3-2 and Figure 3-3 shows that there are two important differences in the way the new models are behaving. Firstly, in the new models, saturation of the disks above and below the canister is almost complete at the 1 yr point that has been plotted. In the previous models these were the regions of substantial remaining gas levels. The reason for this is that these blocks start from an almost completely saturated state, as shown in Table 3-1.

The second difference is that resaturation has progressed very little in the region close to the canister compared to what happened in the models of Section 3.2. This is happening because of the reduced permeability assigned to the inner fill zone around the canister. In the Section 3.2 models, the high permeability of this zone effectively allowed the whole of the canister surface to act as a source for resaturation. With the new value, it is taking a significant amount of time for water to move out from the source points before penetrating the bentonite. The shading of the canister surfaces in the plots of Figure 3-5 and Figure 3-6 shows the limited zones of saturation around each source.

Figure 3-7 shows the model of Figure 3-6, with the higher host rock permeability, after 3yr of water injection. It can be seen that even at this point in time there is significant gas saturation remaining in parts of the system including areas adjacent to the canister wall.

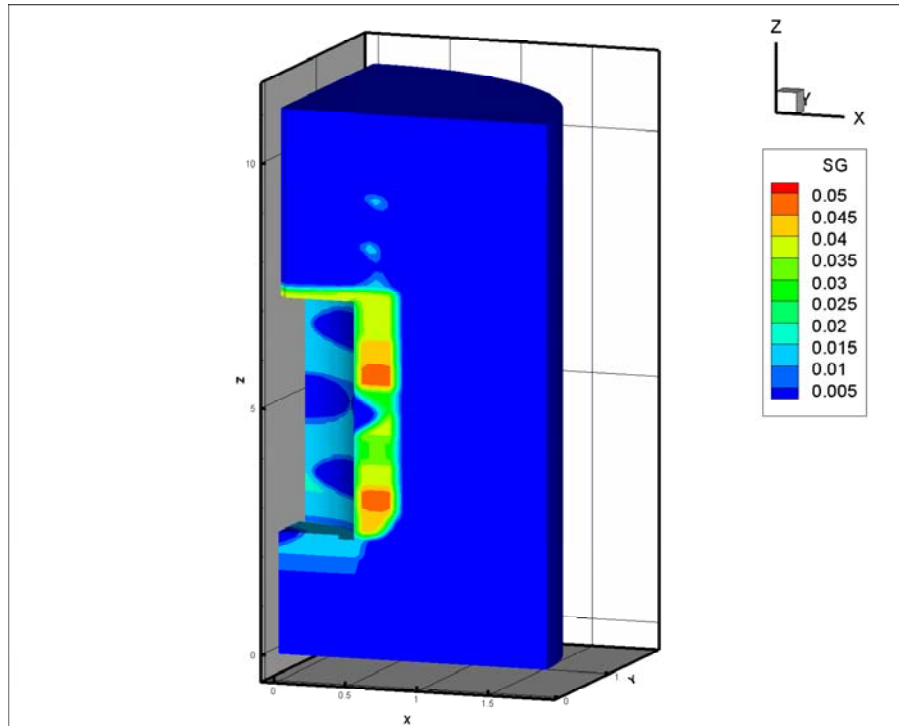


Figure 3-5 Gas saturations after 1yr of water injection for a model with a low permeability host rock (10^{-22} m^2) and a heterogeneous bentonite buffer.

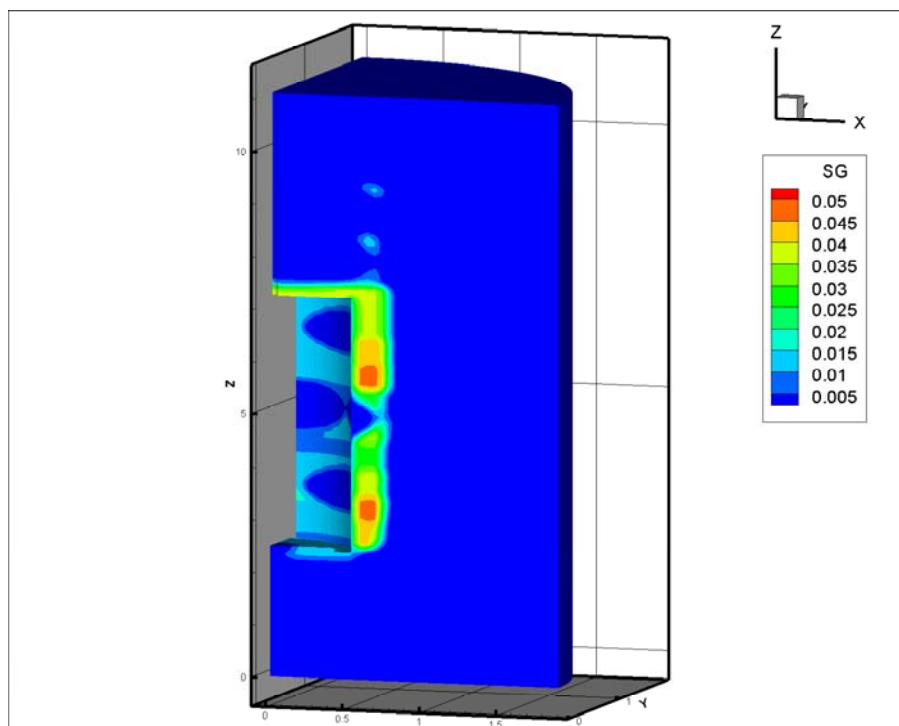


Figure 3-6 Gas saturations after 1yr of water injection for a model with a higher permeability host rock (10^{-19} m^2) and a heterogeneous bentonite buffer.

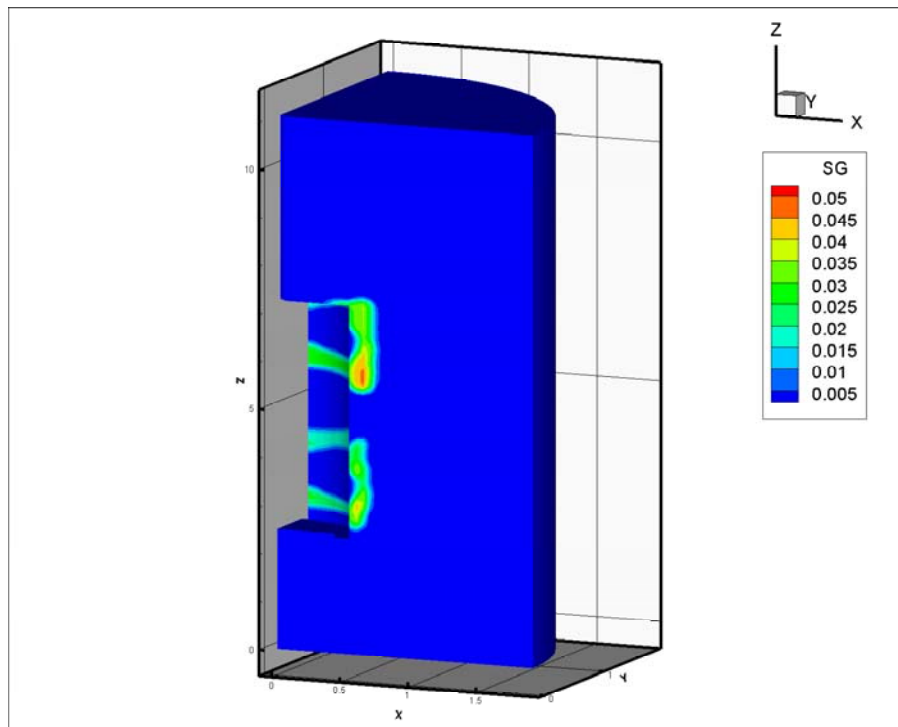


Figure 3-7 Gas saturations after 3yr of water injection for a model with a higher permeability host rock (10^{-19} m^2) and a heterogeneous bentonite buffer.

3.3.2 The effect of higher capillary pressure in the bentonite

It was stated in Section 3.2 that the parameter α was set to 0.981 m^{-1} in the models and that numerical problems limited scope for its reduction in bentonite to a more realistic level, which might be as low as 0.01 m^{-1} . It was not possible to complete a run of the model with such a low value, but one run was made with $\alpha = 0.098 \text{ m}^{-1}$, using the lower permeability for the host formation (10^{-22} m^2). A plot of the results after 1 yr is shown in Figure 3-8. Comparison with Figure 3-5 shows that the differences are relatively minor. The regions with the highest gas saturations are slightly reduced in the new model, but the gas saturations are higher in the inner fill zone between the source points, plotting in green rather than light blue.

3.3.3 The effect of a higher injection pressure

The models in this section have all used the injection pressure sequence detailed in Table 3-2, which rises to a maximum of 5 MPa after 150 days. The model shown in Figure 3-9 was run with the pressure steps in Table 3-2 doubled so that the injection pressures rise to 10 MPa at the same time. This model has the diorite permeability set at 10^{-19} m^2 , so the results should be comparable with those in Figure 3-6. It can be seen that the extra pressure has very little effect on the extent to which resaturation has progressed.

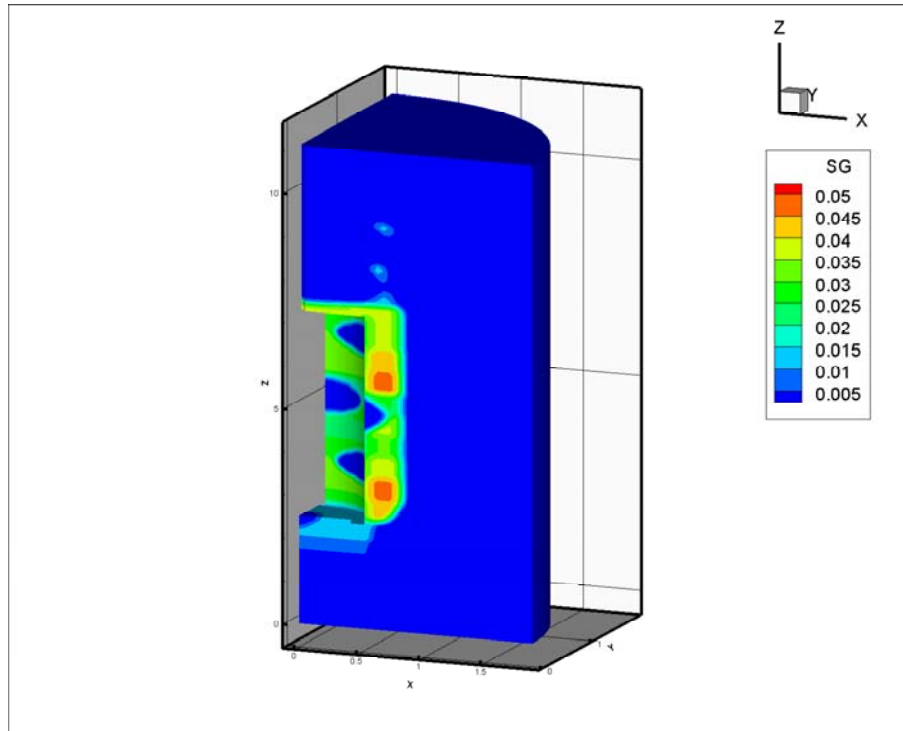


Figure 3-8 Gas saturations after 1yr of water injection for a model with a low permeability host rock (10^{-22} m^2) and a lower α (0.098).

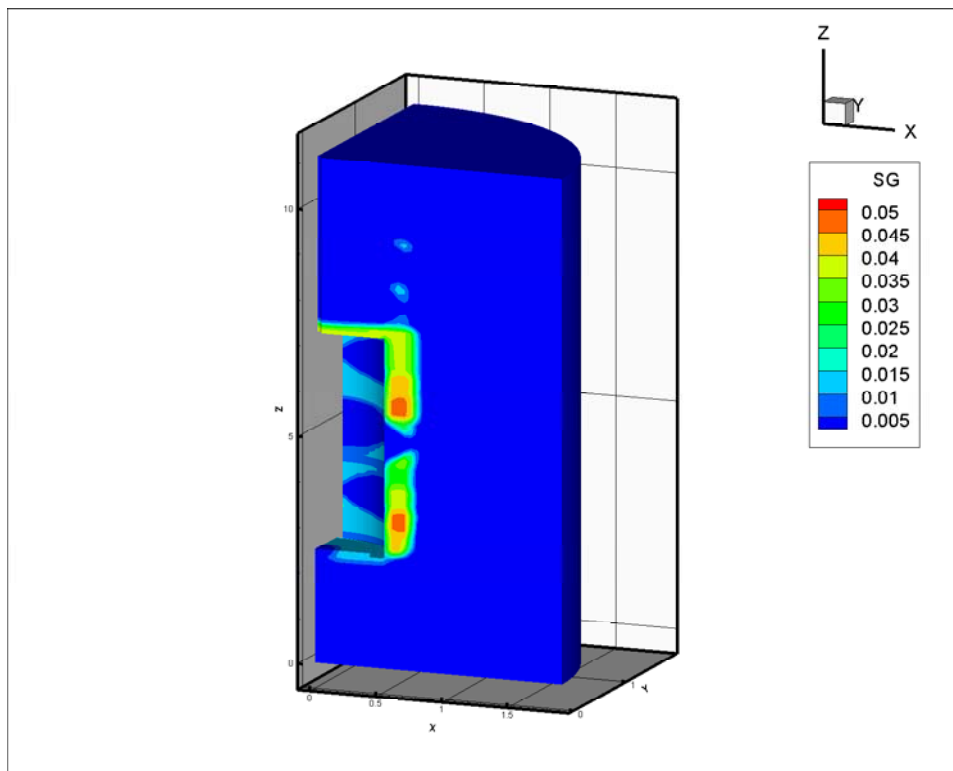


Figure 3-9 Gas saturations after 1yr of water injection for a model with a higher permeability host rock (10^{-19} m^2) and a higher injection pressure (10MPa).

3.3.4 The effect of the inner fill permeability

As noted at the beginning of this section, it was decided to reduce the permeability of the inner fill zone from the value used for the models in Section 3.2 in order to make more conservative assessments of the progress of the resaturation process. A reduction of three orders of magnitude was made and the models in this section have shown that this change has a very substantial effect on the resaturation of the bentonite buffer, particularly for that part of it alongside the canister. The change made to the permeability in fact makes the fill zone only one order of magnitude more permeable than the bulk of the bentonite.

To study the sensitivity to a slightly more permeable fill zone two further models were run with the permeability raised to 10^{-18} m^2 , with the lower and higher host rock permeabilities. The results from these models are shown in Figure 3-10 and Figure 3-11. It can be seen that the resaturation has progressed much further than for the comparable models in Figure 3-5 and Figure 3-6. The faster progress of resaturation is underlined in Figure 3-12 where the model of Figure 3-10 has been continued until a simulated time of 3yr. Here it can be seen that the gas phase has been almost completely removed from the bentonite buffer. Comparison with Figure 3-7 shows how important the inner fill zone of the model is to the resaturation process.

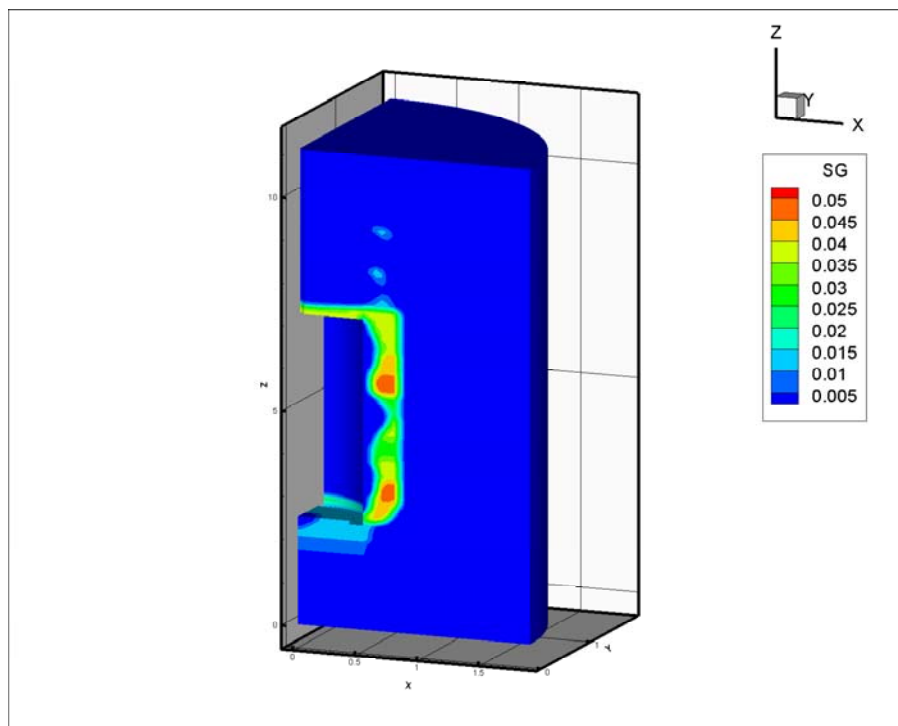


Figure 3-10 Gas saturations after 1yr of water injection for a model with a low host rock permeability (10^{-22} m^2) and an inner fill permeability of 10^{-18} m^2 .

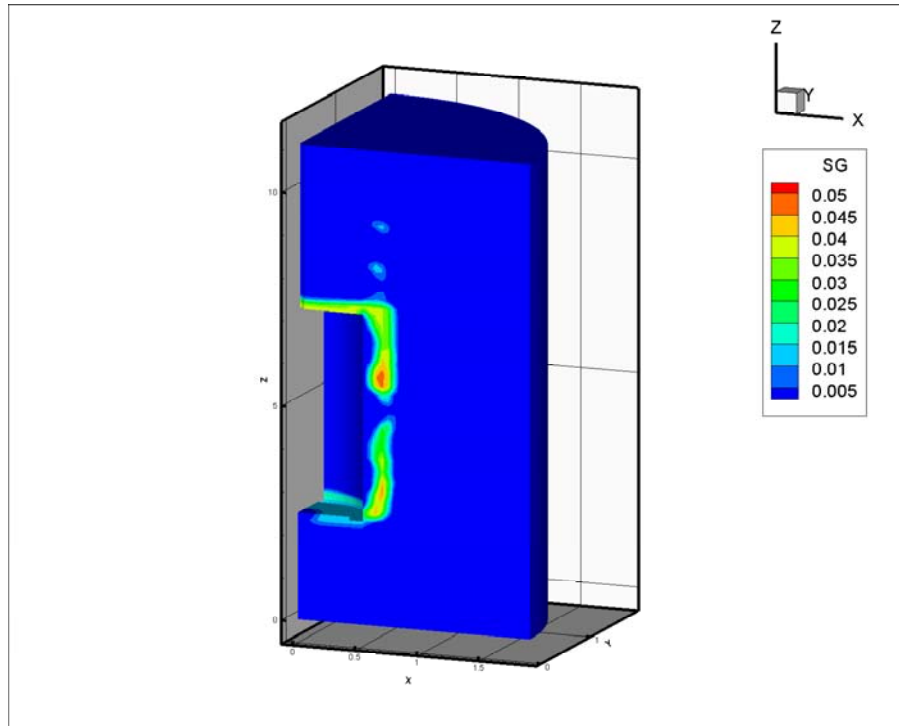


Figure 3-11 Gas saturations after 1yr of water injection for a model with a high host rock permeability (10^{-19} m^2) and an inner fill permeability of 10^{-18} m^2 .

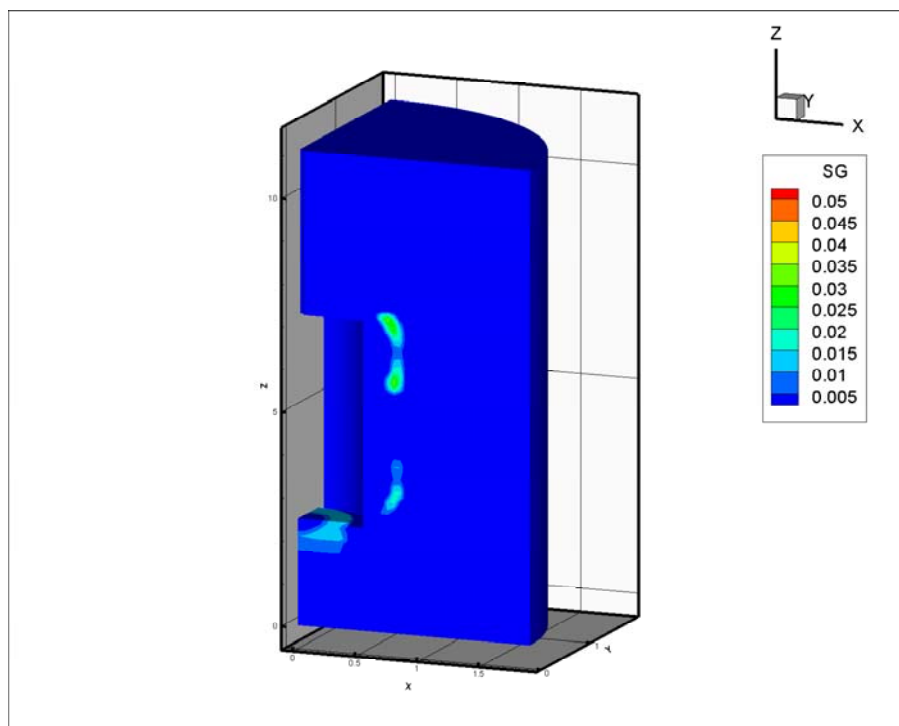


Figure 3-12 Gas saturations after 3yr of water injection for a model with a low host rock permeability (10^{-22} m^2) and an inner fill permeability of 10^{-18} m^2 .

4 Hydration Phase 1: Experimental results

The aim of this phase of testing is to hydrate the bentonite blocks through natural and artificial means, thereby raising the saturation state in the bulk of the buffer to a value close to unity. The time period for hydration will depend on a number of factors, including:

- The initial geotechnical properties of the bentonite blocks (dry density, saturation, moisture content).
- The buffer dimensions, suction gradient and permeability to water.
- The availability of water, which depends on the number, location and discharge rates of the hydration sources.
- The volume of gas voids and the capacity of the buffer to expel trapped air.
- The amount of unfilled void space, including construction gaps that must be filled by clay swelling.

Hydration of the bentonite is undertaken in a series of stages with hydraulic pressure artificially increased at a number of locations within the system in an attempt to reduce hydration times. *In situ* porewater collected from a nearby sealed borehole is used as the injection permeant. During artificial hydration, porewater is actively injected through all of the filters located on the canister surface (excluding the FCT) and the large filter mats sandwiched between blocks C2-C3 and C4-C5 (Figure 4-1).

The deposition hole was closed on the 1st February 2005 signifying the start of the hydration phase. In order to allow *in situ* porewater pressure to equilibrate and provide the bentonite with time to swell and begin closure of the engineering voids, the start of artificial hydration was deferred. During this time, groundwater was flushed through the system in an attempt to remove the bulk of the residual air trapped in the engineering voids. Localised groundwater inflow through a number of highly-conductive discrete fractures quickly resulted in elevated porewater pressures (>870kPa) throughout large sections of the borehole. This led to the formation of conductive channels (piping) and bypass flow, leading to the extrusion of bentonite from the hole and the discharge of groundwater to the gallery floor.

To address this issue, two pressure relief holes (PRH1 and PRH2) were drilled in the surrounding rock mass in an attempt to lower the porewater pressure in the vicinity of the deposition hole. With the insertion of submersible pumps into the pressure relief holes, piping and bypass flow stopped and water pressure within the deposition hole was stabilised. Packer assemblies were inserted into the pressure relief holes on day 413 and the packers inflated on day 415. Individual sections were then closed off over the period from day 476 to day 519.

Artificial hydration began on the 18th May 2005 after 106 days of testing. Table 4-1 shows a summary of key events through November 2007.

4.1 EVOLUTION OF POREWATER PRESSURE

The following sections describe the temporal evolution of porewater pressure in the Lasgit system, reflecting the complex interaction between artificial and natural sources and their cumulative role in the hydration of the buffer clay. Table 4-2 summarises key hydration events occurring during this stage of testing. Table 4-3 provides details of the sequence of events during installation of packers into the pressure relief boreholes.

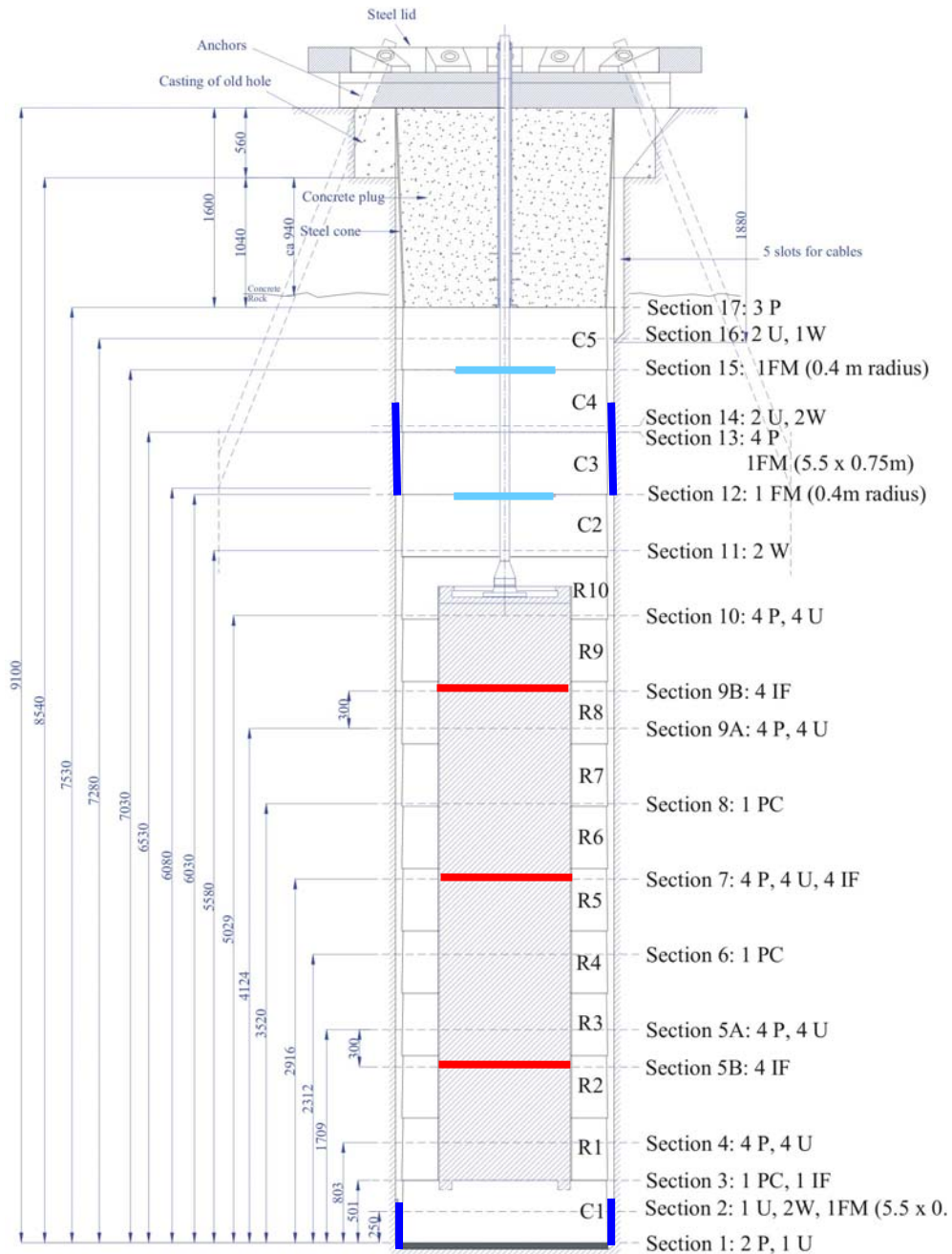


Figure 4-1 Schematic representation of borehole infrastructure taken from the R4 Report by Sandén (2003). Cartesian coordinates and a description of each sensor is included in the R4 report (“P” signifies a total pressure cell, “U” a pore pressure cell, “W” a relative humidity sensor, “PC” a total pressure on canister, “FM” a filter mat and “IF” an injection filter). The dark and light blue lines respectively highlight the position of filter mats bolted to the rock surface and those located between bentonite blocks. The red lines show the planes along which the canister filters are positioned.

4.1.1 Canister filters FL901 to FU912.

Data from the canister filters are shown in Figure 4-2. Artificial hydration began at 106 days at a pressure of 150 kPa. During this initial stage of the test, the pressure in all of the canister filters (excluding the FCT) and the filter mats FB903 and FB904 were controlled using reciprocating pumpset RP2. At 111 days, filter mat FR902 was added to the RP2 circuit and its pressure raised to 150 kPa (the temporary reduction in pressure at 112 days occurred during error checking of

the data acquisition software). Three days later (115 days) the pressure in the RP2 circuit was raised to 250 kPa.

Date	Elapsed time	Description of event
1/02/2005	0	Deposition hole closed and water flushed through system in an attempt to remove air trapped in engineering voids
2/02/2005	1	Extrusion of bentonite plus water into the instrumentation slot around the top of the deposition hole
	1	Canister filters and injection mats connected to the Gas Laboratory (GL)
4/02/2005	3	De-airing of tubework from GL to canister filters and hydration mats
13/02/2005	12	Increased discharge to instrumentation slot.
14/02/2005	13	Pressure lines from filter mats to the Gas lab disconnected to improve drainage from hole in an attempt to moderate the increase in porewater pressure
13/03/2005	40	Interruption in Geokon data acquisition due to corrupted library file
4/04/2005	62	Pressure relief hole 1 drilled in the surrounding rock mass
7/04/2005	65	Submersible pump placed in pressure relief hole 1
12/04/2005	70	Pressure relief hole 2 drilled in the surrounding rock mass
19/04/2005	77	Submersible pump placed in pressure relief hole 2
25/04/2005	83	Air-conditioning unit failed resulting in an increase in laboratory and office temperatures. Test unaffected.
27/04/2005	85	Air-conditioning unit repaired
3/05/2005	91	Submersible pumps switched off
10/05/2005	98	Submersible pumps removed from and packers installed in both pressure relief holes. Packered intervals open to atmospheric pressure and free to drain. Discharge rates monitored on a regular basis from this date onwards.
18/05/2005	106	Start of artificial hydration. Pump pressure in RP2 initially set to 100 kPa (uncalibrated value) to stabilise pressures in all canister filters (except the FCT) and filter mats FB903 and FB904.
	106	RP2 pressure then increased to 150 kPa (uncalibrated value).
23/05/2005	111	Filter mat FR902 opened to pumpset RP2 set at 150 kPa (uncalibrated value).
24/05/2005	112	Error checking of the software required isolation of individual test circuits from the pump system. The momentary reduction in pressure of filter mat FR902 occurred during this process.
27/05/2005	115	Pressure increased in RP2 to 250 kPa (calibrated value) in all canister filters (except the FCT) and filter mats FR902, FB903 and FB904.
2/06/2005	121	Software revision installed. FCT valve opened by accident resulting in a drop in all filter pressures and the discharge of groundwater into the canister void.
7/06/2005	126	FCT valve closed and system pressures restored.
9/06/2005	128	Pressure increased in RP2 to 500 kPa (calibrated value) in all canister filters (except the FCT) and filter mats FB903 and FB904. FR902 left closed so that inflow to other circuits could be measured.
11/06/2005	129	Power supply to acquisition system (Field-Point module) failed leading to a loss of fluid pressure in the system.
13/06/2005	132	Power supply to acquisition system (Field-Point module) replaced, system reset and pressures raised to 500 kPa (calibrated value).
16/06/2005	135	Multi-logger software "crashed" resulting in the loss of Geokon data
21/06/2005	140	Attempted to raise pressure to 1000 kPa (calibrated value). After pumping >800 ml of fluid into FM906 process suspended and pressure reset in all previous open filters to 500 kPa. During this time an additional ~8 litres of fluid were injected into FM906.
22/06/2005	141	Pressure increased in RP2 to 750 kPa (calibrated value) in all canister filters (except the FCT) and filter mats FR902, FB903 and FB904.
		Once stable pressure obtained, then increased in RP2 to 1000 kPa (calibrated value) in all canister filters (except the FCT) and filter mats FR902, FB903 and FB904.

4/07/2005	153	Interruption in LabVIEW control software led to the momentary closure of all automated valves resulting in a number of clearly defined negative pressure transients
7/07/2005	156	Multi-logger software revision installed resulting in a loss of data and a short-term reduction in system pressure
13/07/2005	162	Repair and leak-testing of pumpset RP1 complete. Pressure set to 1000 kPa (calibrated) and thereafter used to control pressure in filter mats FR902, FB903 and FB904 as well as canister filters FM905 to FM908. All other filters pressures (except FR901) remain controlled by RP2.
14/02/05	163	Software fault on RP1 resulted in a temporary loss of pressure to filter mats FR902, FB903 and FB904 as well as canister filters FM905 to FM908.
18/07/2005	167	Pressure increased in RP2 to 2000 kPa (calibrated value). When the pressure in filter FL903 reached ~1800 kPa increases in pressure were observed in FR901 as well as multiple total stress and porewater pressure sensors located within the clay and on the surface of the borehole, indicating the formation of highly conductive channels ("piping"). Pressure in RP2 was immediately lowered to 1200 kPa.
	167	Further attempts were made to substantially increase water pressure in both RP1 and RP2 systems without success. Pressure in both pump systems were then set to 1250 kPa.
19/07/2005	168	Another attempt was undertaken to incrementally raise water pressure to 2000 kPa. When water pressure reached ~1750 kPa in FU910 piping occurred resulting in a rapid increase in monitored porewater pressure and total stress. Pressure in both pump systems was finally set to 1350 kPa resulting in a massive reduction of flow into the system.
20/07/2005	169	Pressure increased in both RP1 and RP2 to 1500 kPa. No piping observed.
9/08/2005	189	New system for monitoring the relative movement of the steel lid to gallery roof was successfully installed (DP905).
10/08/2005	190	Gas pressure inside the canister was gently raised to expel the groundwater which had been accidentally pumped into the void (2/06/2005). This resulted in a temporary increase in FCT pressure and noise in the signal from the canister thermocouple.
23/08/2005	203	Another attempt was undertaken to incrementally raise water pressure to 2000 kPa. When water pressure was raised in FM906 piping reoccurred resulting in a rapid increase in monitored porewater pressures and total stresses coupled with an increase flow rate from both pump systems ($>60 \text{ ml}\cdot\text{min}^{-1}$). Pressure in both pump systems was finally set to 1500 kPa.
22/09/2005	233	Both pump systems taken off-line for <1 day while software upgrades installed. During this period the pressure in the circuits controlled by RP1 and RP2 dropped to ~1200 kPa and ~1100 kPa respectively.
23/09/2005	234	System repressurised to 1500 kPa.
11/10/2005	252	Interruption in data acquisition caused by the "crashing" of the laboratory PC.
13/10/2005	254	PC rebooted and software restarted. When communication with the control systems were re-established the pressure in the FL and FU circuits had increased slightly to ~1600 kPa.
18/01/2006	351	The code was temporary stoppped to disable contour plots. Temporary spike in pressures were observed when the acquisition software was restarted.
6/03/2006	397	Logging system stopped while new acquisition cards were installed to log the new transducers.
7/03/2006	399	Logging system stopped momentarily to back-up sources code. Valve to FB904 failed to automatically open when code restarted. Resulted in a slight drop in pressure - valve reopened <4 hours later.
18/03/2006	410	Revised code uploaded to Lasgit PC.
21/03/2006	413	Logging software stopped while new transducers added to data acquisition system.
	413	System restarted but both pumpsets failed to initalise leading to a reduction in filter pressures overnight.
	413	Packer assemblies installed in PRH1 and PRH2.

22/03/2006	414	Packers inflated – drain valves left open.
23/03/2006	415	Top packer interval on PRH1 ruptured (414.73 days) resulting in the deflation of all packered intervals in PRH1. PRH2 remained inflated.
	415	Ruptured packer replaced and reinflated at 415.08 days. Failed again on pressurisation.
	415	At 415.09 the drain valves to sections PRH2-1 to PRH2-4 closed and pressures monitored to define flowing intervals.
	415	At 415.12 days, the drain valves to PRH2-1 to PRH2-3 were opened momentarily while pressure relief valves installed. PRH2-4 left closed as no significant flux observed.
	415	At 415.15 days drain valve to PRH2-2 opened and pressure relief valve removed and attached to PRH1-1.
	415	Packer interval moved to prevent a third failure and reinflated at 415.21 days.
	415	At 415.26 days the drain valve to PRH1-1 was closed. Data subsequently deleted due to problems with the transducer.
	415	Drain valve to PRH1-1 opened as pressure had increased to around 2.2 MPa.
24/03/2006	415	New calibration values applied to data.
	416	Data corrupted. Code stopped, revised and uploaded less than 2 hours later. Resulted in a small drop in pressure in most of the filter systems.
23/05/2006	476	PRH1-1 on line.
	476	PRH2-4 closed.
31/05/2006	484	PRH2-2 closed.
08/06/2006	492	PRH1-5 closed.
14/06/2006	498	PRH1-4 closed.
16/06/2006	499	Pressurisation system for PRH1 packers began to leak.
20/06/2006	504	PRH1-3 closed.
21/06/2006	504	All PRH pressures (in both holes) in packered intervals begin to decrease as the packers in PRH1 continue to deflate (504.82).
22/06/2006	506	Pressure from PRH1-3 bleeds into PRH1-4 and 1-5 as gas bottle pressure not sufficient to create seal between PRH1-3 and rockface.
26/06/2006	510	Leak fixed in the pressurisation system for PRH1 packers (510.02).
29/06/2006	513	PRH1-2 closed.
05/07/2006	519	PRH1-1 closed.
27/07/2006	541	Computer crashes – was restarted 12 days later when Aspo staff returned from leave.
22/08/2006	567	Pumps taken offline for maintenance. Drops in pressure to all cannister filters, FM2,3,4 and Refill water line.
22/08/2006	567	Total pump volumes inaccurate due to leak whilst maintaining pressure (caused by deposits on barrels). Leakages from the standby pump are therefore included in the total pumped. (Pumps taken for servicing at this point A1/A2).
19/09/2006	595	Calibration of transducers for ~2 days.
05/10/2006	611	Lab temp increased due to compressor overworking. Caused by faulty Isonic valve.
20/11/2006	657	Pressures in all filters (except FR901) raised to 2350kPa (calibrated) using RP2. Connectivity between UFA4 and UFA1 observed when UFA1 pressure raised. FB903 and FB904 also took largest volumes of fluid to pressurise. Total fluid volume used ~44ml.
09/01/2007	707	Inlet water supply switched to fresh water.
11/01/2007	709	Air con system failed until ~710 days.
17/01/2007	715	Maintenance of air conditioning system.
31/01/2007	729	Reconfigured air conditioning system in lab area to redistribute air flow over Isonic values. It took around 2 days for the system to equilibrate resulting in an offset between lab high and low temperatures.
13/02/2007	742	A2 recalibrated. Values not input into sheet as the difference in calibrated value at 2300 kPa was only around 3 kPa and A2 was moved to A1 position on 5/3/07 invalidating the calibration.
14/02/2007	743	Hydration system moved across to pump A2.

15/02/2007	744	Pressure in all hydration circuits dropped as the A2 pump ran out of water. For the next ~6 days the pressure in the hydration system dropped.
16/02/2007	745	B1 and B2 removed for servicing.
16/02/2007	745	Office temperature lowered by 3 degrees.
21/02/2007	750	Pump A2 refilled and hydration pressures restored.
22/02/2007	751	Lab and office temperatures lowered by a further 1 degree to ~13.5 C to bring them in line with canister.
23/02/2007	752	A2 alarm tripped and stopped pump for no obvious reason. Pressure in hydration system fell.
23/02/2007	752	A2 alarm tripped and stopped pump for no obvious reason. Pressure in hydration system fell to around 2 MPa.
24/02/2007	753	A2 restarted and alarm disabled.
05/03/2007	762	A1 removed and pump A2 connected to controller to act as A1. A2 not recalibrated – but opened to atmospheric and pressure zeroed. Calibration now invalid. Pressure in hydration system dropped by around 60 kPa. Raw data filed edited to move pump A2 data to its correct column.
07/03/2007	764	Increased pump A2 by 65kPa to 2387 kPa (to account for the fact that the pump was now out of calibration having been moved to the A1 position) to raise pressure in hydration system to match previous values.
30/03/2007 to 11/04/2007	787 to 799	Air-con temperature increased resulting in a drop in pressure. Temperatures fluctuated for a few days before settling down.
10/04/2007	798	TBG logged on to system and pump over pressured circuits to 4 MPa momentarily. Hydration data deleted from sheet. A small offset noted in the lid displacement data but since it didn't return to the original value when the system was depressurised the offset was left in.
10/04/2007	798	B1 and B2 reinstated. A2 used to control hydration system.
2/05/2007	820	System isolated whilst pumps leak-tested. All hydration circuits dropped in pressure.
3/05/2007	821	Hydration circuits repressurised using B1.
17/05/2007	835	B1 ran out whilst hydrating. Refilled it whilst connected to downhole as no-one onsite at Aspo. Pressures downhole dropped momentarily and then recovered.
25/05/2007	843	All lower filters isolated for start of hydraulic pressure decay test.
5/06/2007	854	PRH transducers calibrated.
8/06/2007	857	Canister filters, filter mats, A1, A2, B1 and B2 transducers calibrated.
	857	FC901 transducer only left in communication with the calibration manifold pressurised by pump B1. Valve to canister closed at all times.
	857	Pump B1 raised by approx 100 kPa to lift the hydration filter pressures to approx the same value as before following calibration of the system.
21/06/2007	870	Jump in hydration circuits caused by swiching from pump B1 to RP1 (A1 and A2).

Table 4-1 Log of dates and events in the Lasgit test history to June 2007. Where stated calibrated values refer to scaled outputs prior to error checking (Section 2.6.1).

The drop in pressure to near atmospheric conditions observed at 121 days was caused by the accidental opening of the FCT valve while upgrading the data acquisition software. System pressures were restored a few days later and the pressure subsequently raised to around 500 kPa at 128 days. The failure of a power unit at 129 days (early on a Saturday morning) resulted in the temporary loss of data and a small reduction in system pressures until the transformer was replaced the following Monday (131 days).

At 141 days into the test history, the pressure within the RP2 circuit was successfully increased to around 750 kPa and then 1000 kPa using the methodology described in Section 2.7. A short interruption to update the control software (lasting ~5.5 hours) resulted in the adoption of a “fail safe” mode of operation, whereby all system valves automatically default to the closed position,

isolating individual test circuits. During this time a number of transducers exhibited clearly defined negative pressure transients. A similar affect was observed at 156 days when an update to the multi-logger (Geokon) software was applied. At 162 days, control of the pressure in canister filters FM905 to FM909 and filter mats FR902, FB903 and FB904 was migrated to pumpset RP1. During this transition a temporary reduction in pressure occurred.

Date	Day	Activity
1/02/2005	0	Closure of deposition hole
13/02/2005	12	High water pressures around the bentonite resulted in by-pass flow. Initial corrective measures proved unsuccessful
04/04/2005	62-70	Pressure relief holes drilled in surrounding rock mass
10/05/2005	98	Submersible pumps removed and pressure relief holes packered
18/05/2005	106	Start of artificial hydration (water pressure 150 kPa)
27/05/2005	115	Artificial porewater pressure increased to 250 kPa
09/06/2005	128	Artificial porewater pressure increased to 500 kPa
21/06/2005	140	Attempted to raise artificial porewater pressure to 1000 kPa (failed)
22/06/2005	141	Artificial porewater pressure increased to 1000 kPa
18/07/2005	167-168	Attempted to raise artificial porewater pressure to 2000 kPa (failed)
20/07/2005	169	Artificial porewater pressure increased to 1500 kPa
23/08/2005	203	Attempted to raise artificial porewater pressure to 2000 kPa (failed)
	203	Artificial porewater pressure reset to 1500 kPa
21/03/2006	413	Packer assemblies installed into pressure relief holes
23/03/2006	415	Packers in pressure relief holes inflated
23/05/2006	476-519	Packer sections in pressure relief holes isolated
20/11/2006	657	Pressures in all filters (except FR901) raised to 2350kPa
25/05/2007	843	Lower canister filters isolated for the start of the first hydraulic test

Table 4-2 Timeline of key hydration events.

Date	Days	Activity
23/03/2006	415	Valves to sections PRH2-1 and PRH2-3 closed. Valve to section PRH1-1 temporarily closed (few hours) but reopened as pressure increased rapidly
23/05/2006	476	Valve to section PRH2-4 closed
31/05/2006	484	Valve to section PRH2-2 closed
08/06/2006	492	Valve to section PRH1-5 closed
14/06/2006	498	Valve to section PRH1-4 closed
20/06/2006	504	Valve to section PRH1-3 closed
21/06/2006	505	All PRH pressures (in both holes) begin to decrease as the packers in PRH1 deflate
26/06/2006	510	Pressurisation system for PRH1 packers repaired
29/06/2006	513	Valve to section PRH1-2 closed
05/07/2006	519	Valve to section PRH1-1 closed

Table 4-3 Sequence of events during the installation of packers into the pressure relief boreholes PRH1 and PRH2.

Between 167 and 168 days several attempts were made to incrementally raise water pressure in the canister filters to a target value of 2000 kPa. When water pressure in filter FL903 reached ~1950 kPa, an increase in pressure was observed in FR901 as well as multiple total stress and porewater pressure sensors located within the clay and on the surface of the borehole - indicating the formation of highly conductive channels (“piping”). The pressure in RP2 was immediately lowered to ~1200 kPa to prevent the possible extrusion of bentonite slurry and the formation of long-term pathways. After a short period of time the pressure in each pump system was incrementally raised to around 1250 kPa without any obvious signs of pathway flow. At this

point in the test history it was decided to increase the pressure in each pump system to approximately 1300 kPa without isolating individual test circuits. This proved successful, so the pressure in the artificial hydration system was increased in 50 kPa steps. When the pressure reached 1450 kPa both reciprocating pump-sets began to rapidly inject water into the system, indicating that one or more conductive pathways had formed. The pressure in each pump system was reduced to around 1250 kPa and the system allowed to stabilise.

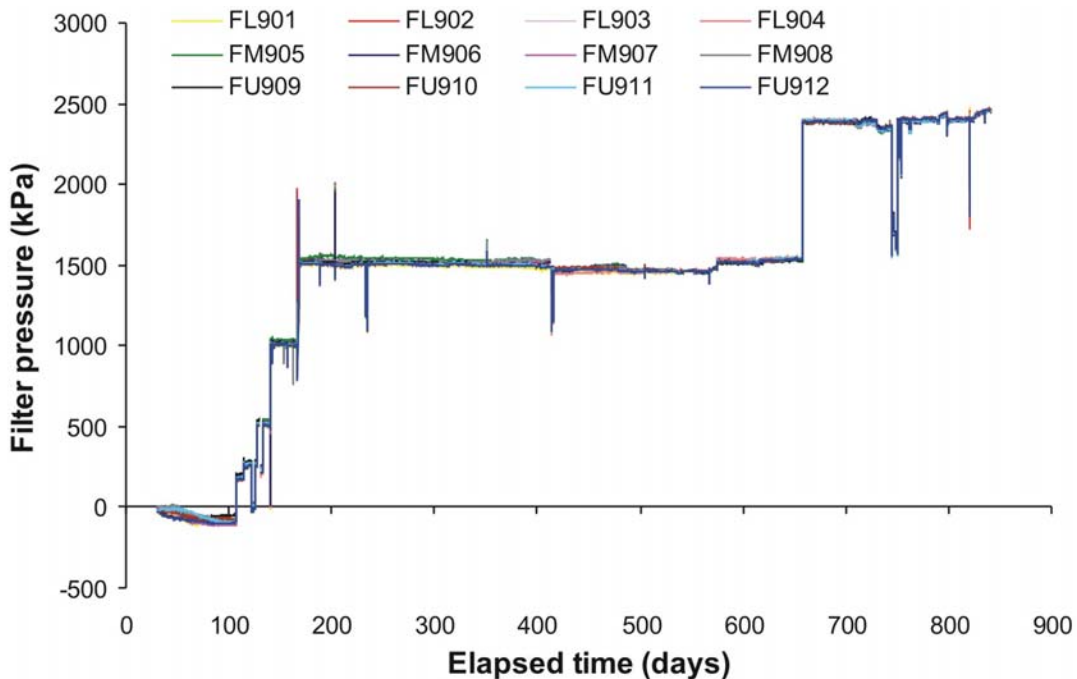


Figure 4-2 Evolution of water pressure within the canister filters.

The next day (elapsed time 168 days), pressure in each of the canister filters and hydration mats was incrementally raised to approximately 1500 kPa without any signs of pathway flow. Another attempt was made to incrementally raise water pressure in the artificial hydration system to 1750 kPa (Section 2.6). This was successful up to the inclusion of FM905, at which point pathway flow re-occurred. The pressure was immediately reduced to around 1500 kPa. However, when an attempt was made to restore the water pressure in FU910, which had declined slightly while isolated from the pumps, pathway flow again occurred. At this point, FU910 was isolated from the rest of the hydration system and the pressure allowed to equilibrate. Shortly afterwards, both pump sets began to rapidly inject water into the system indicating the sudden formation of one or more conductive features. To stabilise the system the pressure in both pump sets was reduced to 1350 kPa. The following day at an elapsed time of 169 days water pressures were incrementally raised to around 1500 kPa in each system without any obvious signs of pathway flow.

These pressure dependent features appear to be relatively short lived with the channels closing when the water pressure is reduced. Figure 4-3 shows a series of intensity plots showing the propagation of a high pressure water zone around the periphery of the borehole during the piping event described above.

At 203 days another attempt was undertaken to incrementally raise porewater pressure in the artificial hydration system to 2000 kPa. As the pressure was increased, piping occurred when the tube work to filter FM906 was opened. This resulted in a rapid inflow of water and an increase in monitored porewater pressure and total stress. Pressure in both pump systems was immediately reset to 1500 kPa and the system allowed to re-stabilise at the lower pressure.

At 233 days after closure of the deposition hole both pump sets were taken off-line for around 1 day while software upgrades were applied to the system. During this time each test circuit exhibited a small decrease in water pressure. However, when a similar activity occurred 21 days later the pressure in the lower and upper filter arrays actually increased to around 1600 kPa.

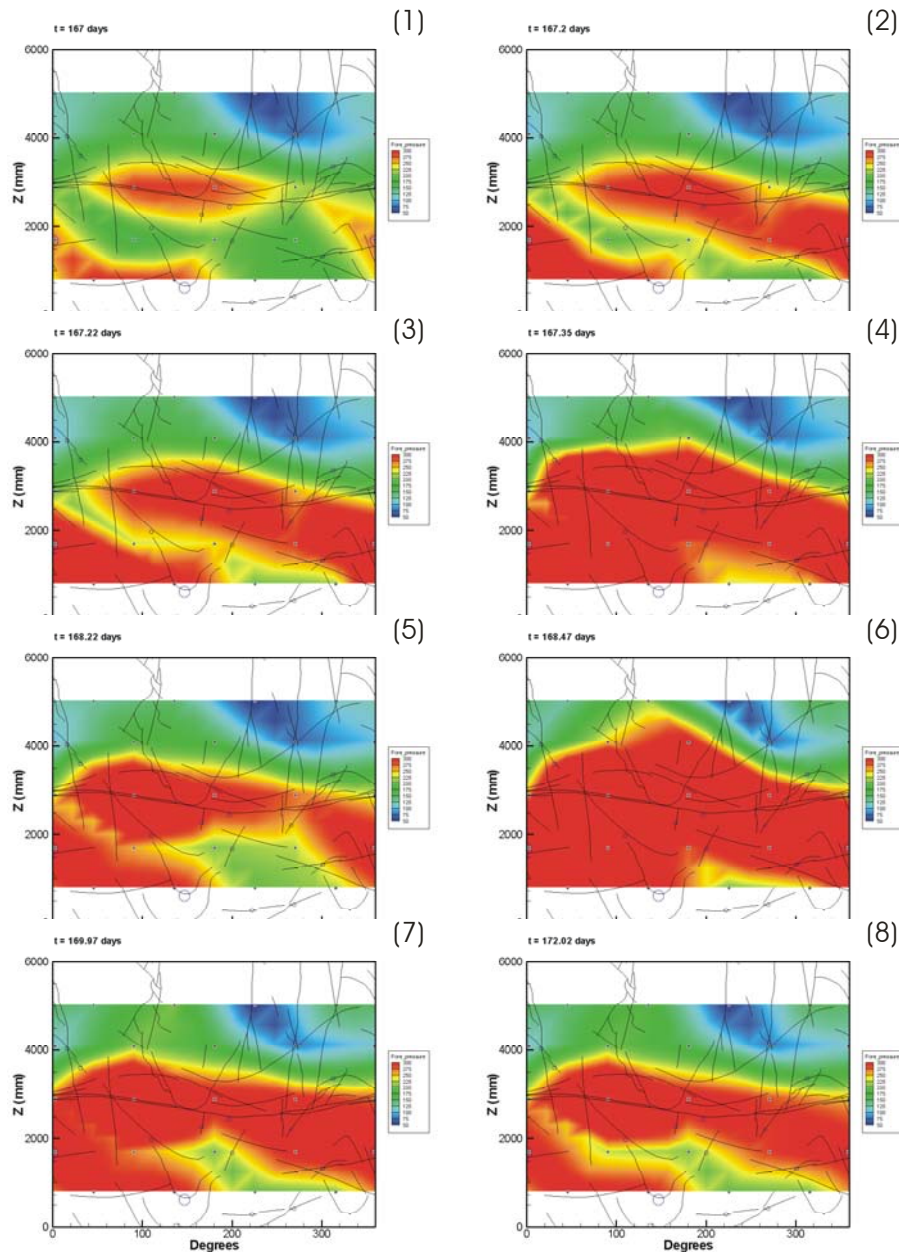


Figure 4-3 Evolution of water pressure at the borehole wall due to hydraulically induced piping during artificial hydration activities. The series of images start at 167 days and finish at 172 days.

At 657 days, after the pressure relief holes had been closed for about 140 days, the pressures on the canister filters and filter mats FR902, FB903, and FB904 were all raised to around 2350 kPa. A six day drop in pressure occurred at 744 days when pump A2 ran out of water. A further drop in pressure occurred at 821 days when the injection pumps were leak tested. Phase 1 of hydration was completed 842 days after the start of the testing.

4.1.2 Filter mats FR901, FR902, FB903 and FB904

Data from the filter mat sensors are shown in Figure 4-4. The erratic output from the transducers during the first 14 days of testing is primarily due to de-airing of the tube work (post-closure of the deposition hole) and the depressurisation of system components in an early attempt to moderate the rapid build-up of porewater pressure which occurred during the early stages of the hydration test. Towards the end of this period the pressure lines from each filter mat were disconnected from the Gas Laboratory where they emerged from the deposition hole, in an attempt to improve discharge rates out of the arrays. As a mechanism for moderating pore pressure build-up, this was unsuccessful and the problem was only solved by drilling the two pressure relief holes described at the start of Section 4.

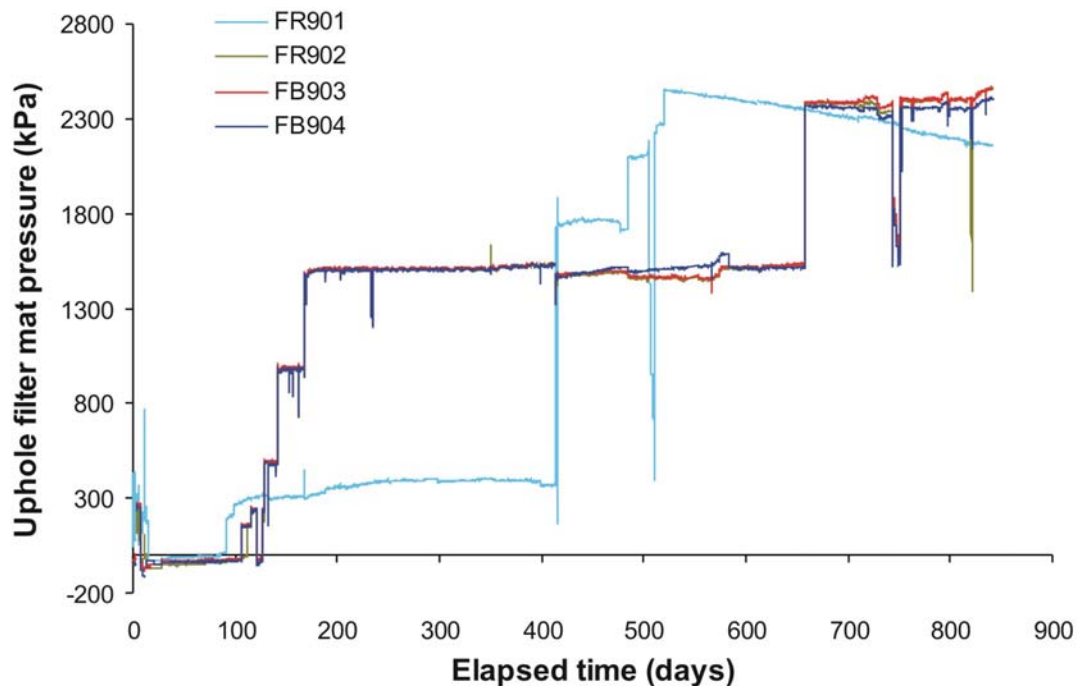


Figure 4-4 Evolution of water pressure in the filter mats located on the borehole wall and within the bentonite blocks. Filter mat FR901 is in direct communication with the drain holes and was therefore allowed to evolve independently from the other filter mats.

The water pressure in the upper filter mat (FR902) located on the rock face and the two filter mats (FB903 and FB904) sandwiched between bentonite blocks C2-C3 and C4-C5 respectively (Figure 4-1), have all been subject to the same artificial pressure history as the canister filters described in Section 4.1.1. The water pressure in the base filter mat FR901 (Figure 4-4) is in direct hydraulic communication with the drain holes and as such has been left to evolve independently from the rest of the system. The rise in pressure of FR901 at 167 days is caused by the “piping” event through the bentonite discussed in Section 4.1.1.

Close inspection of the data from FR901 shows a small but progressive increase in porewater pressure between 200 and 400 days. While the cause of this response is unclear it may indicate some form of time dependent (temporal) evolution in the hydraulic characteristics of the surrounding rock mass. Clogging and associated permeability reduction of fracture pathways may explain this response. It is also interesting to note that the hydrogeological regime in the Assembly Hall area of the HRL appears to have changed during the operation of Lasgit, with fresh discharges observed from previously dormant fractures.

The pressure at FR901 increases abruptly at 415 days when the packers were installed in the pressure relief holes and in a series of further steps as the various packered sections were isolated, reaching a peak of about 2450 kPa at 520 days. After that there has been a steady decline in the pressure. The cause for this behaviour remains unclear but may relate to a regional decline caused by engineering works elsewhere at the Äspö site.

4.1.3 Porewater pressure within the bentonite

Porewater pressure within the bentonite is measured at 6 discrete locations. Figure 4-5 shows spikes in porewater pressure at 128 (UB923), 140 (UB924) and 167 days (UB902). These features were caused by localised channelling through the clay as porewater pressure was increased in the canister filters. It is interesting to note that channelling occurs at multiple locations at different times within the clay rather than being consistently focused in one specific location. The small increase in pressure at 203 days in UB902 corresponds with another attempt to raise water pressure in the artificial hydration system.

Pressures in UB901 and UB902 show a clear effect from the installation of packers in the pressure relief holes with pressures rising steadily from that point on, although UB901 appears to have levelled off after 770 days at about 300 kPa. Pressures in UB923 and UB924 rose steadily from 200 days on with little apparent effect from the changes to the pressure relief holes, though UB923 exhibited a small increase in pressure at around 485 days probably caused by the closure of the packered interval PRH2-2. At about 600 days pressure in UB923 levelled off at about 200 kPa, but pressure in UB924 continued to rise steadily through to 840 days. Pressures in UB925 and UB926 remained largely unchanged until the introduction of packers in the pressure relief holes, which resulted in a small but noticeable increase in the rate of change of pressure in UB925. In contrast, UB926 exhibited little additional pressure sensitivity until around 489 days, when the rate of pressure increase rose, steepening markedly after about 720 days and again at 760 days. The latter date roughly corresponds to the observed levelling seen in UB901 and may indicate a readjustment of the ingress of water in the buffer clay.

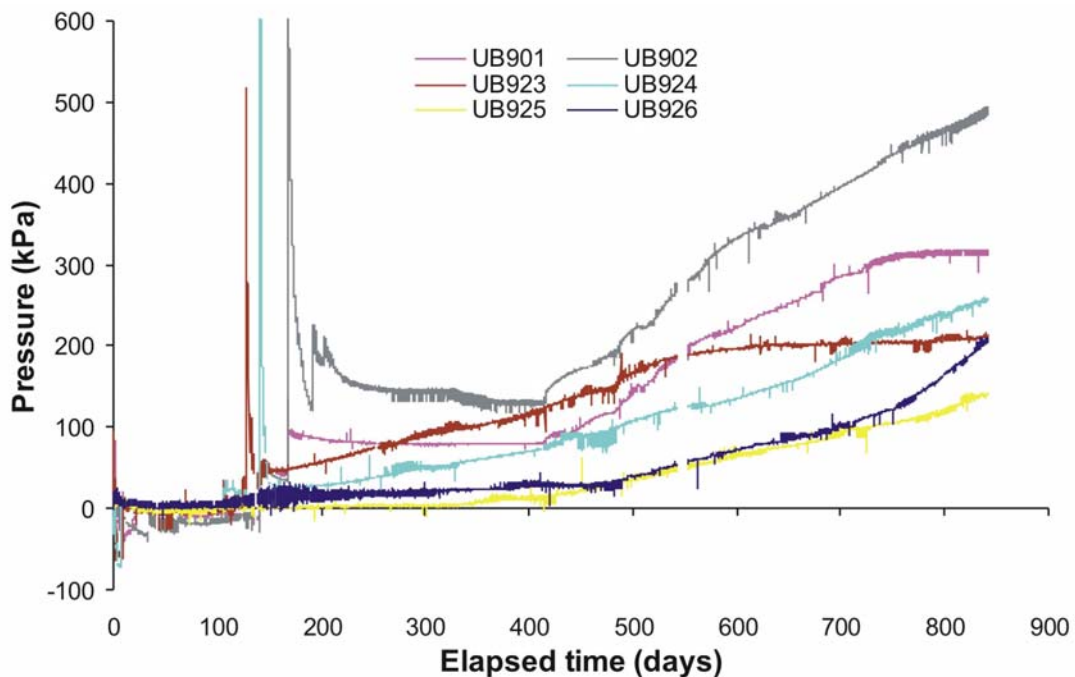


Figure 4-5 Variation in porewater within the bentonite at the 6 monitoring points. The large spikes in the data correspond with attempts to increase porewater pressure within the artificial hydration system early in the test history.

While all porewater pressure sensors are fully operational, the integrated thermocouple within UB924 is not functioning. However, this does not affect the functionality of the test which is performed under isothermal conditions. Thermocouple values from the neighbouring device (UB923) are now used to correct outputs from the affected sensor.

It is clear from the data presented in Figure 4-5 that porewater pressures within the clay remain very low when compared to the *in situ* boundary condition (Section 4.1.5), and that the bentonite remains in a state of hydraulic disequilibrium. This is an important observation when interpreting the subsequent hydraulic and gas test phases.

4.1.4 Porewater pressure measured at the rock wall (UR903 to UR922)

Porewater pressure is measured at 20 separate locations on the borehole surface and the data are shown in Figure 4-6. Once the pressure relief holes were drilled in the surrounding rock mass, the pressure in the deposition hole stabilised and local increases in porewater pressure at 141, 167, 168 and 203 days were caused by the movement of water along temporary channels when water pressure in the filter assemblies was increased (Figure 4-2). These pathways appear to be ephemeral features which seal when the water pressure is allowed to decay. It is interesting to note that many of the sensors actually exhibit a similar progressive increase in value with time as that observed by FR901. Analysis of the spatial and temporal increases in porewater pressure may provide an insight into the possible changes in the hydraulic boundary condition suggested in Section 4.1.1.

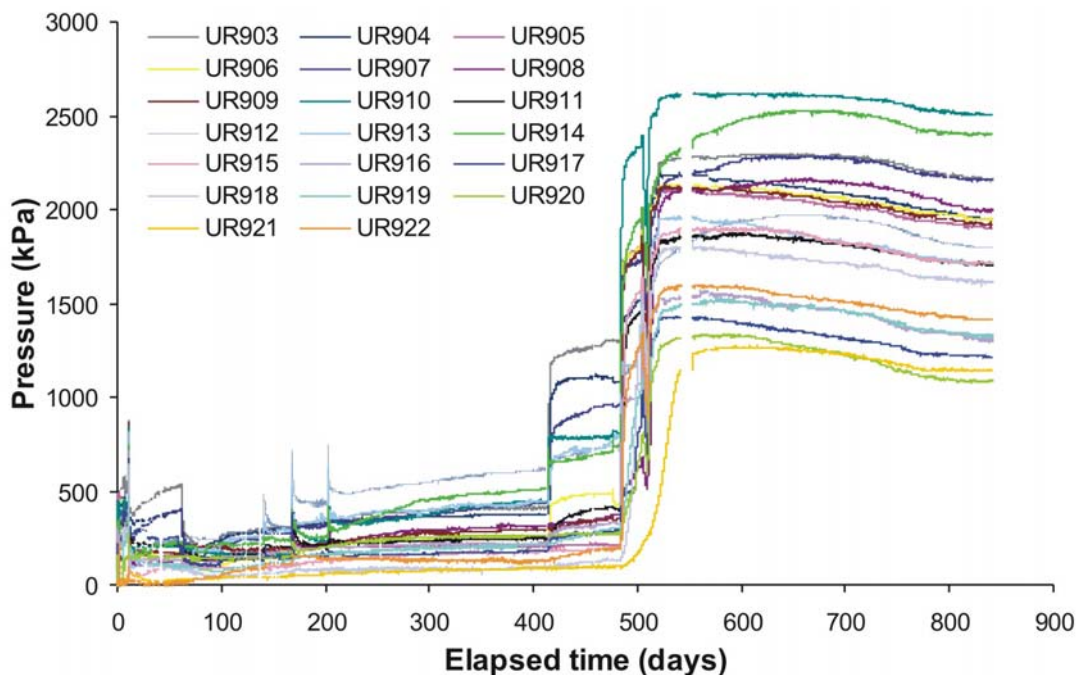


Figure 4-6 Variation in porewater pressure with time measured at the rock face. The spikes in the data from 141 days to 203 days correlate with attempts to increase porewater pressure in the artificial hydration system. The rapid increase in pressure from around 415 days relate to changes in the boundary condition during the installation of packers in PRH1 and 2 and their subsequent closure.

The intensity plots (Figure 4-7) show the spatial and temporal evolution in porewater pressure measured at the interface between the rock wall and the bentonite from 130 to 272 days. Examination of the initial data, images [1] and [2], clearly shows a zone of elevated porewater extending from the base of the plot diagonally upwards from left to right. The “pulses” in high

water pressure, images [3] and [5], stem from a number of attempts to raise porewater pressure in the artificial hydration system resulting in piping of water through the buffer. The pressure in these regions quickly decays with time, images [4] and [6] respectively, indicating that these pressure-induced pathways are no longer conductive. As hydration progresses, a small increase in porewater pressure can be observed left of centre in plots [7] and [8]. The origin for this expanding zone of porewater pressure is unclear but may relate to the suggested evolution in the near-field hydrogeological behaviour discussed earlier.

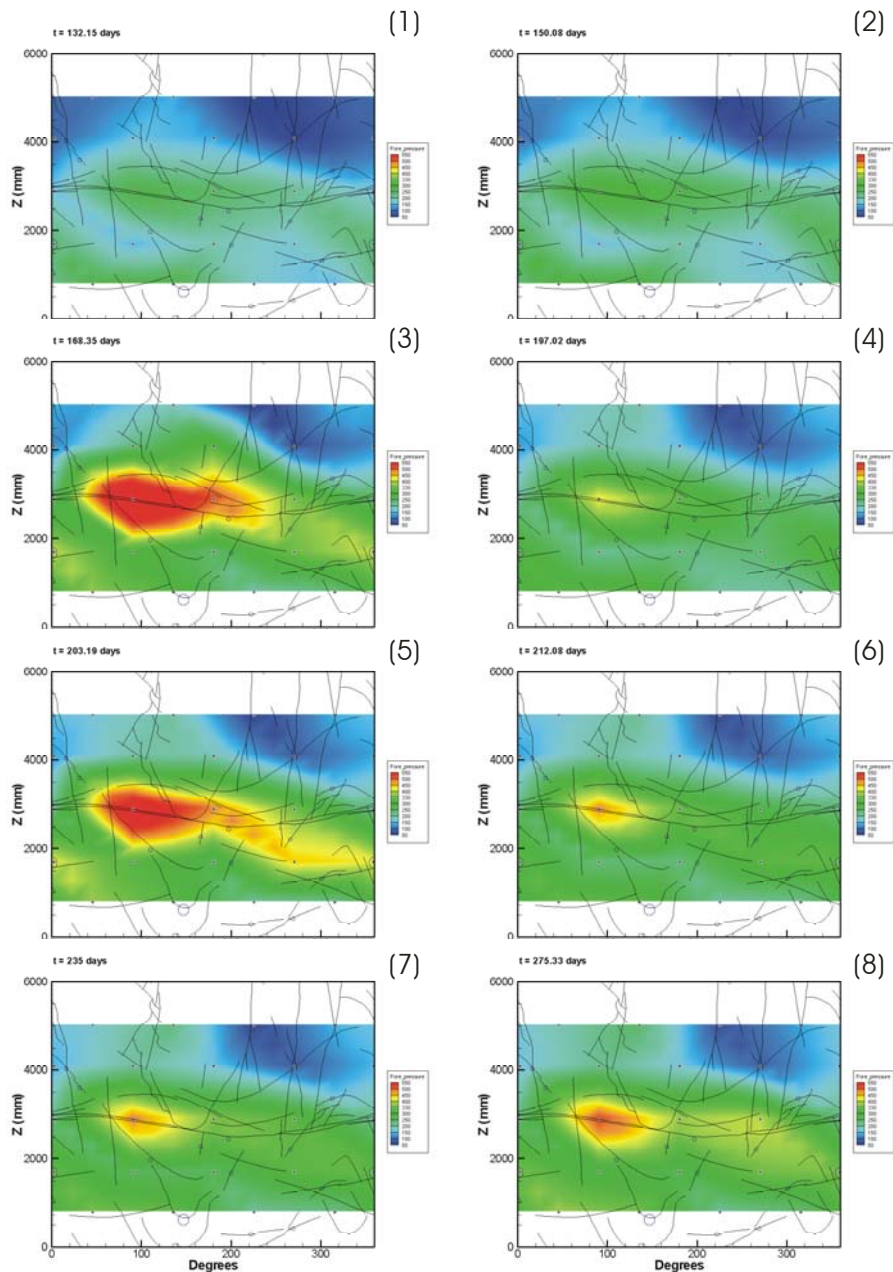


Figure 4-7 Evolution in porewater pressure measured at the interface between the rock wall and the bentonite from 132 to 275 days. The series of images show a general increase in porewater pressure. The high pressure zones in images (3) and (5) relate to piping events during artificial hydration activities.

In the intensity plots of Figure 4-8 the changes of pore pressure during the closure of the pressure relief hole packers can be traced. Comparing images [1] and [2] shows that the introduction of the packers raised pressures at the base of the hole sharply. Then, as the packer sections were

closed the zone of highest pressures migrated to an area around 270 degrees and 2 m up from the base of the hole (note the changes in the colour scale between [2] and [3]). Following the completion of the changes in the pressure relief holes there has been a gradual reduction in the overall levels of the pore pressures, which is also seen in Figure 4-6, with little change in the pattern of pressure variations.

Close inspection of the data in Figure 4-6 indicates a reduction in the rate of pressure decay in a number of porewater pressure sensors at around 775 days. Indeed, a number of sensors (907, 910, 911, 912, 913, 914, 915, 917, 919, 920, 921 and 922) appear to level at around 818 days. However, porewater pressures in the lower sections of the borehole continue to exhibit a general trend of reducing porewater pressure. As in Section 4.1.2 (FR901) the cause for this behaviour remains unclear.

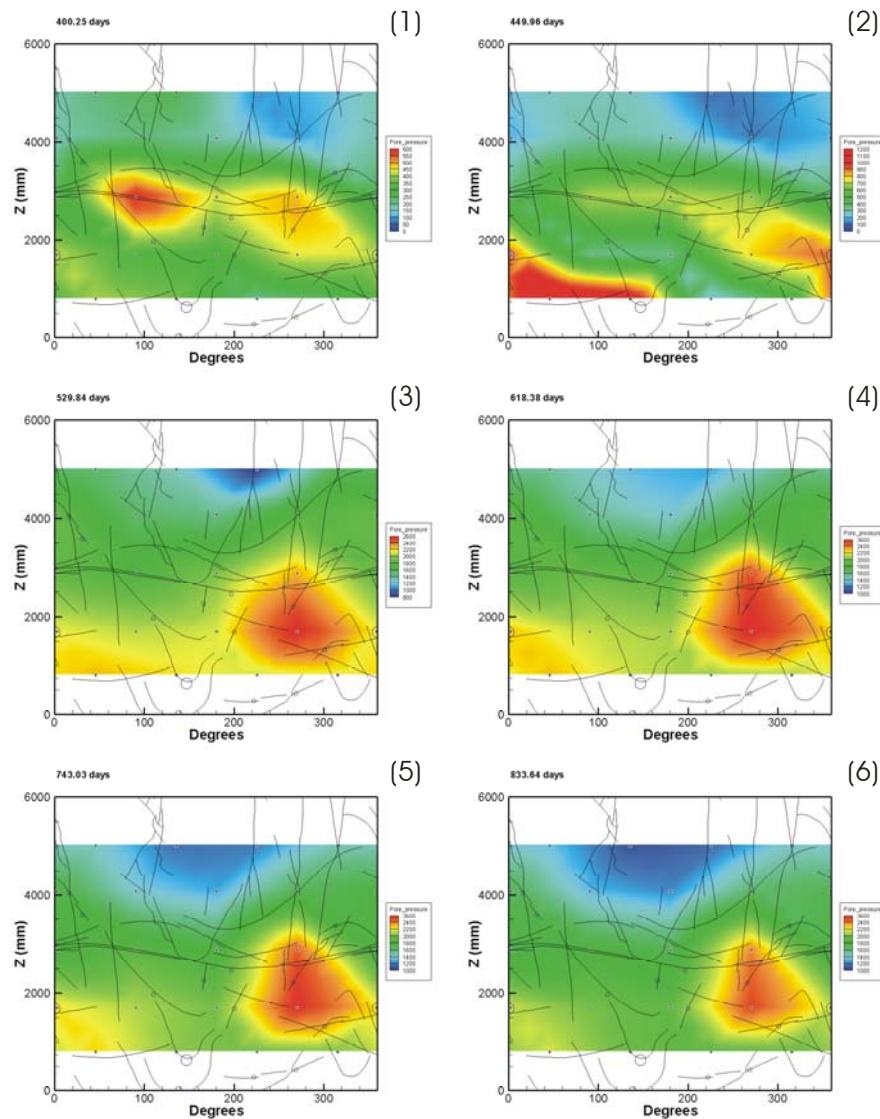


Figure 4-8 Evolution of pore pressure at the deposition hole wall from 400 to 840 days.

4.1.5 Porewater pressure in the pressure relief holes

Pressure data from the individual packered sections of the two pressure relief boreholes are shown in Figure 4-9. After the packers have been inflated and the sections isolated the pressures form a pattern that is maintained through the rest of the test, but with the overall magnitude of the pressures declining gradually with time. Section PRH1-1 has the highest pressure at 2540

kPa on day 525 and declining to 2230 kPa. Section PRH2-1 is next highest with a pressure of 2360 kPa on day 525, declining to 2130 kPa. The five sections PRH1-2, PRH1-3, PRH2-2, PRH2-3, and PRH2-4 all plot together with pressures of about 2070 kPa on day 525, declining to about 1830 kPa. Section PRH1-4 reaches a pressure of 1550 kPa on day 525 and declines to 1300 kPa. The lowest pressures are found in section PRH1-5 which reaches about 1255 kPa on day 525, rises slightly to about 1290 kPa on day 590 and then declines to about 1050 kPa.

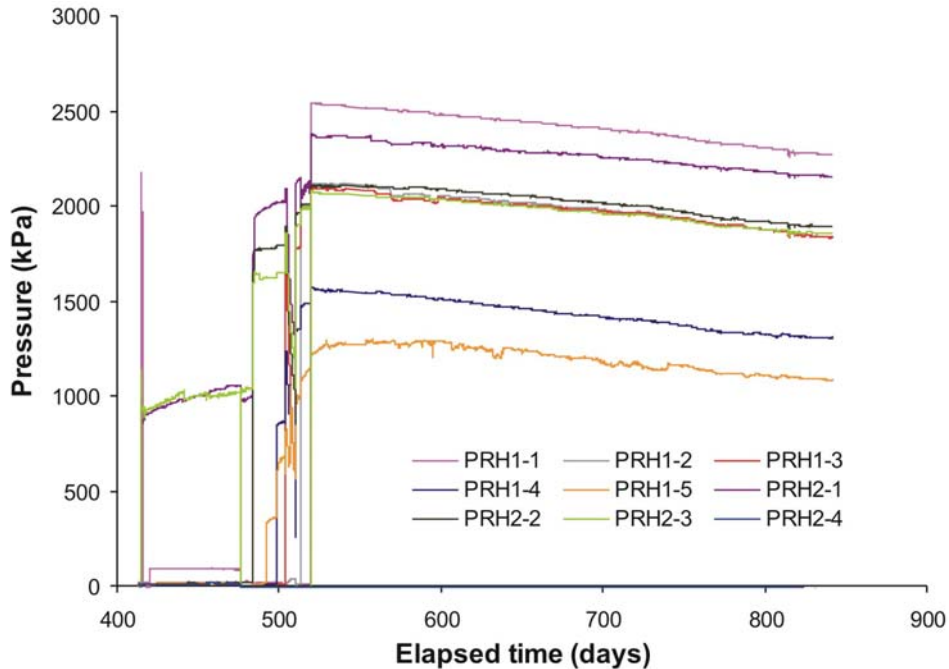


Figure 4-9 Porewater pressures measured in the packed sections of the pressure relief boreholes.

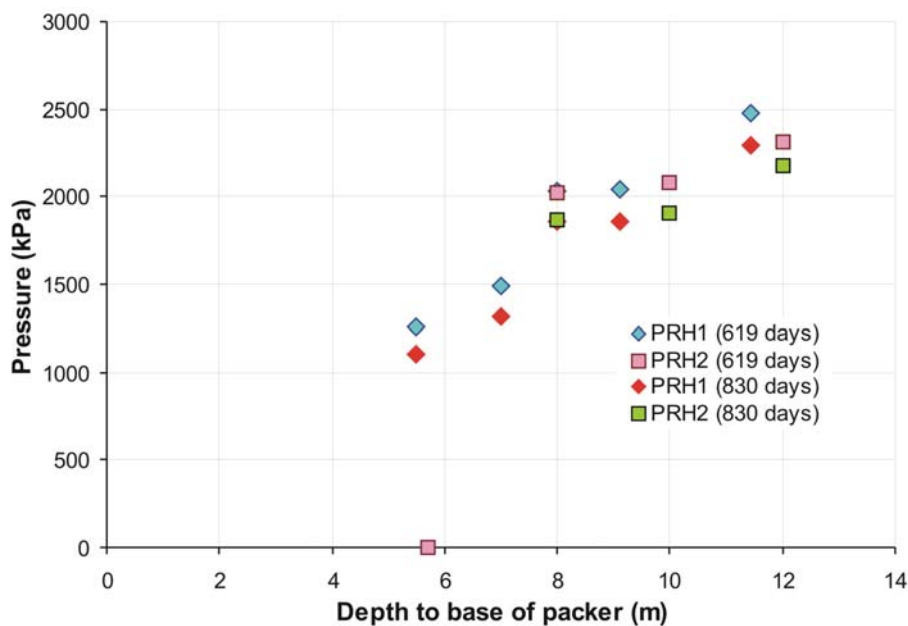


Figure 4-10 Evolution of pressure in packed intervals within PRH1 and PRH2.

Close inspection of the PRH transducer outputs exhibit qualitatively similar responses for most devices to those observed by the porewater pressure sensors mounted on the rock wall (Section

4.1.4) at around 775 and 816 days. This indicates that the hydraulic boundary conditions around the Lasgit borehole have evolved during the test. This behaviour could be related to periodic construction work related to the commissioning and decommissioning of new tests at the Äspö site. While no such activities could be identified for the event at 775 days, the change in porewater pressures observed at 816 days correlates with over-coring activities of the LTDE project which is located in a niche just above the Lasgit test site.

A cross-plot of the porewater pressure against depth to base of each packered interval for both PRH's (Figure 4-10), indicates a fairly linear trend with pressure decreasing towards the gallery floor. The data clearly demonstrates the decreasing trend in local porewater pressure with time, strongly indicating some form of temporal evolution in the local hydrogeological boundary condition.

4.2 EVOLUTION OF TOTAL STRESS

Total stress within the Lasgit system is measured at 32 locations within the borehole. Sensors mounted on the canister, rock wall and within the clay can be used to determine both the axial and radial components of stress and the distribution of values throughout the borehole

4.2.1 Radial stress measured at the rock wall (PR903 to PR922)

Data from total pressure sensors PR903 to PR922 are plotted in Figure 4-11. As in previous sections, the small increases in radial stress at 141, 167, 168 and 203 days are all caused by localised piping events when water pressure in the canister filters and hydration mats were increased, resulting in hydraulic flow through/across the bentonite. These events are generally short-lived with the radial stress traces returning to their predicted trend-lines within a few days. The absence of any lasting effects supports the results presented in Harrington and Horseman (2003) examining the validity of the effective stress law. In the absence of piping events the rate at which radial stress increases within the deposition hole is insensitive to the absolute value of porewater pressure applied to the filter assemblies. This confirms the predictive modelling work described in Section 3.

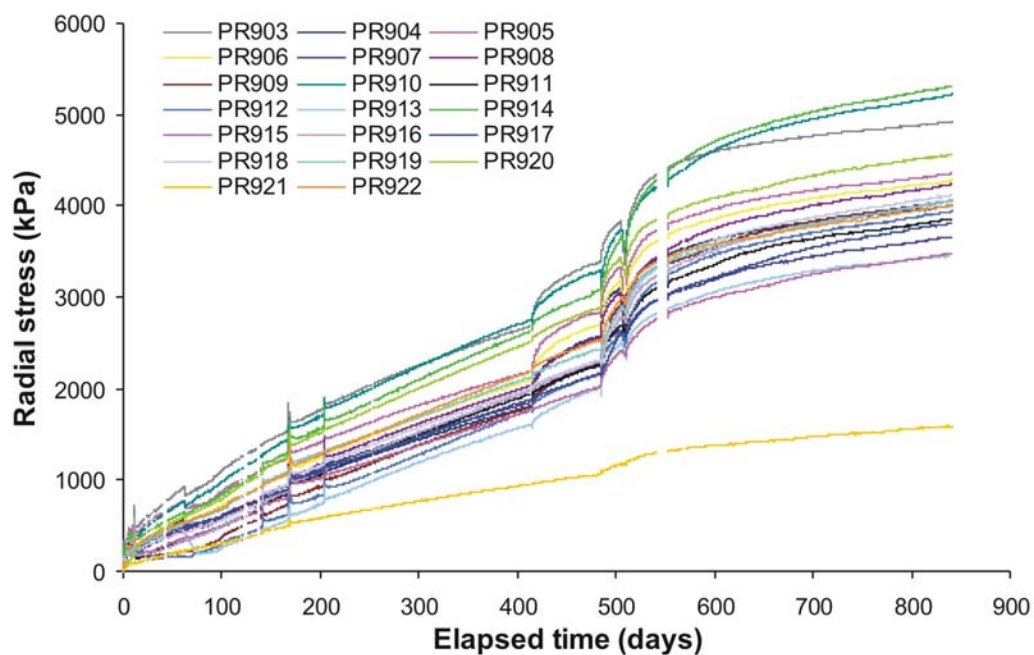


Figure 4-11 Variation in radial stress with time. In the absence of preferential flow (piping), the rate at which total stress increases is insensitive to the absolute value of porewater pressure applied to the filters.

The intensity plots (Figure 4-12) show the spatial and temporal evolution in radial stress measured around the canister between the rock wall and the bentonite from 75 to 272 days.

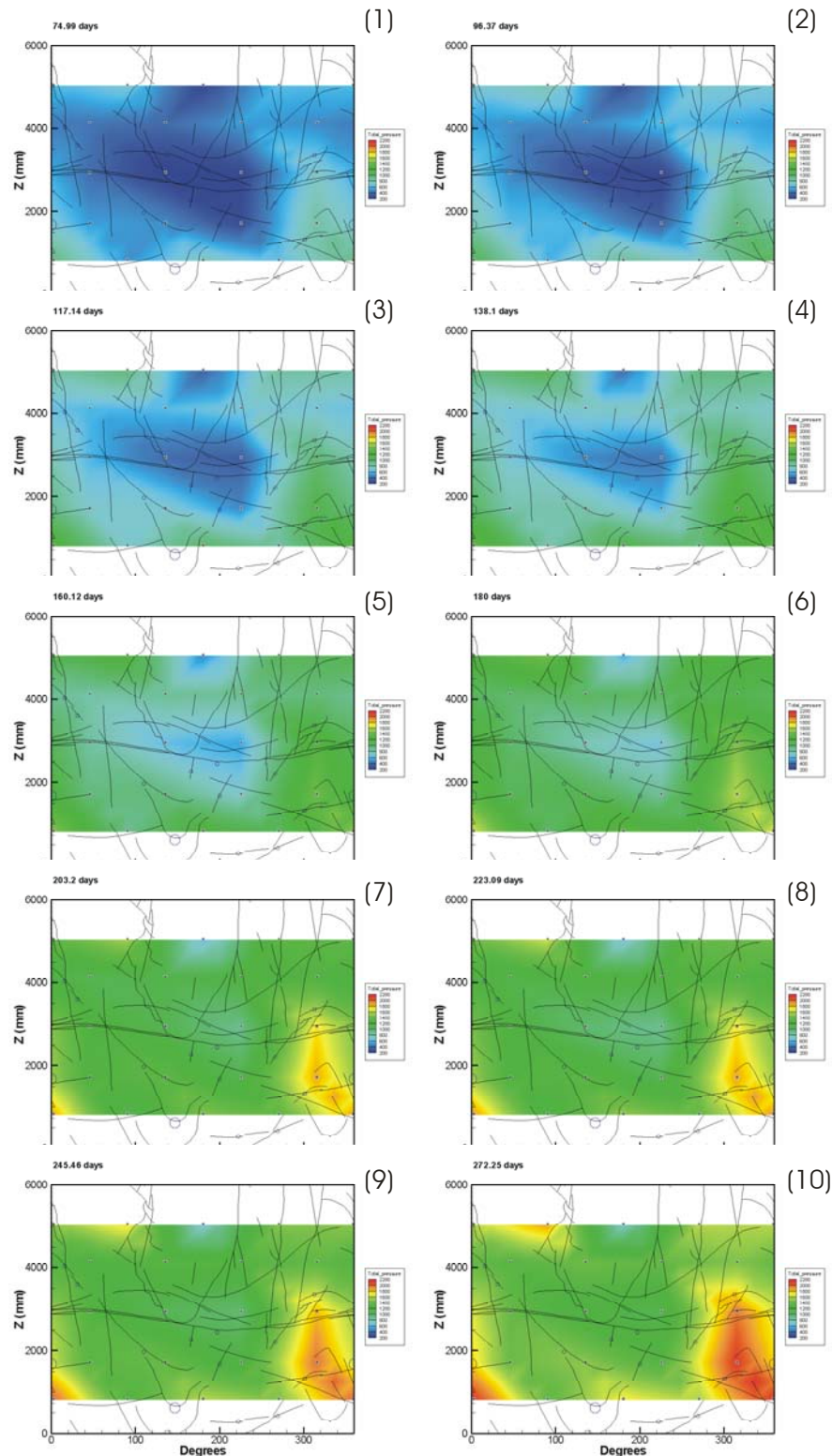


Figure 4-12 Evolution in radial stress around the deposition hole wall from 75 to 272 days. From image [5] onwards a narrow zone of high pressure can be seen propagating upwards.

Inspection of the data clearly shows a narrow zone of elevated stress propagating vertically upwards to around 3.5m by an elapsed time of 270 days. This zone appears to be expanding as the test progresses. At this stage of the hydration history, the remaining buffer exhibits a fairly uniform distribution in stress with the exception of the upper zone, at around 5m, which has

somewhat larger variations in stress. This could be explained by the close proximity of the large filter mat located between blocks C2 and C3 causing preferential swelling of the clay.

Comparison of the images in Figure 4-7 [8] and Figure 4-12 [10] shows a rather poor correlation between pore pressure and radial stress at a similar point in time. Given the quasi-static nature of the boundary condition, it is unclear what mechanism is directly responsible for the preferential swelling of the clay observed propagating upwards from the base of the borehole.

The intensity plots in Figure 4-13 show that the pattern of stress around the deposition hole wall does not change greatly through the installation of packers into the pressure relief holes except for a general rise in stress levels, which is also apparent in Figure 4-11.

It is also apparent from Figure 4-11 and the intensity plots of Figure 4-13 that the readings from sensor PR921 are anomalously low compared to those from all other sensors. The reason for this behaviour is not known at present.

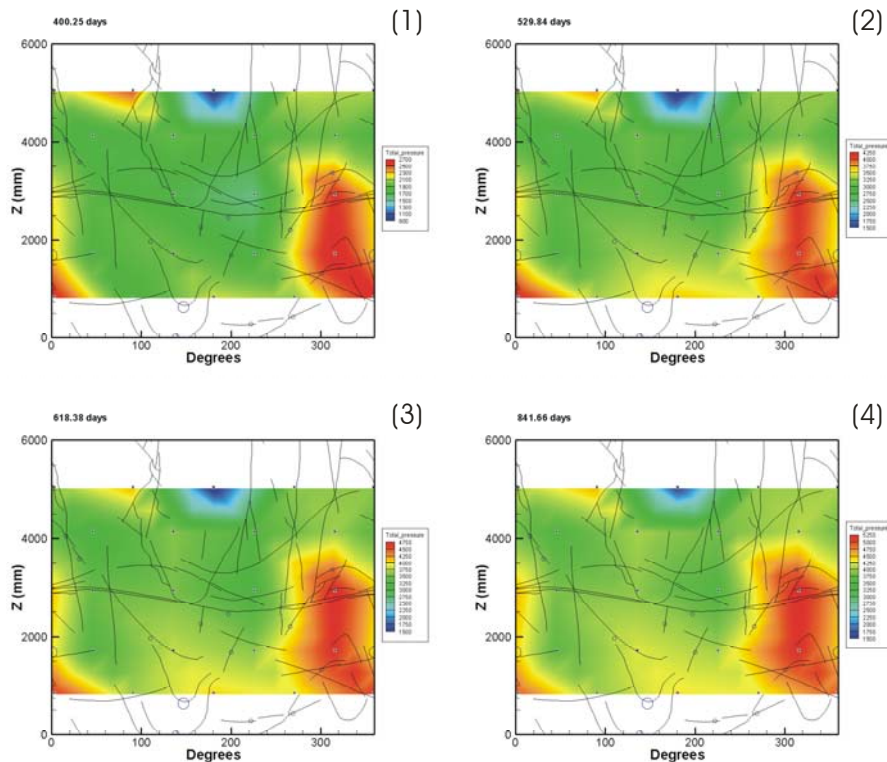


Figure 4-13 Evolution of radial stress around the deposition hole wall from 400 to 840 days.

4.2.2 Net horizontal stress

It is apparent from the intensity plots of Figure 4-12 and Figure 4-13 that high radial stresses are concentrated along the part of the deposition hole wall that is at about 300° and that stress varies mainly with angular position rather than with depth. To examine this in more detail the data were divided into 16 angular strips and the stress values averaged over depth. This gives a set of pressures that can be represented as vectors in the horizontal plane as shown in Figure 4-14. Since these pressures act upon equal area segments of the hole wall they can be added vectorially to give a net horizontal force acting on the hole. The data from PR903 to PR922 have been used to generate this net force vector throughout the hydration phase of the project. Its magnitude as a function of time is plotted in Figure 4-15 and its locus in the horizontal plane is shown in Figure 4-16.

It can be seen in Figure 4-15 that the magnitude of the net force had levelled off by about the time that packers were installed into the pressure relief holes. During the installation of the packers there were some significant adjustments to the net stress and afterwards the net stress

increased more rapidly. This has now almost levelled off again, but there is no sign yet of it reducing, as would be expected of the system as it approaches an equilibrium state.

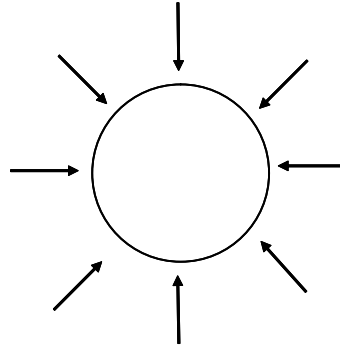


Figure 4-14 Depth averaged radial stresses represented as vectors in the horizontal plane.

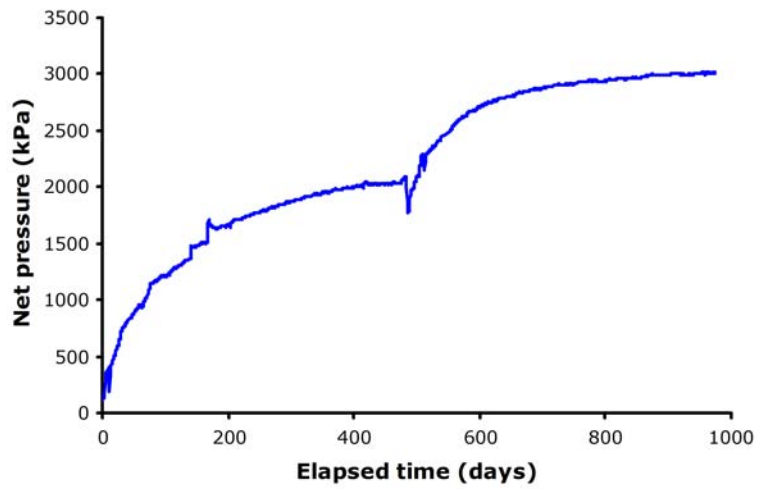


Figure 4-15 Evolution of the magnitude of the net horizontal stress with time during the hydration phase.

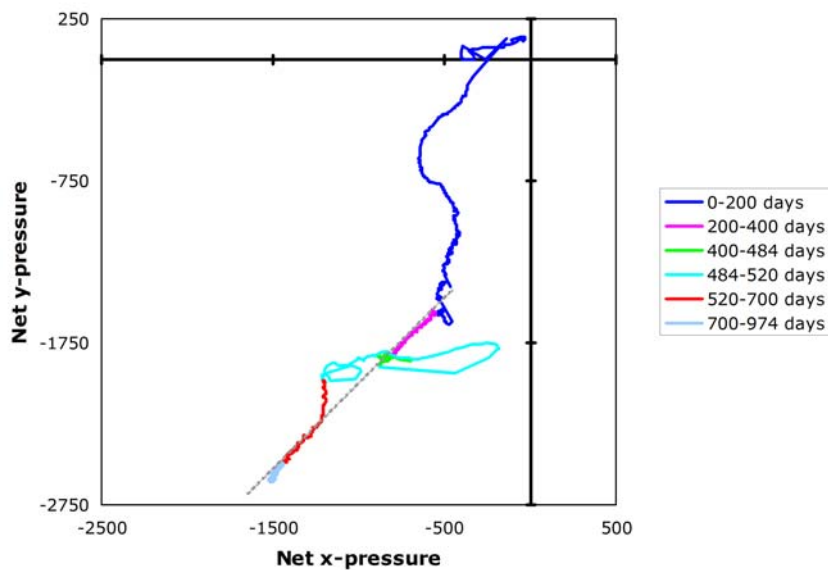


Figure 4-16 Evolution of the locus of the net horizontal stress with time during the hydration phase.

Similarly, the locus plot in Figure 4-16 shows a fairly erratic path during the first 200 days of hydration but then settling to an almost linear path between 200 and 400 days. The packer installation is shown as a further period of erratic change in the net pressure locus but following that the path returns to the same line that it was following during the period from 200 to 400 days. The rate of movement has greatly slowed during the last 300 days but there is clearly no indication of a return to the origin for an equilibrium state.

4.2.3 Radial and axial stress on the canister (PC901 to PC903)

Axial and radial stress around the canister has increased steadily during the course of the hydration history (Figure 4-17). At an elapsed time of 878 days radial stress on the canister surface ranged from 4620 kPa to 4810 kPa. The radial stress monitored by PC903 increased at 167 and 203 days (due to piping) attaining a value close to that of the artificially applied porewater pressure. This indicates that device PC903 is in good calibration and operating correctly. Spontaneous increases in pressure for all sensors correlate with the experimental activities discussed in Section 4.1.1.

At 878 days axial stress acting on the base of the canister (monitored by PC901) was 3810 kPa. This value is relatively low when compared to the equivalent outputs from axial stress sensors located within the bentonite above the canister (Section 4.2.4) and the Glotzls cells (Section 4.3) located on three of the rock anchors. This suggests that a poor contact probably exists between the face of the stress sensor and the clay, indicating that the clay in this region of the system is poorly hydrated.

In the absence of pathway flow the rate at which stress around the canister increases is insensitive to the absolute value of porewater pressure applied to the filter assemblies. A similar result was observed for the development of radial stress at the rock wall (Section 4.2.1).

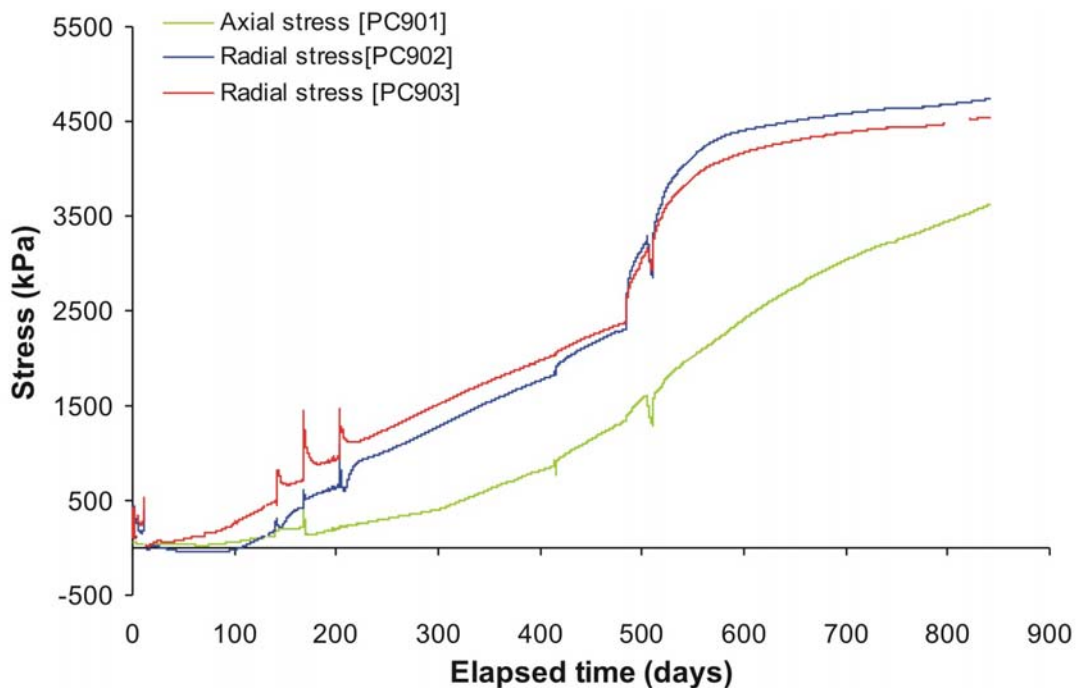


Figure 4-17 Development of axial and radial pressure on the side and base of canister.

Analysis of the stress data in Figure 4-17 also indicates a small inflection at around 775 days, with the rate of stress increase rising marginally after this time. This observation correlates with the previous responses noted in Sections 4.1.4 and 4.1.5.

4.2.4 Axial stress within the bentonite (PB901, PB902, and PB923 to PB929)

Data from the axial stress sensors is shown in Figure 4-18. The variability in axial stress within the bentonite was considerable during the first 200 days, but significantly reduced during the next 200 days, with all sensors (except PB901 which is located directly under the canister) ranging from 2770 to 3560 kPa at an elapsed time of 400 days. Following installation of the packers in the pressure relief holes, however, the variability has increased again to some degree with values ranging from 4740 to 5910 kPa at 841 days.

Outputs from these devices generally demonstrate only a minor sensitivity to changes in porewater pressure. These events often correlate with other experimental activities such as changes in artificial hydration pressure or drilling and abstraction of groundwater from the pressure relief holes. In general, the rate at which axial stress increases within the clay seems fairly insensitive to the absolute value of water pressure applied to the canister and hydration filters.

The intensity plots shown in Figure 4-19 have been constructed using the axial stress data from all sensors, except PB901. The plot clearly shows the development of non-uniform axial stresses across the major axis of the emplacement hole, which may help to explain the minor differences in lid displacement observed in Section 4.4. Since the completion of packer installation in the pressure relief holes the general distribution of axial stress has been relatively stable (images [3] to [6]) with just a gradual extension of the high pressure zone about PB928 towards the centre of the section.

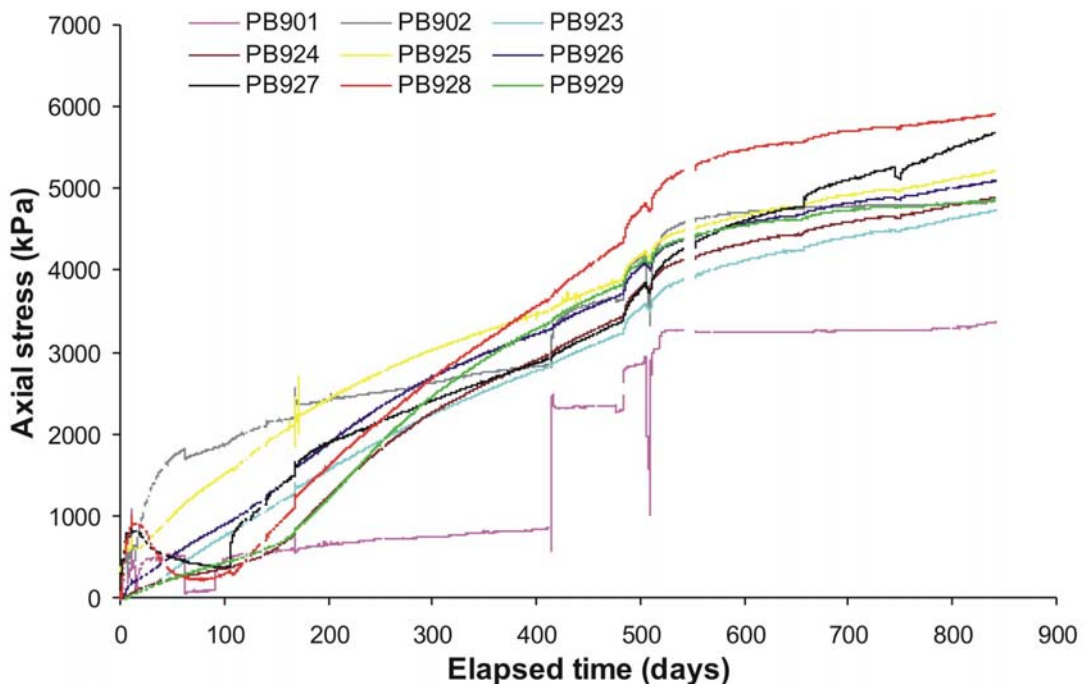


Figure 4-18 Development of axial stress measured at 12 locations within the buffer.

Both stress sensors located in the base of the deposition hole (PB901 and PB902) exhibit a small but noticeable increase in the rate of pressure rise at around 775 days. This affect is most pronounced in PB901 which is located directly beneath the canister. This observation correlates with previous data from the porewater pressure sensors mounted on the rock wall and would suggest that the hydrogeological boundary condition changes at this time, with the effect most pronounced in the base of the deposition hole.

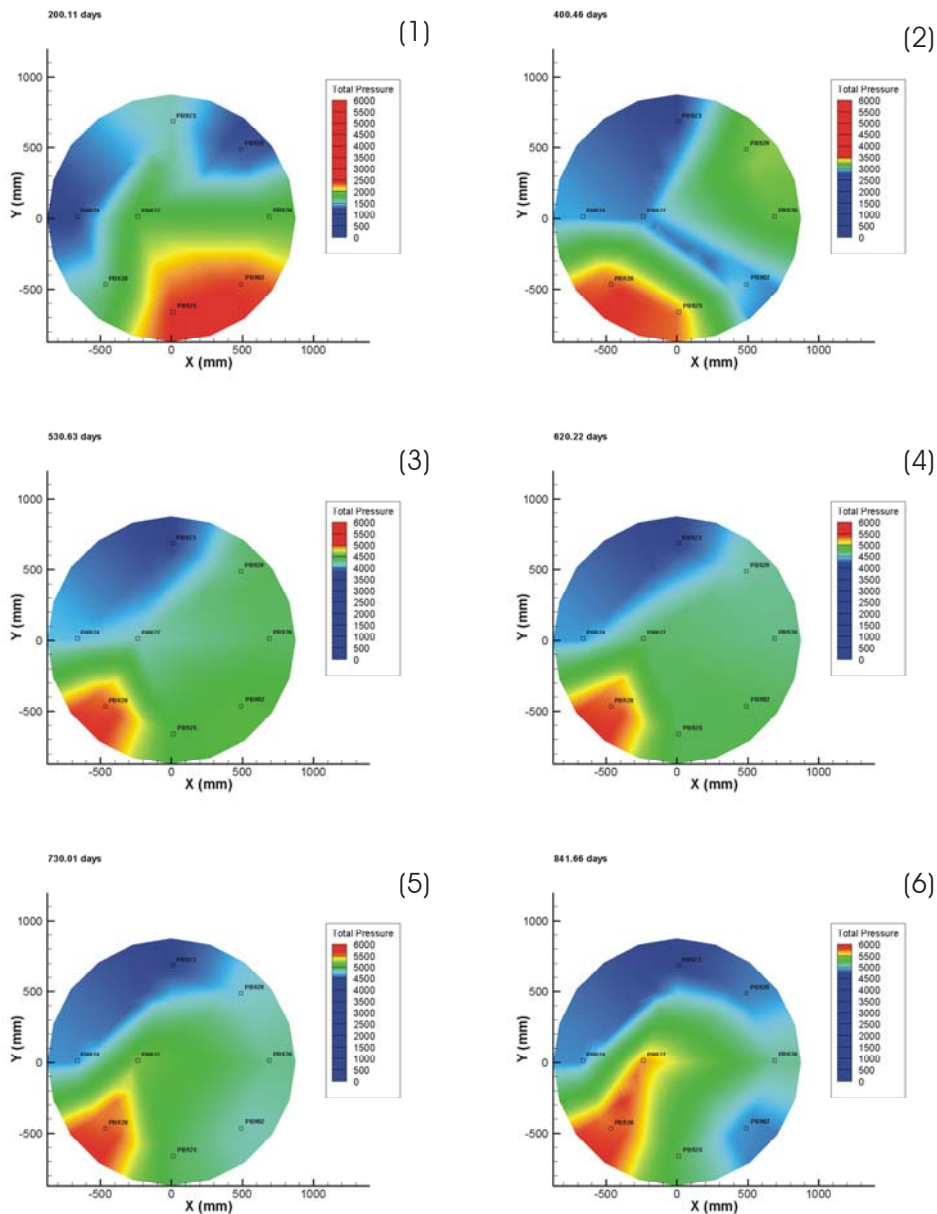


Figure 4-19 Intensity plots showing the distribution of axial stress across the borehole from day 200 to 847. The range of colour variations has been adjusted to the range of stress values in each plot to highlight the variation over the section.

4.3 EVOLUTION OF WATER CONTENT IN THE BENTONITE BUFFER

Figure 4-20 shows the suction pressures recorded at the seven psychrometers WB901 to WB907 embedded at locations within the bentonite buffer as shown in Figure 4-1 (see also Table 2-6). It can be seen that suction at each location is declining, confirming that resaturation is progressing, although the rate of hydration does appear to be slowing. Greatest progress has been made near the filter mats above the canister whilst the least progress occurs just below the canister. There is no data available yet from WB903. While a number of psychrometers appear to be levelling (e.g. WB902), close inspection of the data reveals a steady downward trend.

It is anticipated that when the buffer bentonite is in hydraulic equilibrium, psychrometer values will plateau at a finite (positive) suction, caused by the natural salinity of the Äspö groundwater. However, the data in Figure 4-20 clearly shows that most, if not all of the clay, remains in a state of suction. It is important to remember that clay can be in suction even when fully saturated.

Ideally, in relation to future testing, the clay should be in a state of hydraulic equilibrium, otherwise, the suction introduces an unknown variable in the interpretation of the results.

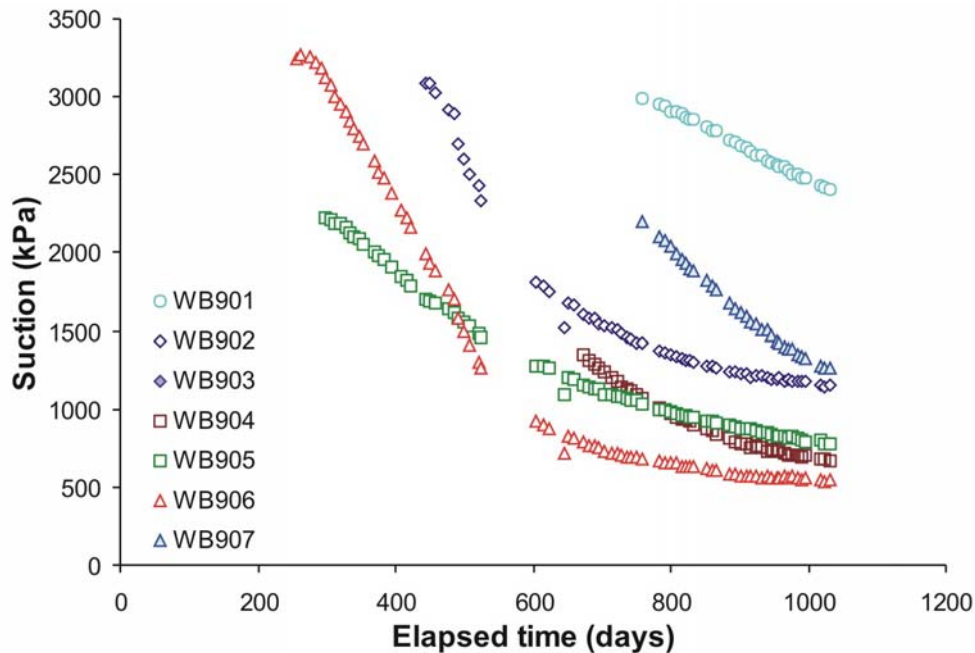


Figure 4-20 Suction pressures recorded at sensors WB901 to WB907 for the entire test.

4.4 AXIAL FORCE ACTING ON THE STEEL LID

Figure 4-21 shows a plot of the axial force (measured by the Glotzl cells) applied by the lid to the concrete plug and bentonite column. The initial reduction in the axial force can be explained by a time dependent relaxation of forces due to compression of the bentonite blocks and the engineering void space. Differences in sensor output can be explained by minor errors in the factory calibration of each device (i.e. <0.4% FSR).

From around 40 days (LP902) and 80 days (LP901/903) the load cells begin to exhibit a positive gradient, suggesting that the continuum axial swelling pressure within the bentonite is greater than the initial pre-stress applied by the lid. From approximately 220 days onwards, all three load cells show a small but progressive reduction in force. This can be explained by convexing deformation of the steel lid in response to the large axial forces developed in the system as the bentonite continues to swell. This hypothesis is supported by the strain data presented in Section 4.5.

Following packer installation the forces on sensors LP901 and LP902 started to increase steadily, with a slight steepening of gradient at about 755 days. The force on sensor LP902 also increased initially but then levelled off at about 600 days until 755 days when the force began to rise again. This would suggest uneven loading of the lid which is in line with the axial stress data presented in Section 4.2.4. From 755 days onward the forces at LP901 and LP903 are equal whilst LP902 has maintained an excess of 170 kN over them.

The data in Figure 4-21 clearly shows that axial forces within the deposition hole continue to evolve with time. At present, there is no sign based on the output from the Glotzl load cells that any of the sensors will imminently asymptote at a finite value in the near future.

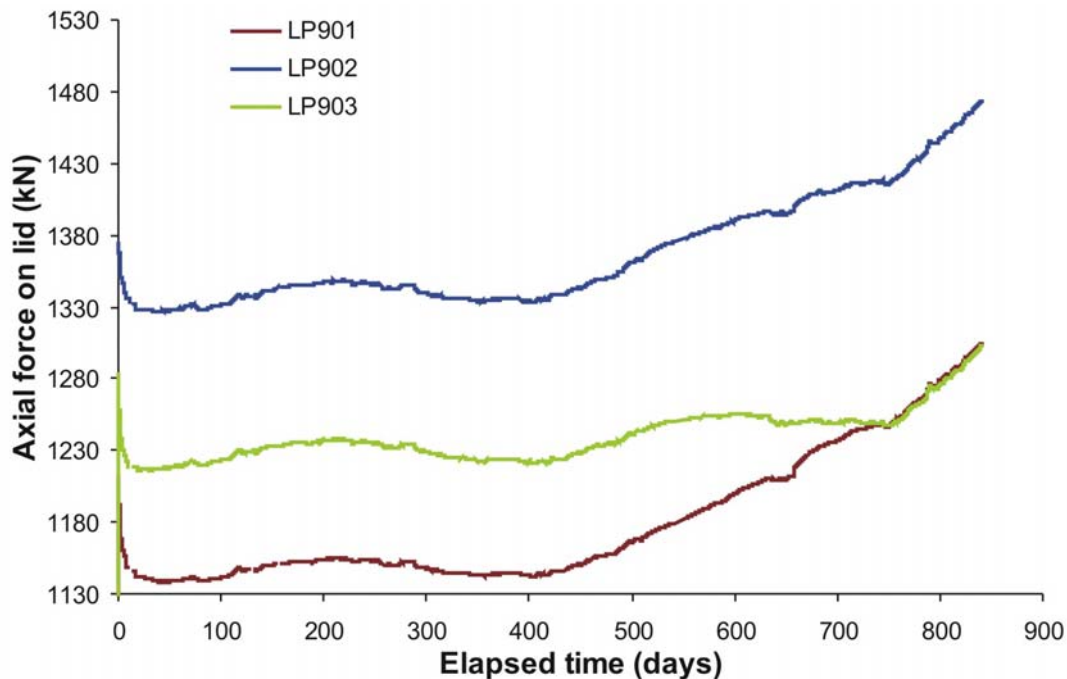


Figure 4-21 Axial force acting on steel lid measured by 3 load cells attached to separate rock anchors.

4.5 DISPLACEMENT OF LID AND CANISTER

Data from sensors DP901 to DP905 is plotted in Figure 4-22. Sensors DP902-905 continuously monitor movement of the steel lid relative to both the gallery floor and ceiling whilst DP901, attached between the Monel pipe and lid, detects relative changes in canister position. Post closure of the deposition hole, sensors DP902 to DP904 exhibit a negative transient signifying a fairly uniform drop in lid height with respect to the gallery floor. This can be explained by the relaxation in the initial pre-stressing applied to the lid (Section 4.4). Comparison of the data from Figure 4-22 with that in Figure 4-2, suggests movements of the lid are insensitive to changes in the porewater pressure applied to the filter arrays. In contrast, displacement of the canister appears highly sensitive to changes in porewater pressure. Examination of the data clearly shows that after the first 16 days of testing where porewater pressures varied considerably, the canister moves progressively upwards associated with preferential hydration of bentonite around the base of the deposition hole. This trend continues until the first pressure relief hole is drilled at 62 days, at which point the canister reverses direction and moves slightly downwards away from the lid. This is probably due to the reduction in porewater pressure within the Lasgit borehole. A second upward trend is then observed at around 91 days corresponding to the removal of the submersible pumps from both pressure relief holes.

In general, once artificial hydration begins at 106 days, the canister reverses direction moving away from the lid as hydration preferentially occurs above the canister through the large filter mats FB903/4. At an elapsed time of 415 days, at the initial installation of packers into the pressure relief holes, the canister resumed an upward movement which continued, with minor interruption around 500 days during packer inflation, until about 660 days when the direction of motion was reversed again. By 880 days the canister displacement is at -1.58 mm.

Analysis of the lid displacement data shows a general progressive drop in lid height, relative to the gallery floor, ranging from -0.12 mm to -0.17 mm at 400 days. The data from DP902 to DP904 would seem to suggest a slight distortion of the lid may have occurred as it deformed to accommodate the uneven distribution in axial stress shown in Figure 4-19.

At 189 days, the original DP905 sensor was replaced with a new measurement system which included a high resolution displacement transducer. The device clearly shows a small but

progressive uplift of the steel lid relative to the gallery roof, supporting the hypothesis of convex deformation presented in Section 4.4. This type of deformation could also help to explain the minor drop in axial force observed by LP901 to LP903 from around 220 days onwards (Figure 4-21).

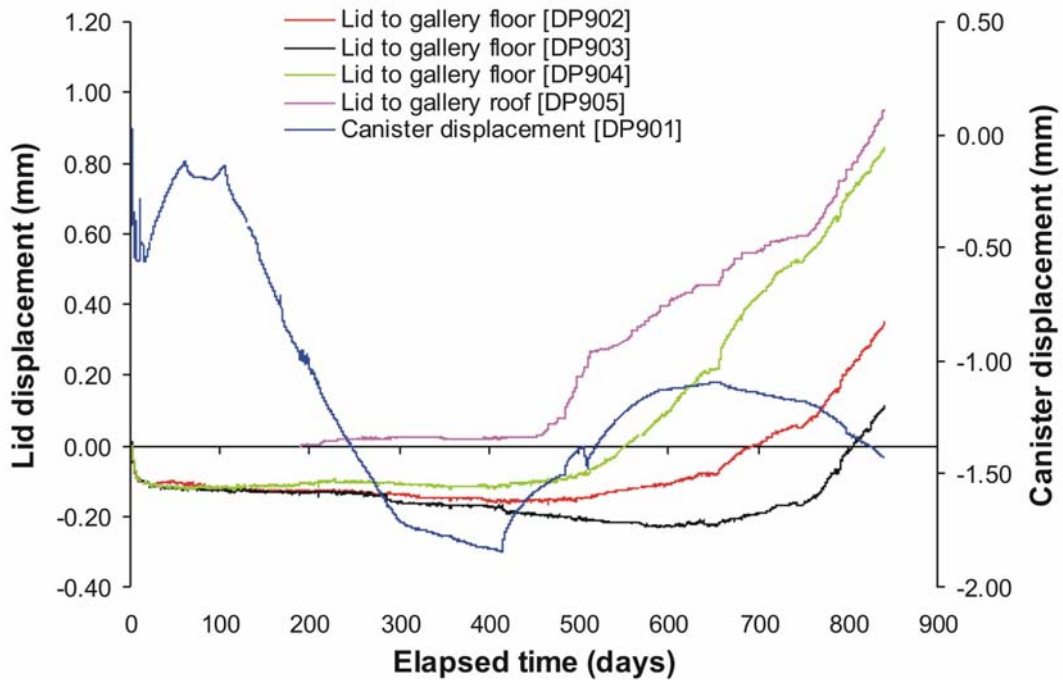


Figure 4-22 Linear displacement of the steel lid and copper canister. Movements of the lid are measured relative to both the gallery floor and ceiling. Movements of the canister are measured relative to the steel lid.

Following the initial installation of packers into the pressure relief holes at 415 days the displacements measured at DP902 to DP904 start to diverge with DP904 rising, DP903 falling, and DP902 remaining steady until about 480 days. DP905 shows no response until about 460 days when it starts to rise sharply. Gradually displacements at DP902 to DP904 change to a progressively steeper upward gradient until from about 760 days all sensors DP902 to DP905 are moving upwards at similar rates. By 842 days displacements range from +0.12 mm at DP903 to +0.96 mm at DP905.

Inspection of the data in Figure 4-22 clearly confirms the observations from previous sections that the forces and strains within the Lasgit test remain in a state of disequilibrium.

4.6 DISCHARGE RATES FROM LASGIT DEPOSITION HOLE

Discharge rates from the Lasgit deposition hole are shown in Figure 4-23. As flux from the canister filters reduces with time (negligible flow after 15 days), the discharge rate to the slot and tube work AR901-904 all increase. At 30 days into the test, flux to the instrumentation slot is stopped by collecting fluid directly from one of the neighbouring rock anchor holes. During this early stage of the test the total volumetric flow rate out of the system remains fairly constant at around 240 L.day⁻¹.

When the first pressure relief hole (PRH1) was completed on the 5th April 2005 (day 63) the discharge rate from AR901-904 tube work immediately reduced to a negligible amount, while at the same time flux to the anchor hole also declined by nearly 30% to around 105 L.day⁻¹.

However, when a submersible pump was installed in PRH1 (at around 64 days), it had no significant effect on the monitored discharge rates.

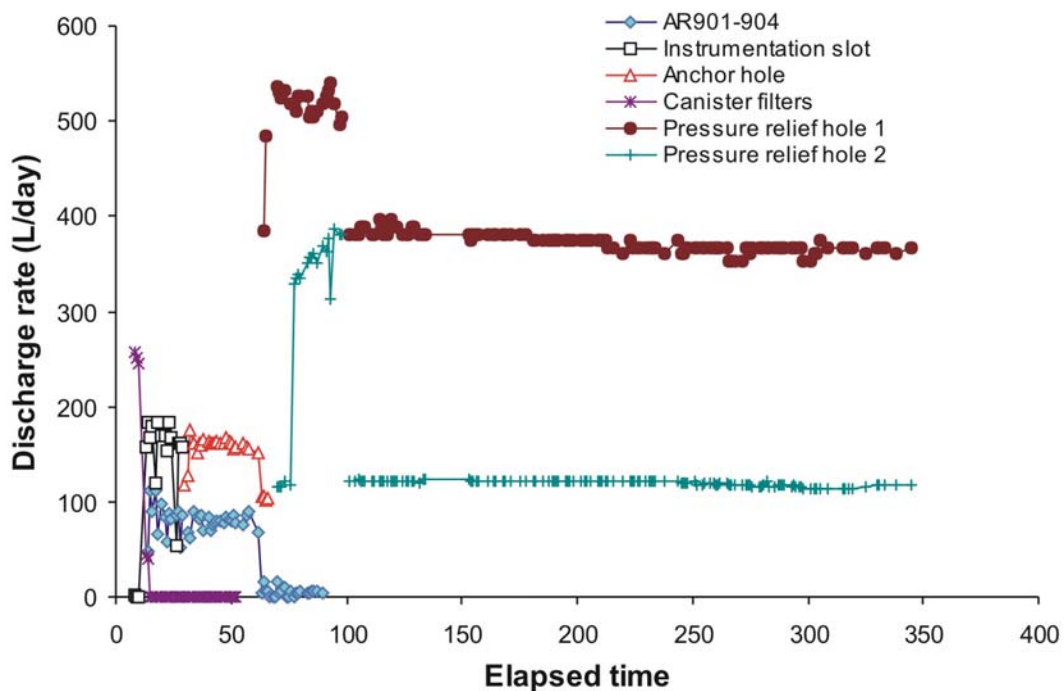


Figure 4-23 Discharge rates from the Lasgit deposition hole.

The second pressure relief hole (PRH2) was completed on 12th April 2005 (day 70). While this had the desired affect of reducing flux to a negligible quantity to the anchor hole, it had no observed effect on the discharge rate from PRH1. Even when a submersible pump was installed 5 days later and the discharge rate from PRH2 increased by 300%, there was no observed change in volumetric flow rate from PRH1. While the data is somewhat contradictory it would seem to suggest that the Lasgit borehole is bisected by at least two non-communicating fracture zones.

Close inspection of the data from PRH2 from 100 to around 300 days shows a small progressive reduction in discharge rate, suggesting a temporal reduction in the transmissivity of the fracture systems. A similar response is observed from PRH1 until around 225 days when discharge rates level at around 365L/day. Data from the PRH holes supports the general hypothesis suggested in Section 4.1.2 regarding the temporal evolution of permeability within the rock mass surrounding the Lasgit hole. This affect may also be caused by a regional decline in ground water pressure as suggested in Section 4.1.2

4.7 VOLUMETRIC FLOW RATE INTO ARTIFICIAL HYDRATION SYSTEM

Artificial hydration began on the 18th May 2005 at an elapsed time of 106 days. The pressure in each hydration filter was initially controlled using pumpset RP2. The methodology for raising porewater pressure is described in Section 2.7. During the course of the hydration procedure, porewater pressure was increased in a series of steps which are described in Section 4.1.1 and Table 4-2. The volumetric flow rate into the hydration system is shown in Figure 4-24. Inspection of the data clearly shows that flow rate into the system spontaneously increases as the pressure is raised. This is then followed by a well defined negative transient leading to a slow and extremely protracted reduction in volumetric flow. Analysis of the data shows that the rate of flux into the system is not particularly sensitive to the modest pressures applied to the filters, confirming the predictive modelling work presented in Section 3.

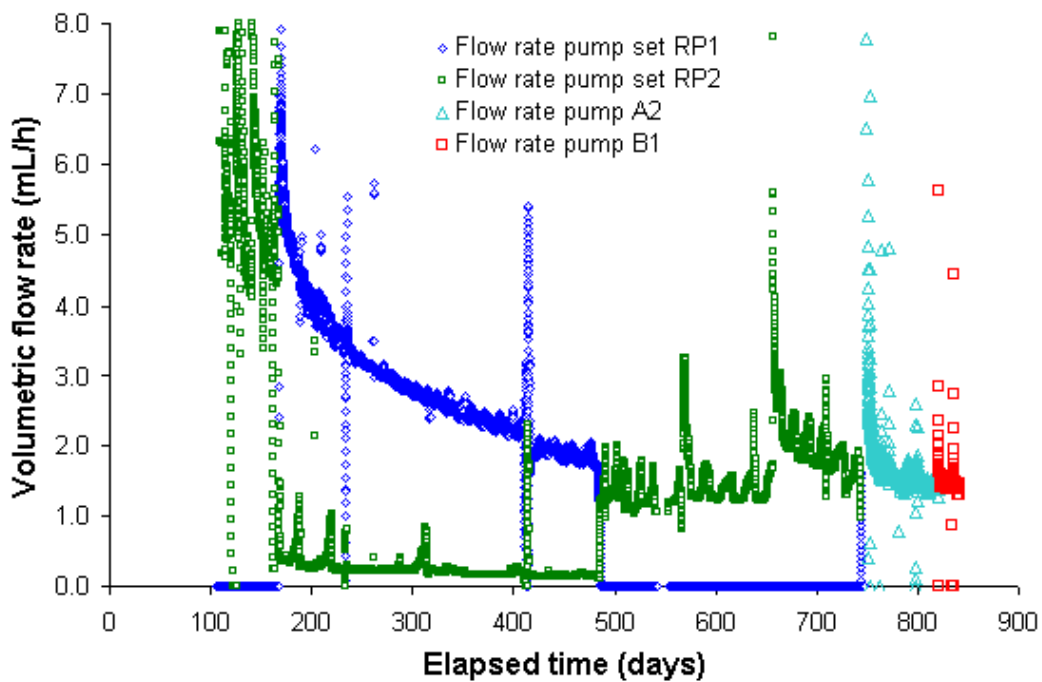


Figure 4-24 Volumetric flow rate into the artificial hydration systems. From 485 days onwards, control of the separate hydration systems alternated between individual pumps or pumpsets while repairs (due to corrosion and scoring of the barrels) were afforded to decommissioned systems.

A second set of reciprocating syringe pumps (RP1) were commissioned 162 days into the test. From this point onwards, pumpset RP1 controlled porewater pressure in the filters located at the mid-plane of the canister (FM905 to FM908) and the large hydration mats FR902, FB903 and FB904. This arrangement of pumps provides a mechanism to estimate the distribution of flow into the system between the canister filters and the large hydration mats (Table 4-4). Volumetric flow rate through the mid-plane filters is estimated by determining the flux through the upper and lower filter arrays and then applying a ratio factor based on the surface area open to flow.

Time	Volumetric flow rate (mL.hr ⁻¹)			Percentage flux through canister filters	Percentage flux through hydration mats
	Canister filters	Hydration mats	Total flux		
200	0.39	3.92	4.32	9	91
250	0.33	3.07	3.40	10	90
300	0.35	2.59	2.93	12	88
350	0.29	2.34	2.63	11	89
400	0.29	2.09	2.38	12	88
450	0.21	1.72	1.93	11	89

Table 4-4 Volumetric flow rate into the canister filters and artificial hydration systems (flux values in the table have been rounded to 2 decimal places and have been time averaged approximately 0.25 days either side of the quoted time).

Examination of the data in Table 4-4 shows that around 89% of the total flux pumped into the Lasgit system has been through the large hydration filters. This is somewhat lower than expected from a purely hydraulic perspective, as the large filter arrays constitute over 98% of the total surface area open to flow. This would seem to suggest that the zone around the canister has a higher permeability than the rest of the clay buffer. Volumetric flow rate into the filter mats

exhibit a small but progressive decrease in volumetric flow. This observation can be explained by preferential swelling of the clay in the vicinity of the mats, resulting in a reduction in the permeability of the clay. This effect may also be compounded by compaction of the filter mats which are subject to high compressive forces.

A similar general trend of decreasing flow rate with time is observed for the ingress of water through the canister filters. It is clear from the data that the general proportion of flux into the clay from the various hydration sources remains fairly constant with time, suggesting that a reduction in clay permeability is the primary cause for the apparent reduction in volumetric flow rate observed in Table 4-4.

4.8 LABORATORY UTILITIES

4.8.1 Temperature

Temperature in the Gas Laboratory, canister and Assembly Hall area are continuously monitored by a series of thermocouples (Figure 4-25). Apart from minor failures of the air-conditioning system at elapsed times of 83 and 710 days, the laboratory and office temperatures remained fairly constant (approximately $\pm 0.5^\circ\text{C}$) until an adjustment to the office temperature was made at 745 days. An upward drift of about 2°C has been experienced between 750 and 870 days. The HRL air temperature shows a clear annual variation, cycling between about 11°C and 16°C . The canister also shows an annual variation, but with a much smaller range of 13.0°C to 13.8°C , and with a phase offset of about 90 days from the HRL.

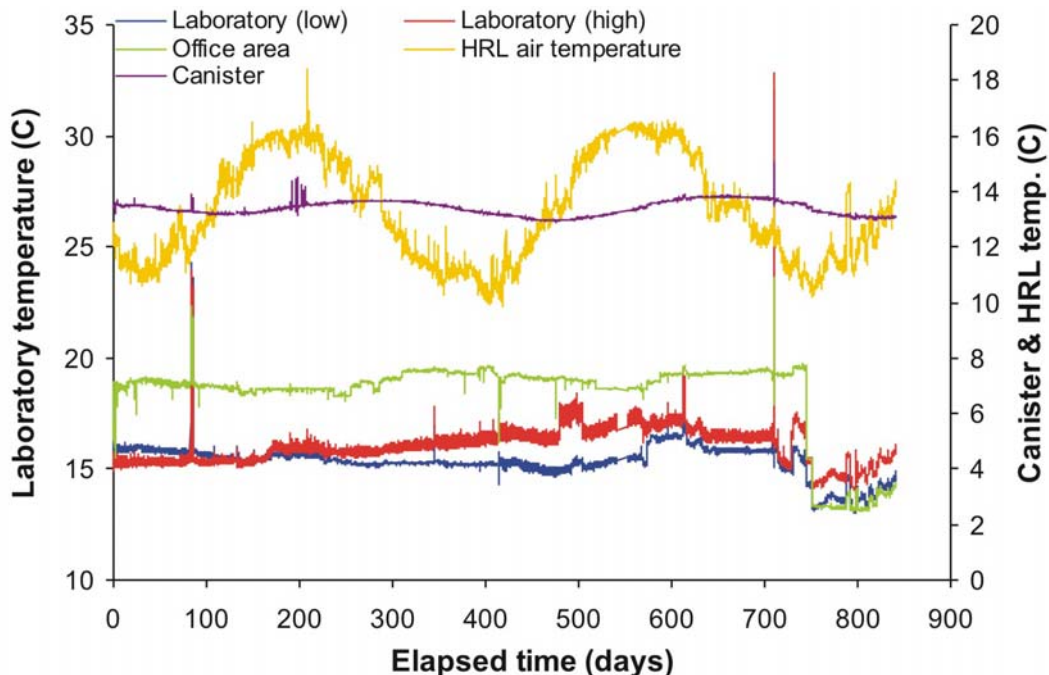


Figure 4-25 Temperatures recorded in the Gas Laboratory, office, canister, and HRL.

4.8.2 Compressed air and water pressure

Figure 4-26 shows a plot of the pressure history for the compressed air and hydraulic feeds to the Gas Laboratory. The apparent noise in the compressed air pressure response (green line) can be simply explained by the frequency with which the system re-pressurises in order to maintain the required air pressure. The sudden drops in water pressure (red line) during the early stage of history are caused when the reservoir tanks for the TBT experiment were refilled. To minimise

this effect the feed pipe to the Gas Laboratory was upgraded by installing a dedicated large diameter pipe at around 90 days.

The hydraulic pressure in the supply borehole remained fairly constant for the first part of the test history at around 600 kPa. However, from approximately 220 days a slow progressive reduction in borehole pressure is observed. The cause for this response is unclear but would seem to support the general hypothesis that the hydrogeological properties of the rock mass in the vicinity of the Lasgit borehole are temporally evolving. This could be caused by a number of reasons from clogging and permeability reduction along conductive fractures near the Lasgit deposition hole, to operational activities (e.g. driving new tunnel headings, sinking of new borehole and deposition holes, block sampling, setup of new experiments, etc.) performed at different locations within the HRL. Pressure rose again between 550 and 650 days, but then dropped down once more, with a step of about 50 kPa at about 707 days when the inlet supply was switched to fresh water, to address the problem of pump damage caused by scoring and corrosion of the barrels. Pressure has remained close to 500 kPa since 707 days.

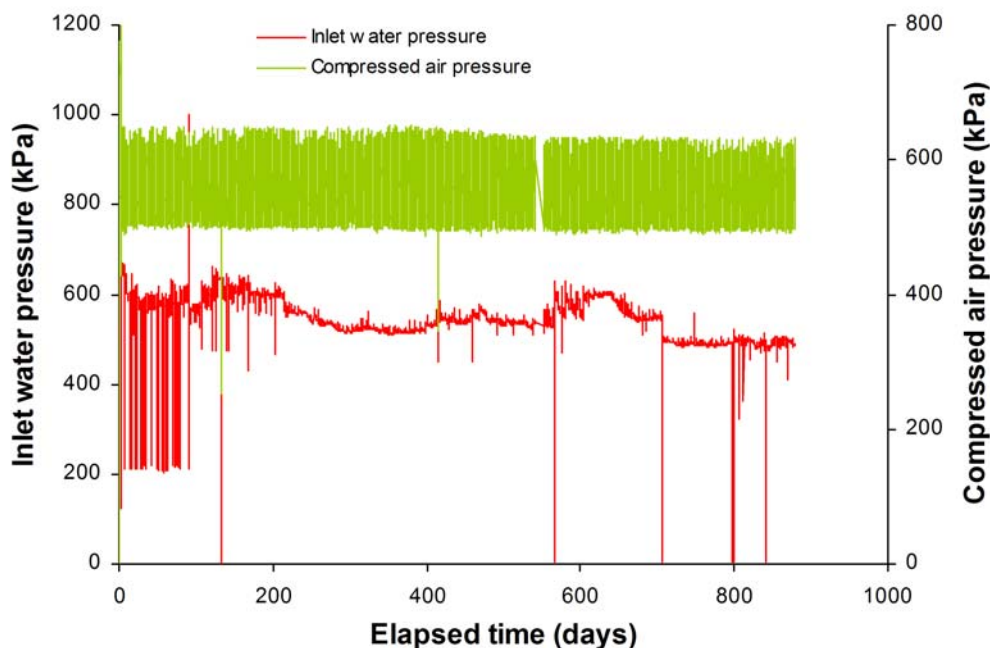


Figure 4-26 Plot showing the variation in pressure for both the compressed air lines and the water inlet feed from a near-by borehole. From 707 days onwards, the water inlet feed was switched to a fresh water supply.

5 Hydraulic and gas injection tests

At the request of project stakeholders a preliminary gas injection history was planned for 2007 with a view to verifying the operation and data reduction methodologies outlined in the original concept report and to provide qualitative data on hydraulic and gas transport parameters for a bentonite buffer during the hydration process. It was decided that preliminary mass transport measurements would be undertaken in FL903, one of the 100mm filters positioned in the lower canister array.

On 25th May 2007 (day 843), the lower filter arrays (FL901 to FL904) were isolated from all neighbouring test circuits and the pressures allowed to decay to provide information on the spatial distribution of local porewater pressures in the vicinity of each filter. Then on 21st June (day 870) a constant head test was started using FL903, with the pressure on that filter raised to

4.3 MPa. During this hydraulic testing the remaining filters in the lower level remained isolated from the artificial hydration system and their pressure allowed to evolve in order to provide temporal data on local porewater pressures within the buffer clay. At the same time, artificial hydration continued through all remaining canister filters and hydration mats. Pressure on FL903 was maintained at 4.3 MPa until 19th July (day 898), when it was reduced to 560 kPa and then held at that level until 7th August (day 917). During this period the flow rates into and out of FL903 were monitored.

On 7th August (day 917) gas injection into FL903 was begun. Starting with an estimated gas volume of 1280 cm³, the gas was pressurised by introducing water into the gas reservoir at a steady rate until 20th August (day 930) when the test was temporarily stopped and the injection pressure held constant. This continued until 11th September (day 952) when the gas volume was reset to around 1273 cm³ and pressurisation resumed, continuing until 3rd October (day 974) when the gas injection was stopped and the pressure decay in FL903 was monitored through to the end of October. To examine the evolution of hydraulic properties following a gas injection event, a repeat hydraulic test was performed immediately after the cessation of gas injection. This had the additional benefit of flushing gas from the system and aiding the hydration of the clay. This phase of the test history is ongoing at the time of preparing this report.

It should be noted that outputs and parameters quoted in the following sections are provisional, awaiting recalibration of the Lasgit system. However, given previous experience, this should have a negligible effect (if any) on the estimation of transport parameters.

5.1 BASLINE HYDRAULIC TEST RESULTS

The pressure responses at filters FL901 to FL904 during the course of the hydraulic test (days 843 to 917) are shown in Figure 5-1 and the flow rates at FL903 during the two steps of the constant head test (days 870 to 917) are shown in Figure 5-2. For comparison, the porewater pressures on the deposition hole wall at sensors UR907 to UR910 are shown in Figure 5-3. These sensors are located at the same elevation as the injection filters FL901 to FL904. It can be seen that the pressures in all the injection filters rapidly drop well below pressures present at the deposition hole wall, strongly suggesting that a significant volume of the bentonite buffer near the canister remains in a partially saturated state. This explanation (rather than simple hydraulic disequilibrium) seems probable as it would require a much lower bentonite permeability to yield such low pressures (measured at FL901, 902 and 904) after extended periods of hydration. If such permeabilities were the case then the response to the shut-ins would take much longer than observed in Figure 5-1.

It can also be seen that the pressures at the various injection filters decline at different rates. These rates seem to reflect the sizes of the filters, with the smallest filter, FL902, falling most rapidly to about 300 kPa within 15 days of the start of the shut-in. (The cause of the pressure discontinuity at 857 days in this sensor is not known.) The two largest filters, FL901 and FL903, remain at the highest pressure at 870 days, at 820 and 900 kPa respectively, and the intermediate sized filter, FL904, falls to about 480 kPa by 870 days. These observations are consistent with the suggestion that the volume of bentonite around each filter that has been resaturated is proportional to the size of the filter. However the fact that the pressure at FL903 initially falls more rapidly than either FL901 or FL904 shows there are additional factors involved. One will be the differences in the porewater pressures at the deposition hole wall opposite each of the injection filters (Figure 5-3), which may have caused local variations in the degree of resaturation. Another may be some degree of heterogeneity within the buffer as it swells, which may also be affected by any eccentricity in the position of the canister with respect to the bentonite blocks.

The flow rate data in Figure 5-2 show that there is a transient of about 10 days after each of the two pressure changes in FL903 before the flows settle to a fairly steady level, although the data following the second pressure change at 898 days is considerably noisier.

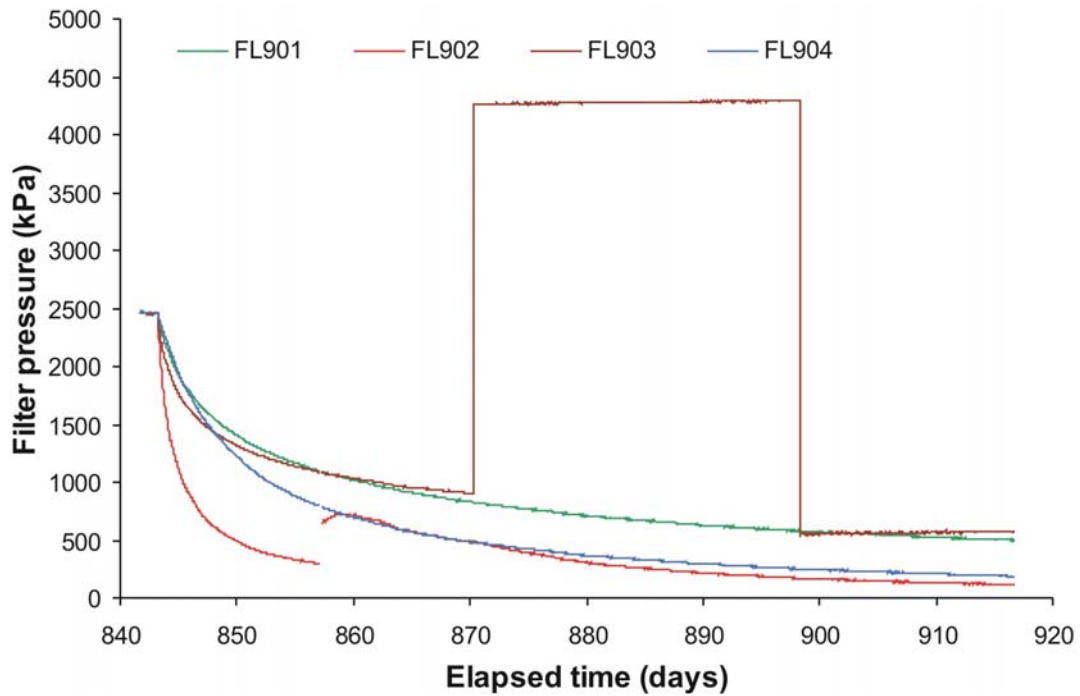


Figure 5-1 Pressures observed at the lower canister filters FL901 to FL904 during the hydraulic test.

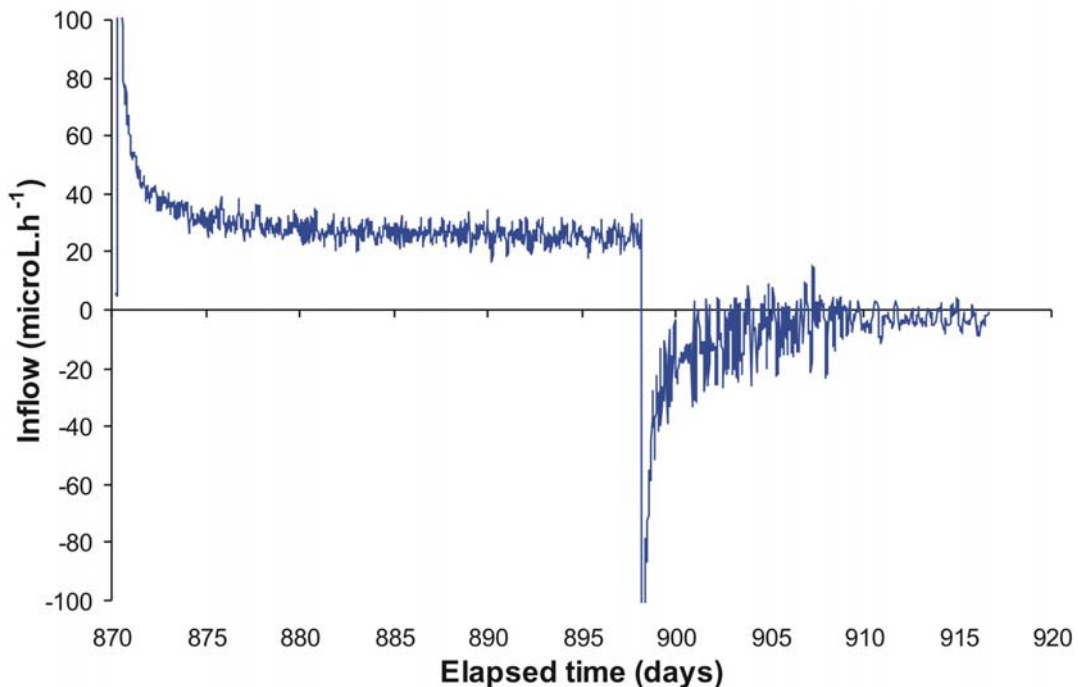


Figure 5-2 Flow rate observed at lower canister filter FL903 during the constant pressure phases of the hydraulic test.

5.1.1 Hydraulic test modelling

In order to obtain estimates of the hydraulic conductivity and specific storage of the bentonite from these data it will be necessary to develop a model of the flow processes that are occurring.

As noted above, the data strongly suggest that a significant volume of partially saturated material remains around the canister, and the extent of this partially saturated zone varies with location around the canister, so that the initial state of the system for any model of the test cannot be specified *a-priori*. Instead, it will be necessary to model the whole of the hydration phase of the Lasgit project in order to arrive at a suitable spatial definition of the initial saturation state for the hydraulic test. Running such a detailed simulation with a full multi-phase model such as TOUGH2 would take too long for this preliminary assessment so a simple finite element groundwater flow code with variable saturation capability was used for these calculations.

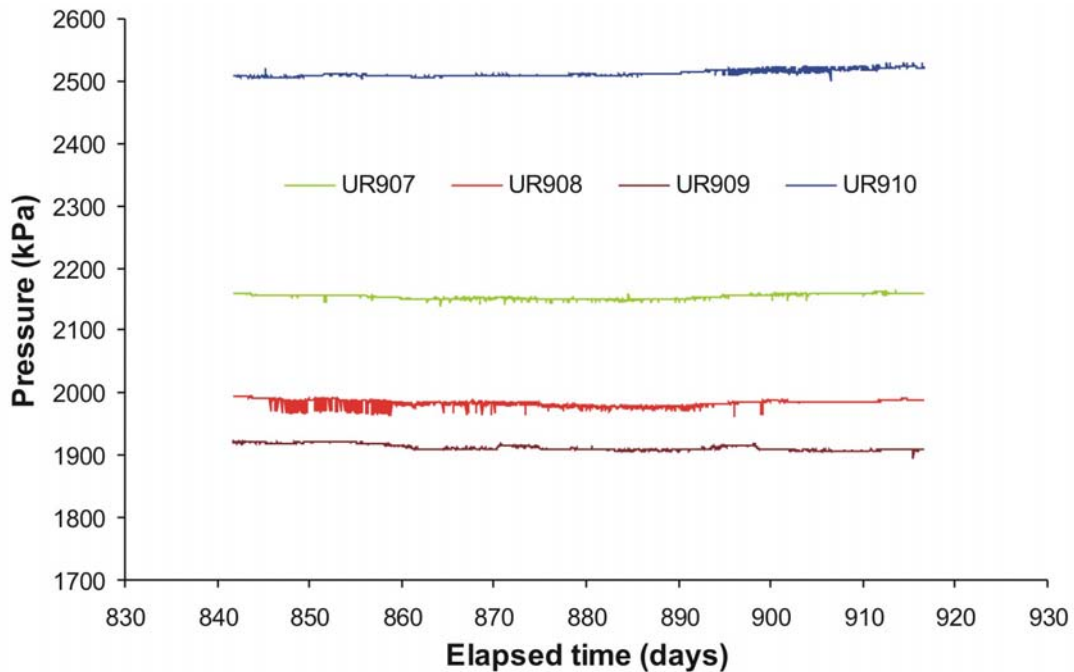


Figure 5-3 Porewater pressures observed at deposition hole wall sensors UR907 to UR910 during the hydraulic test.

Attempting to model variably saturated flow in the full bentonite buffer in 3D with sufficient grid refinement to accurately resolve flow processes around filters as small as 10 mm in diameter is clearly not feasible with the currently available resources. However, a preliminary model of one quarter of a cylinder centred on one filter and extending just 0.7m up and down the canister from the filter was constructed to test the possibility of using such a model to interpret the test data (the initial void space around the canister was represented in the model). The mesh created contained 86,000 nodes on 507,000 tetrahedral elements and took about 5.5 h. to run a single simulation of the hydration and hydraulic test phases of the experiment. The results of a simulation of the hydration phase that assumed a hydraulic conductivity of $1.3 \times 10^{-13} \text{ ms}^{-1}$ and a specific storage of $1.5 \times 10^{-4} \text{ m}^{-1}$ is shown in Figure 5-4.

This model gives a useful general picture of the likely saturation state of the bentonite around an injection filter at the end of the initial hydration phase, but detailed examination of the solution suggests that the mesh is still not sufficiently refined to give accurate results. At the same time, the run times are such that the model would be very difficult to use for data interpretation so a slightly simplified and more efficient approach was sought. After some experimentation, a 2D axially symmetric model was chosen, centred on an injection filter and with the axis of symmetry projecting perpendicular to the canister towards the deposition hole wall. Using a mesh of about 2000 nodes on about 4000 triangular elements a single simulation could be run in about 40 s. This makes it possible to obtain fits to data for each of the filters in a reasonable timescale. Figure 5-5 shows the fits obtained to the shut-in pressure data, using separate

parameter values for each filter and Table 5-1 shows the parameter values used for each model. It can be seen that relatively similar values for hydraulic conductivity have been obtained but that there is quite a wide range of specific storage values.

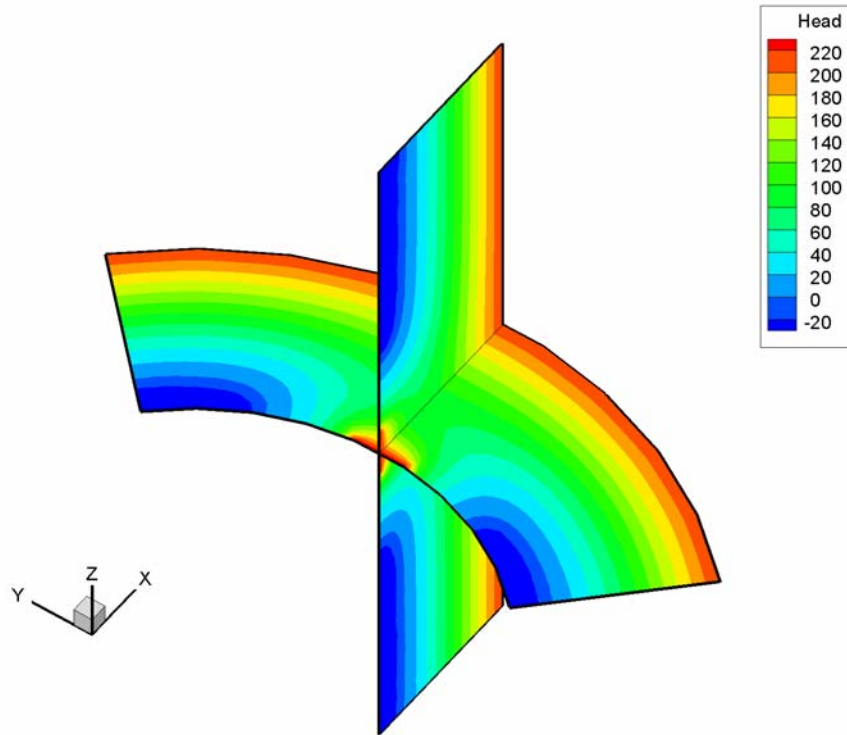


Figure 5-4 Pressure heads in a finite element model of single phase variably saturated flow around filter FL901 after 840 days of hydration. Dark blue bands indicate remaining zones of partially saturated material.

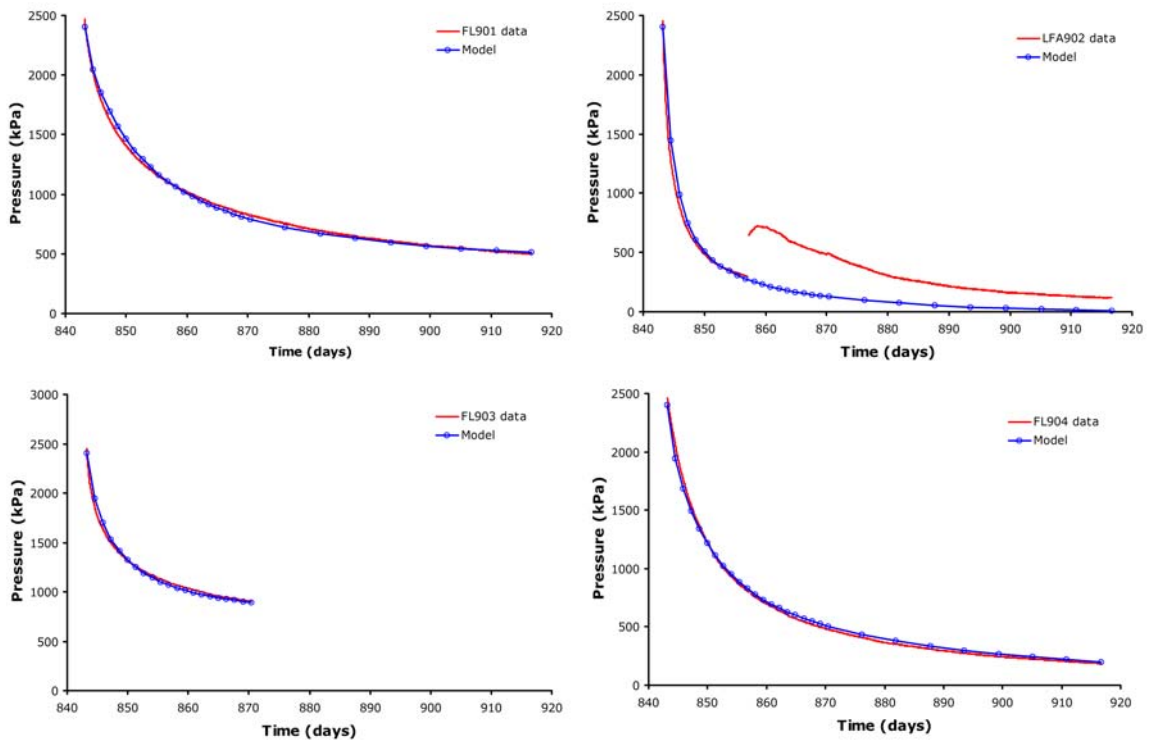


Figure 5-5 Comparison of model simulations to shut-in pressure data for the injection filters FL901 to FL904 during the hydraulic test.

	$K \text{ (ms}^{-1}\text{)}$	$S_s \text{ (m}^{-1}\text{)}$
FL901	1.10×10^{-13}	1.20×10^{-4}
FL902	0.90×10^{-13}	5.50×10^{-4}
FL903	1.24×10^{-13}	0.55×10^{-4}
FL904	1.58×10^{-13}	4.00×10^{-4}

Table 5-1 Hydraulic parameters obtained from fits to shut-in pressure curves for injection filters FL901 to FL904.

The same model can be used to model the constant head steps applied to FL903, but in this case comparing the flow rate data to the model simulation. However, using the parameters from the shut-in phase gives a poor fit to the flow rate data, as shown in Figure 5-6. A revised model provides a much improved fit with $K = 0.75 \times 10^{-13} \text{ ms}^{-1}$ and $S_s = 0.25 \times 10^{-4} \text{ m}^{-1}$.

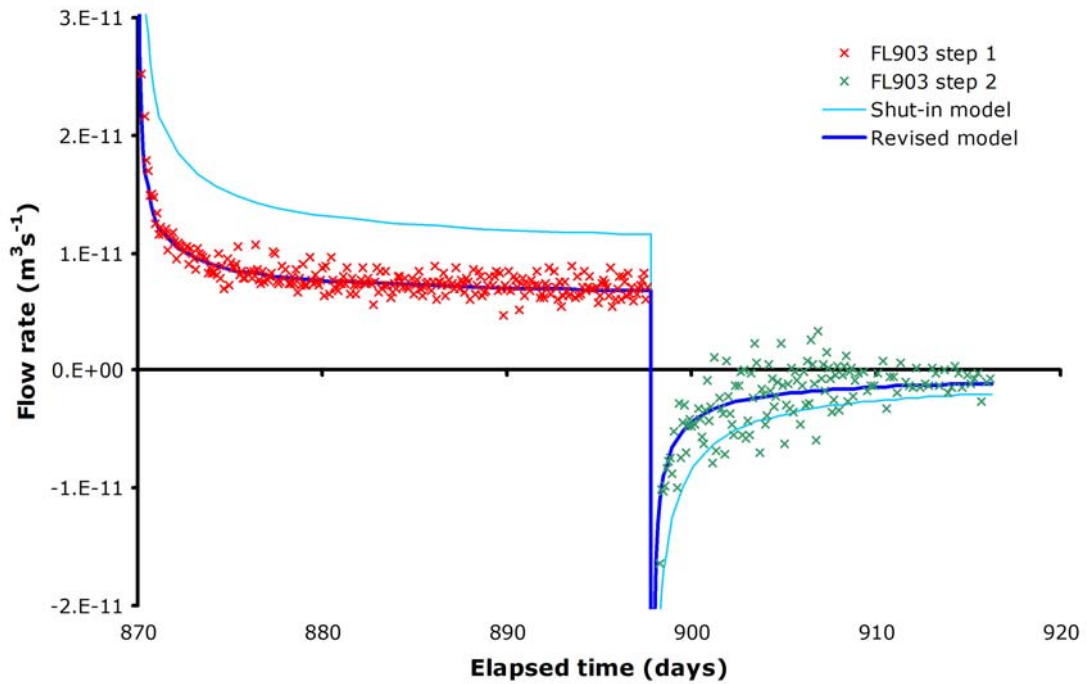


Figure 5-6 Comparison of model simulations with flow rates at FL903 during the constant pressure test steps.

These models used to derive the initial conditions for the filter shut-in calculations also give an indication of the progress of the resaturation of the bentonite in this part of the borehole. Figure 5-7 shows the simulated pressures, plotted as hydraulic heads, at each filter at 840 days, close to the end of the hydration phase, the parameters for the individual fits from Table 5-1 being used in each case. In these plots the two darkest blue bands show the extent of unsaturated conditions. It can be seen that the unsaturated zone is much more extensive near the smallest filter, FL902, than near the larger filters FL901 and FL903.

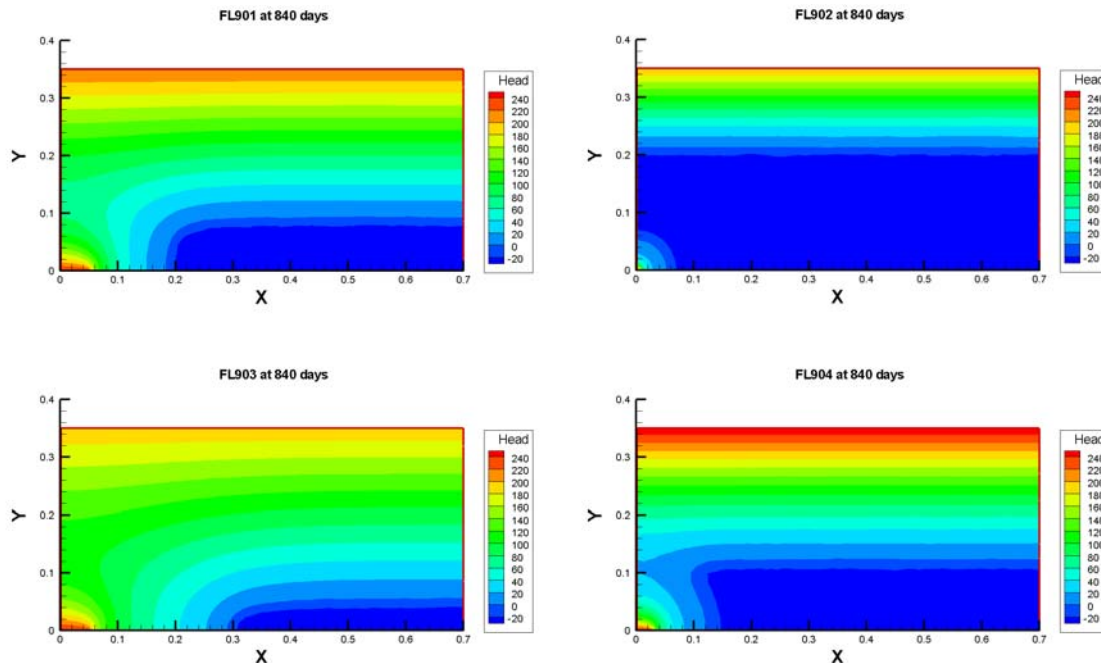


Figure 5-7 Simulated pressure heads around each filter at 840 days, the end of the hydration phase.

5.2 GAS INJECTION TEST RESULTS

Gas injection testing began on 7th August 2007 (day 917) through canister filter FL903. Gas with an initial volume of 1.28 L was introduced and pressurised by pumping water into the reservoir. On 20th August (day 930) FL903 was isolated until 11th September (day 952) when a new gas volume of 1.24 L was introduced and pressurisation restarted. This second phase of pressurisation was continued until 3rd October (day 974) when the filter was again isolated and the gas pressure allowed to decay. The observed gas pressure at the filter is shown in Figure 5-8, which also shows the predicted pressure for a confined ideal gas. It should be noted both predicted gas pressure and the derived volumetric flow rate of gas into the deposition hole are strongly dependent on the start volume of gas.

During the first phase of gas pressurisation (days 917 to 930) the observed pressure starts to depart from the pressure predicted for an ideal gas² at about day 924. Figure 5-9 shows this period in more detail together with the estimated rate of flow of gas into the clay (Section 2.8). These data suggest that the gas starts to flow into the buffer at a pressure of about 775 kPa, which is much lower than the expected gas entry pressure for saturated intact bentonite. It therefore seems likely that gas is flowing between the bentonite and the canister and possibly between bentonite blocks (the interface between bentonite rings 2 and 3 lies just 50 mm above the injection filter).

When gas pressurisation stopped at 930 days and the pressure was held constant, flow into the clay dramatically reduced by around 98.5%, indicating that propagation of the main gas pathway(s) practically ceases when the pressure stops rising. In its most basic form, this can be viewed as the expansion of gas pathway(s), conceptually little different to that of inflating a balloon, where the walls of the latter represent the pathway surfaces within the clay. The small continuous flux observed following this event may result from the movement of gas along small-

² The initial start volume of gas was estimated by fitting the early predicted pressure response to that of the measured values from FL903. The start gas volume for the second test phase was estimated at the end of the test by displacing the remaining gas with water through the FL903 drain vent. Given the importance of this parameter, in future tests, additional effort will be placed on its measurement prior to gas injection.

scale pre-existing features which are only present because the bentonite remains in suction and is not in hydraulic equilibrium. If correct, these fluxes should reduce in magnitude during later tests as hydration of the buffer progresses. Given the sudden reduction in flow, it seems clear from the data that gas is not flowing within the original porosity of the clay and that the initial network of gas pathways fails to locate an adequate sink capable of accommodating the previous flux.

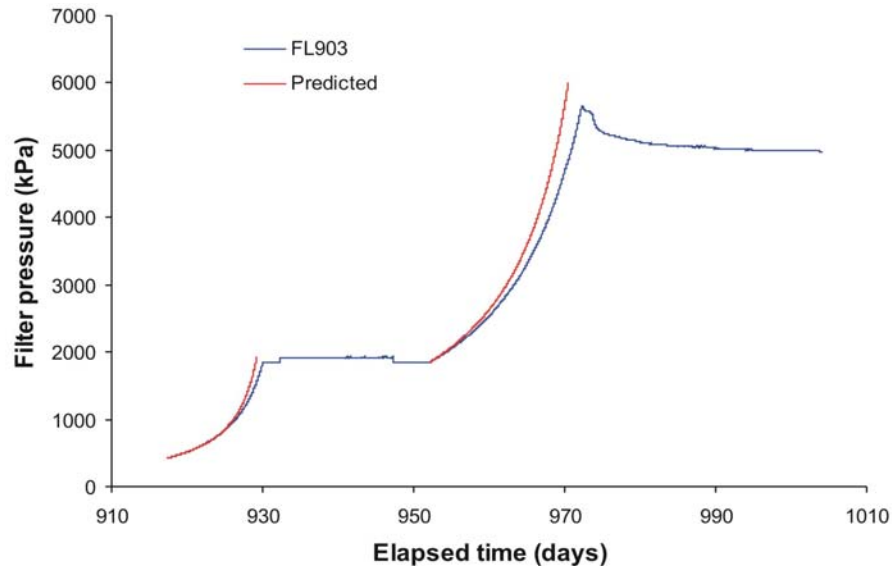


Figure 5-8 Comparison of predicted and observed gas pressures at FL903 during the gas injection test.

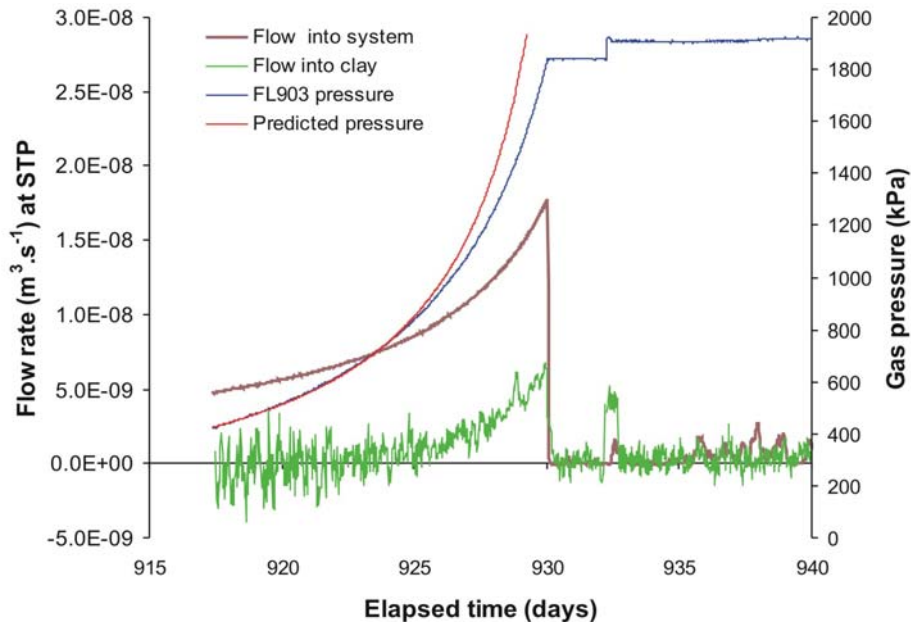


Figure 5-9 Estimated rate of gas flow into the system and the clay compared to the predicted and observed gas pressures during the first phase of the gas injection test.

Following the onset of the second phase of gas pressurisation (day 952) the observed pressure starts to deviate from the predicted ideal gas compression curve immediately (see Figure 5-10), indicating that the pathway continues to extend without any delay. The gas flow rate during this second phase rises gradually with time until about day 970 at which point it rises much more sharply until gas pressurisation is stopped again at day 974. The sharp rise in gas flow rate

occurs when the gas pressure is marginally greater (approximately 0.32 MPa) than the local total stress measured on the rock wall, but is around 0.23 MPa lower than the average radial stress monitored on the canister surface. Axial stress measured at PB902 was also marginally higher than the gas pressure (around 0.27 MPa). Gas pressure continues to increase reaching a peak pressure of 5.66 MPa at day 972.3. This is followed by a small spontaneous negative transient leading to a quasi steady state illustrated in Figure 5-11 at a gas pressure of around 5.5 MPa. This behaviour is qualitatively similar to results from laboratory scale tests reported by Horseman et al. (1999) and Harrington and Horseman (2003).

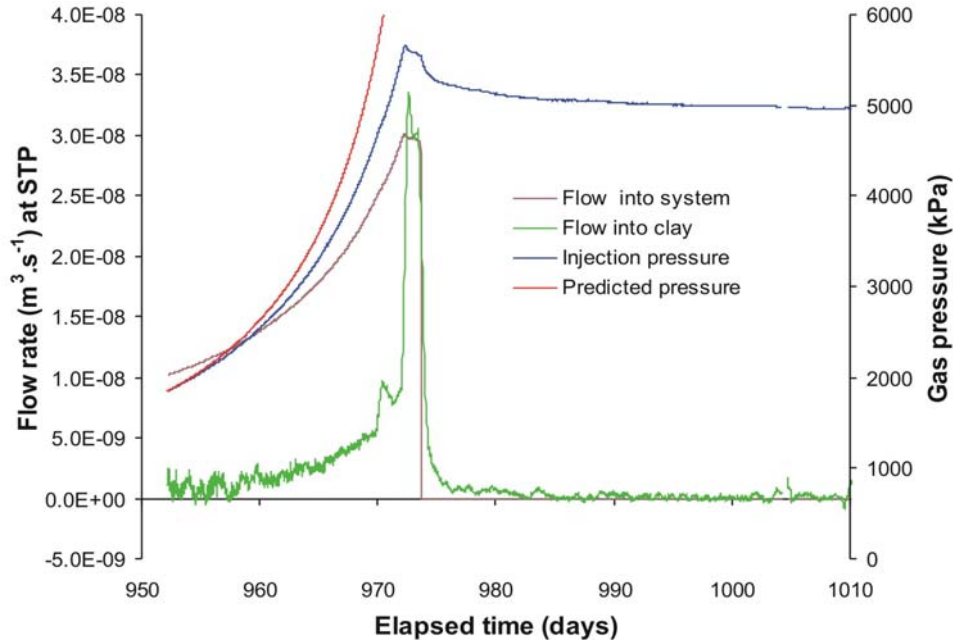


Figure 5-10 Estimated rate of gas flow into the clay compared to the predicted and observed gas pressures during the second phase of the gas injection test.

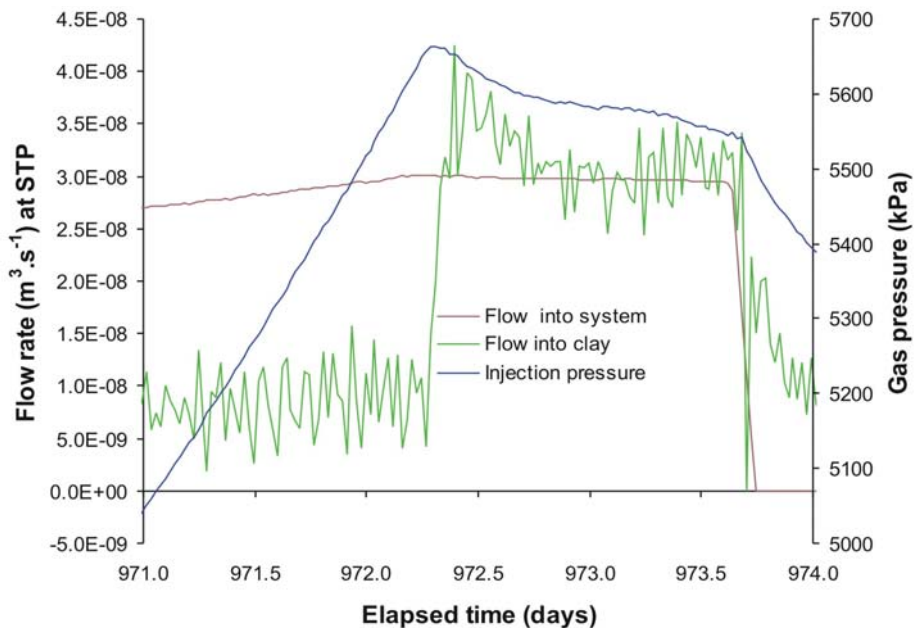


Figure 5-11 Unsmoothed flow rate and pressure responses around peak gas pressure. Gas flow into the clay rapidly increases following the peak which is followed by a small spontaneous negative transient.

The injection pump was stopped at 974 days and the gas pressure allowed to decay to provide an estimate for the apparent capillary threshold pressure. It can be seen in Figure 5-10 and Figure 5-11 that just before injection is stopped, the post peak gas flux exhibits dynamic behaviour (over and undershooting flux into the system) suggestive of unstable gas flow. Following the cessation of injection the flux declines rapidly at first but then enters an extended period of very small flows³. This is reflected in the pressure response which drops rapidly initially but then decays very slowly towards an asymptotic capillary threshold pressure, Figure 5-12, which is tentatively estimated to be around 4900 kPa (the average radial stress measured on the canister is 4900 kPa which is very close to the axial stress measured at PB902). This result, if correct, suggests a strong correlation between gas transport and total stress and supports the observations reported by Harrington and Horseman (2003). The breaks in slope in the pressure decay curve (Figure 5-12) are indicative of the sealing and temporary formation of highly unstable gas pathways.

However, this observation raises a simple question: why does the gas pressure appear to asymptote at a value far in excess of that required to initiate gas flow? To help answer this question we must return to the conceptual model of the “expanding balloon” mentioned earlier. Initial results (with gas pressure below total stress) demonstrate that in the absence of a sink, continued gas penetration of the buffer and or canister interface, required an increasing gas pressure to drive major pathway propagation⁴. The fact that the subsequent gas pressure asymptotes at a value close to that of the local total stress, may suggest that the small amount of gas injected during the test remains resident in the buffer/deposition hole and has not found a suitable sink or egress point from the system (i.e. expansion of the pathway continues until the internal gas pressure declines to a value equal to that of the local total stress).

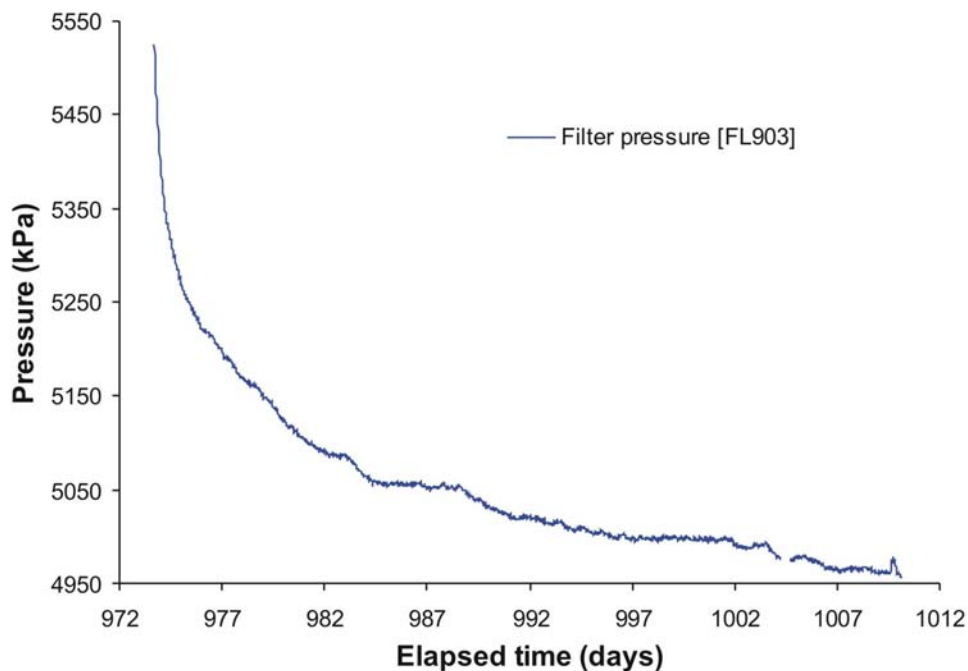


Figure 5-12 Shut-in response for filter FL903. The inflections in the pressure decay response are suggestive of dynamic gas flow and pathway closure.

³ These fluxes are significantly smaller than that observed during the earlier constant pressure phase (which was probably due to flux along small-scale pre-existing features) and suggests that gas pressures within this zone have risen sufficiently to suppress the flow rate.

⁴ The small continuous flux noted from the initial constant pressure gas test was probably along pre-existing small-scale features, which are only present because the bentonite remains in suction and is not in hydraulic equilibrium.

Figure 5-13 and Figure 5-14 show details of the radial stress and pore pressure responses to the sharp increase of gas flow, prior to and just after the peak gas pressure of the second gas injection phase, in a selection of sensors close to the injection filter FL903. It is notable that the most pronounced responses are seen in the sensors from section 4 (see Figure 4-1), which are 600 mm below the injection point, rather than the section 5A sensors, which are 300 mm above it. Examination of the data indicates changes in stress and porewater pressure begin at the peak in gas pressure.

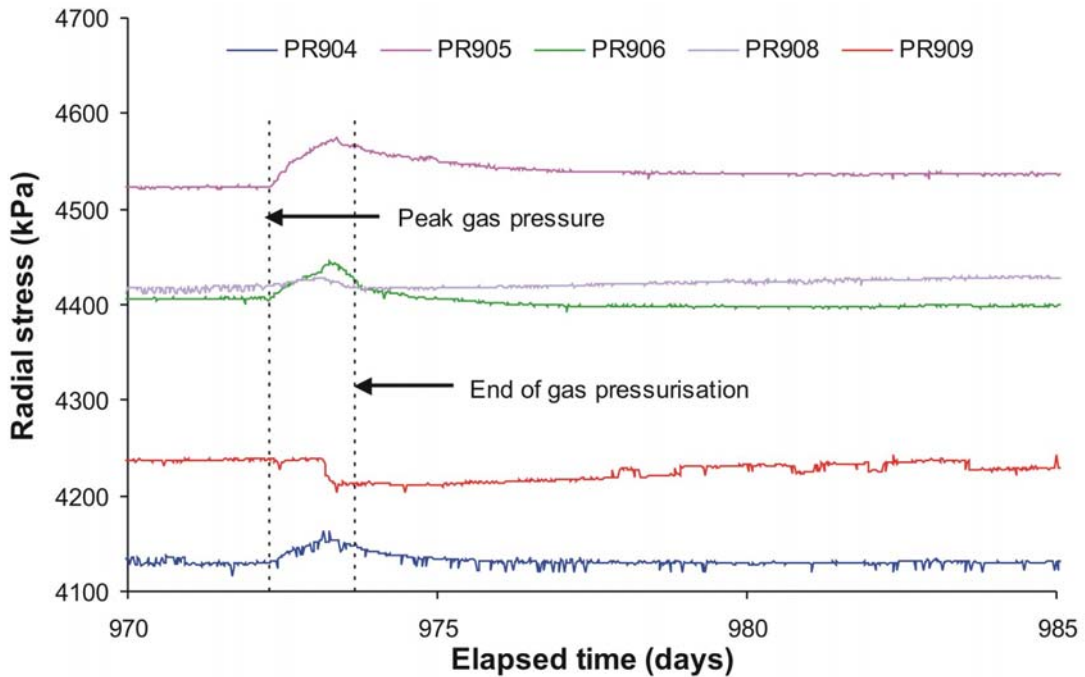


Figure 5-13 Radial stresses observed in a selection of sensors close to FL903 at the end of the second gas pressurisation phase.

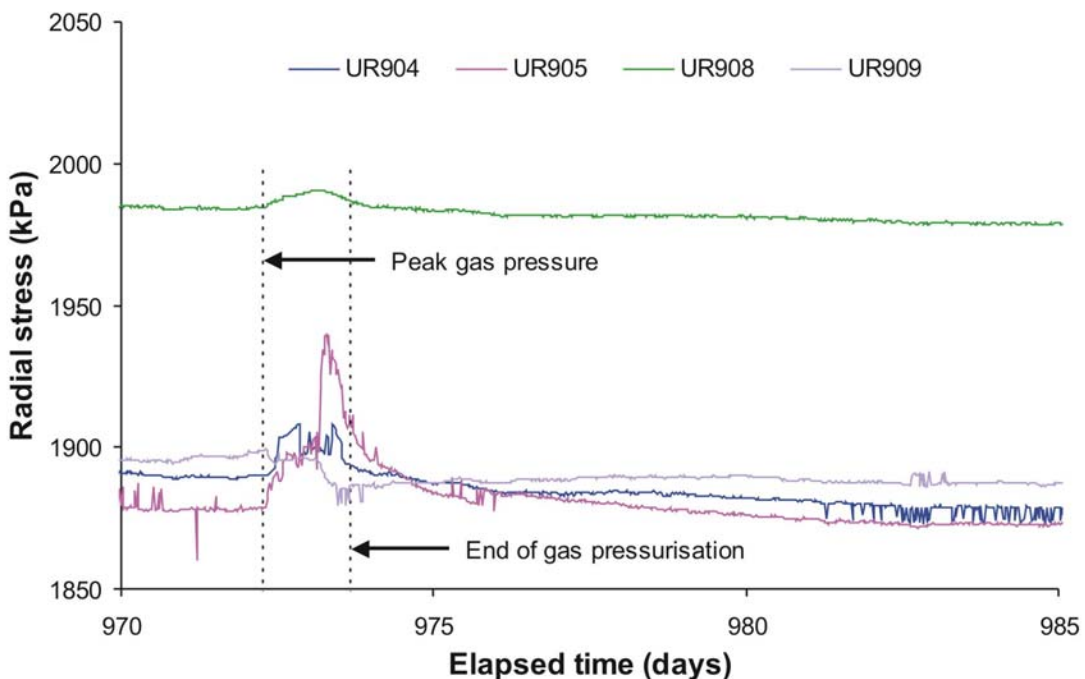


Figure 5-14 Pore pressures observed in a selection of sensors close to FL903 at the end of the second gas pressurisation phase.

Figure 5-15 and Figure 5-16 show the temporal evolution in radial stress and porewater pressure during this time (normalised to zero at 972.02 days). Figure 5-15 shows a well pronounced increase in radial stress around the entire base of the deposition hole, with the highest increase noted in the vertical plane below the point of injection. This indicates the gas preferentially moved downwards, probably along the interface between the canister and buffer. It is notable that the radial stress immediately adjacent to FL903 actually decreases during this time. A similar observation is also seen in the porewater pressure trace (Figure 5-16). The cause of this behaviour remains unclear.

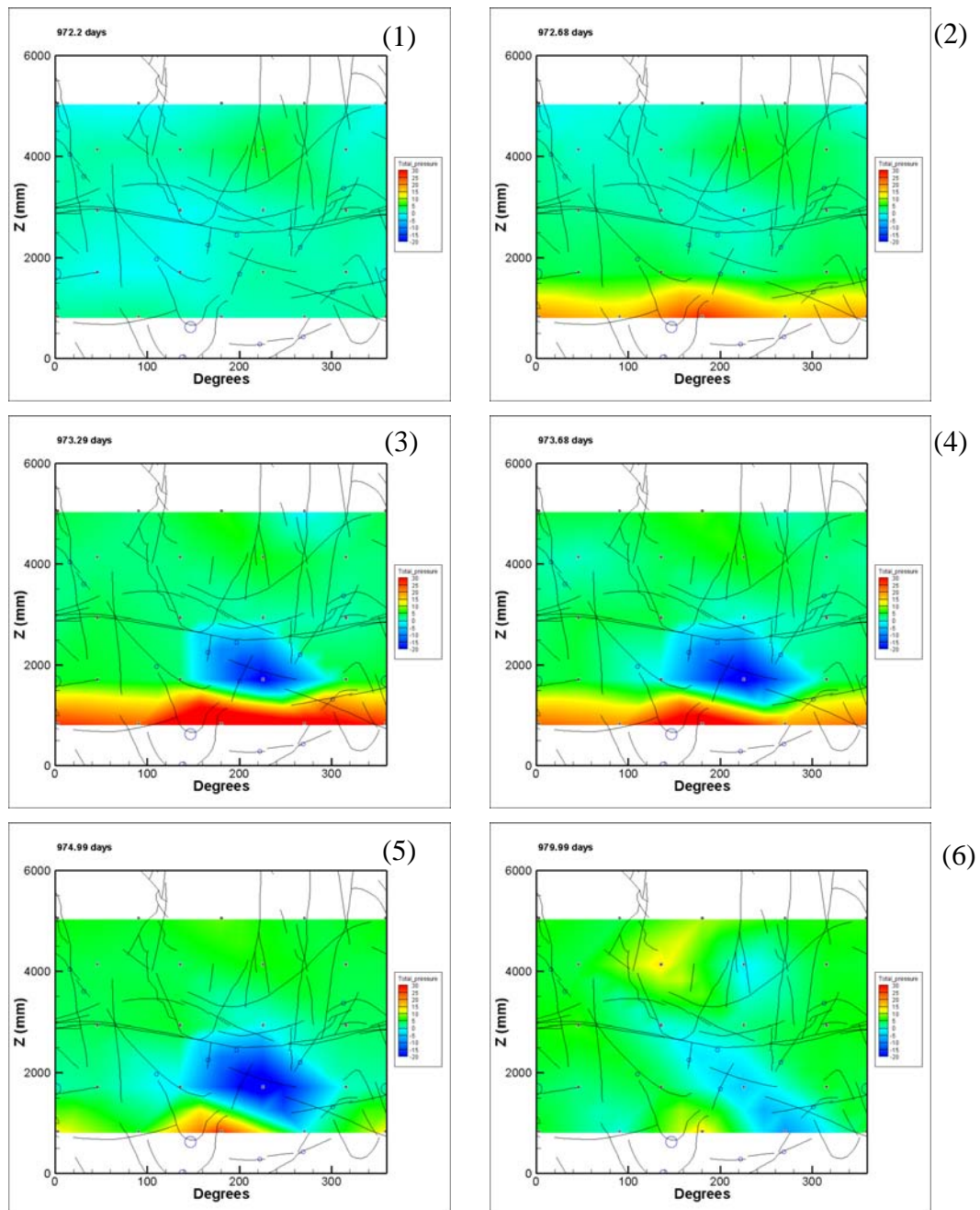


Figure 5-15 Evolution in normalised radial stress around the deposition hole wall prior to and after the peak in gas pressure (days 972.2 to 979.99). The intensity plots indicate a general increase in radial stress around the base of the deposition hole. Adjacent to the filter radial stresses appears to decline momentarily.

Detailed inspection of the porewater pressure intensity plots (Figure 5-16) generally confirms the above observations, though initial results suggest that the pulse in porewater pressure dissipates at a faster rate than that of the radial stress. This may relate to the fact that significant sections of the buffer clay remain in a state of suction.

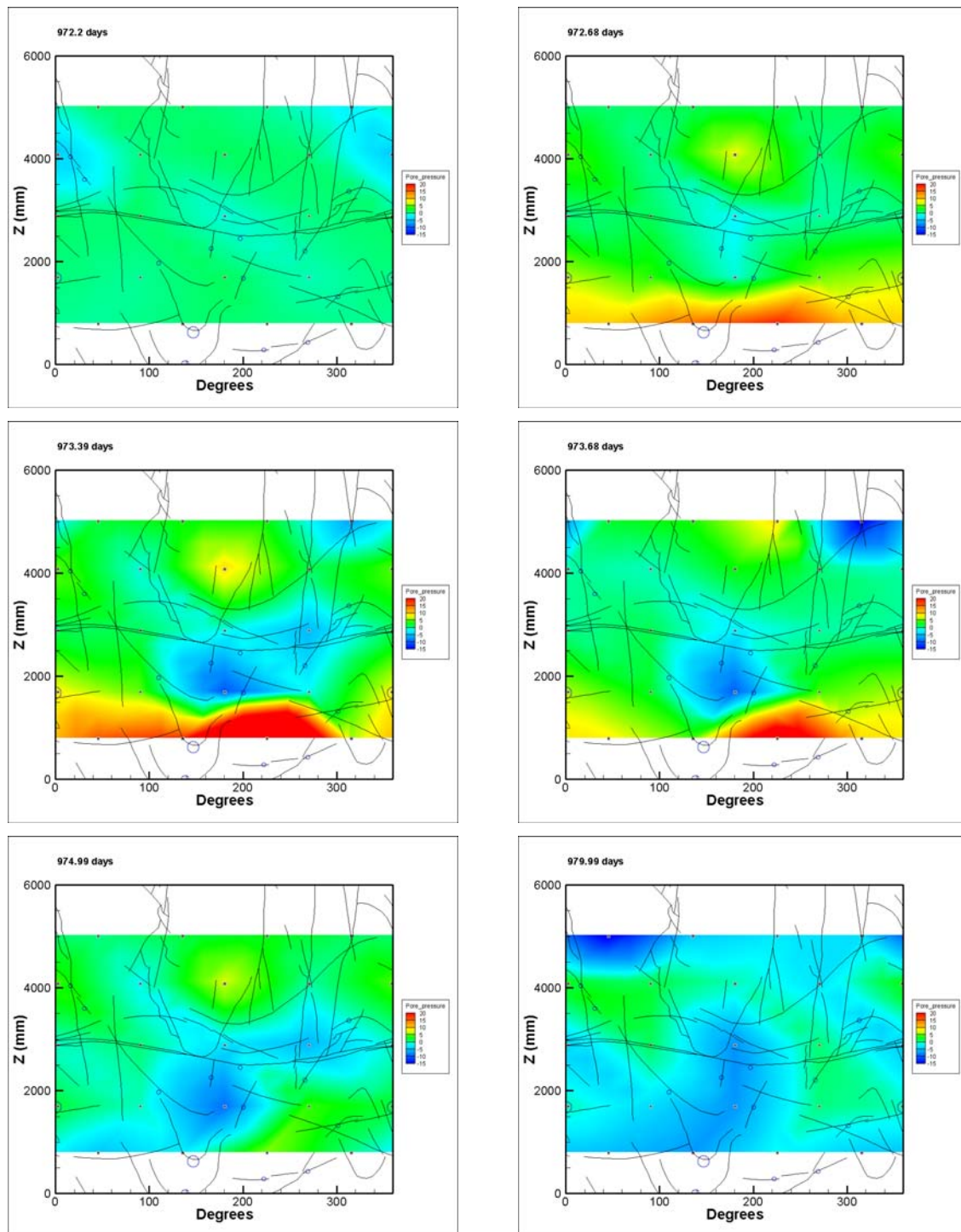


Figure 5-16 Evolution in normalised porewater pressure around the deposition hole wall prior to and after the peak in gas pressure (days 972.2 to 979.99). The intensity plots indicate a general increase in porewater pressure around the base of the deposition hole focussed in the vertical plane of the source filter (FL903). Adjacent to the filter porewater pressure appears to decline momentarily.

Analysis of the porewater pressure sensors located within the buffer show no obvious sensitivity to the injection of gas. In contrast, axial stress sensors located beneath and above the canister appear to register the passage of gas, probably detecting reflected stresses normal to the gas flow path (Figure 5-17). Indeed, the slow and then rapid increase in PB902 immediately following the peak gas pressure is strongly indicative of the time dependent propagation of gas pathways.

A small inflection (reduction) in the rate of increase in axial stress at the base of the canister (PB901) occurs around 0.85 days after the peak in gas pressure. A reduction in stress can only be caused by the removal of load. This would suggest some form of displacement has occurred within the system as a result of gas injection.

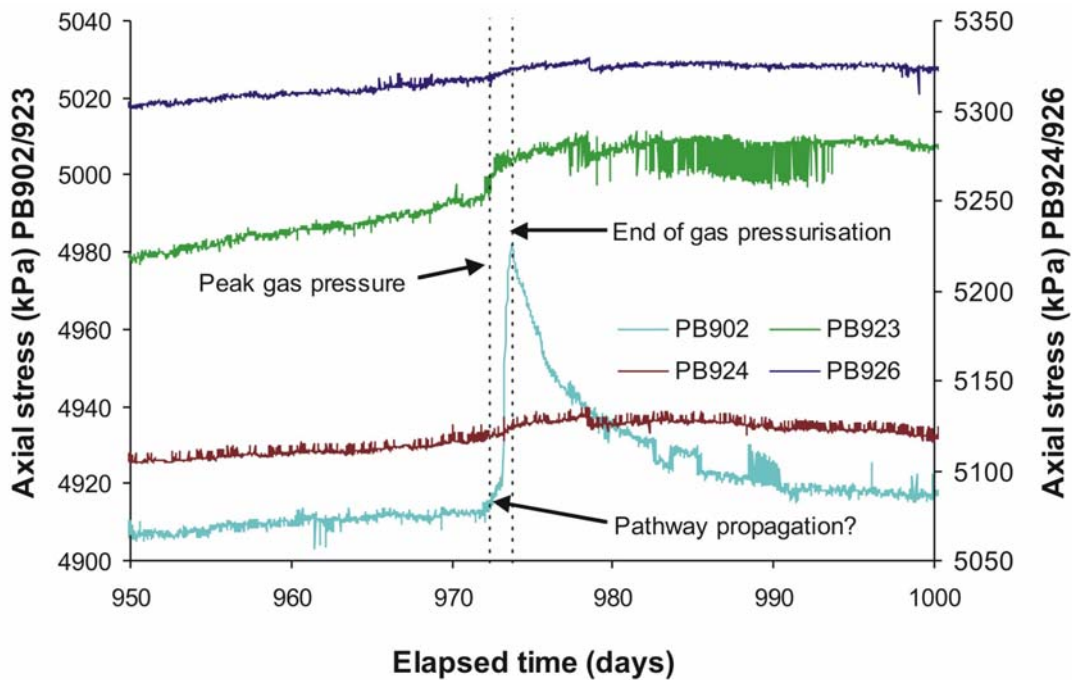


Figure 5-17 Selected axial stress data during the second phase of gas injection. The strongest response is observed by PB902, which, located below the canister, exhibits signs of time depended pathway flow.

While it is difficult with the available data to make definitive statements regarding the exact direction and number of gas flow paths, it seems highly probable that the gas moved generally downwards away from the filter and then along the interface between blocks C1 and R1 and/or R1 and R2. The fact that the gas pressure asymptotes at a value close to the local total stress, may suggest that the small amount of gas injected during the test remained resident in the buffer/deposition hole. This observation compliments the findings of the predictive modelling work described in Section 3, which identified the effectiveness of the seal between canister and bentonite as a critical parameter in determining the overall time taken to resaturate the facility. This is also logical as there is a clear axial stress gradient running from high to low from the top of the deposition hole (PB928 ~6.0 MPa) to the lowest stress sensor (PB902 ~4.9 MPa). Under most conditions gas would propagate along such a stress vector.

However, the observed general coupling between gas, stress and porewater pressure at the repository scale is extremely important and is strongly indicative of pathway dilatancy as a gas transport mechanism. These observations are qualitatively similar to those reported by Horseman et al. (2004).

5.3 HYDRAULIC TEST POST GAS INJECTION

To examine the affect if any on the hydraulic properties of the buffer following gas injection, a second hydraulic test was performed. Prior to the start of this test, the drain valve to FL903 was opened to atmospheric pressure and the gas in the test system vented. Water was then injected in order to help sweep residual gas from the injection system. Once a steady stream of water was discharged from the drain valve, it was closed and the hydraulic pressure in the test system raised to 4.4 MPa (very close to the original test pressure in Section 5). Figure 5-18 shows the evolution in flow rate from both hydraulic tests plotted against the duration of each test.

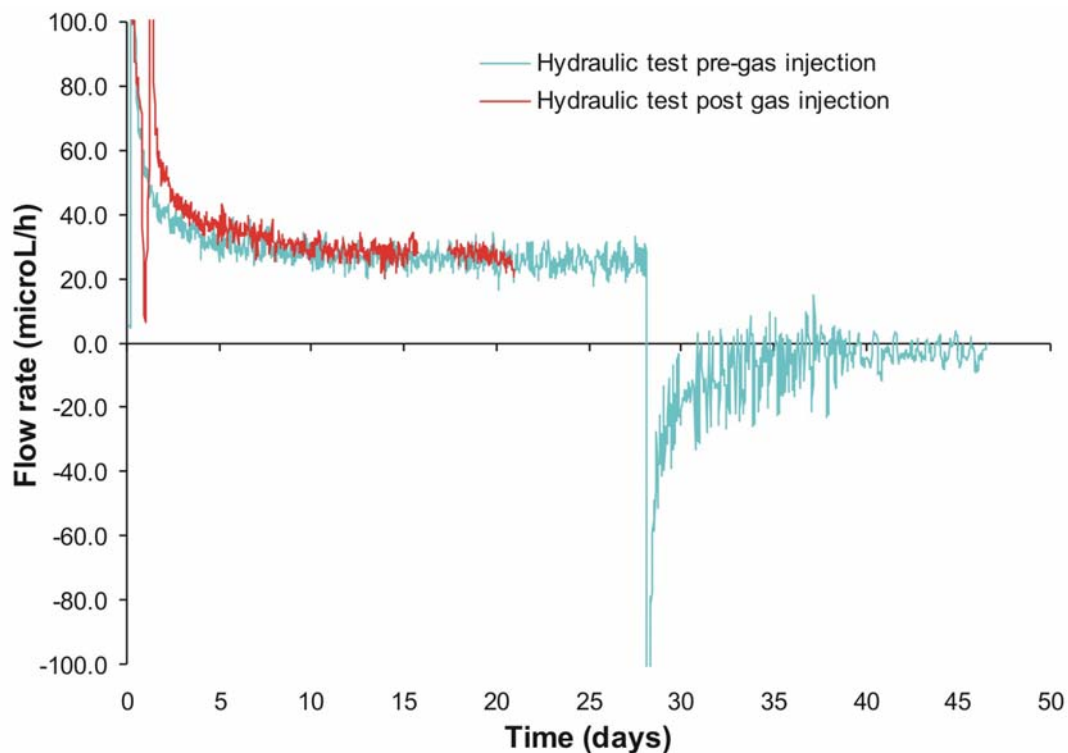


Figure 5-18 Evolution in flow rate for hydraulic tests performed before and after gas injection.

While modelling of the post-gas hydraulic data has not been performed, a visual inspection of Figure 5-18 clearly indicates that little if any significant change in permeability has occurred due to the injection of gas. The slight offset in the red line during the early section of the test, is indicative of a small change in hydraulic storage. Based on the data available, the nascent gas pathways would appear to have no significant effect on the engineering performance of the buffer. This is not particularly surprising given the limited duration of the gas tests and the quantities of helium injected.

6 Summary

The deposition hole was closed on the 1st February 2005 signifying the start of the hydration phase. Groundwater inflow through a number of highly-conductive discrete fractures quickly resulted in elevated porewater pressures throughout large sections of the borehole. This resulted in the formation of conductive channels (piping) leading to bypass flow, the extrusion of bentonite from the hole and the discharge of groundwater to the gallery floor. This problem was addressed by drilling two pressure relief holes in the surrounding rock mass to lower the porewater pressure in the vicinity of the deposition hole.

Artificial hydration began on the 18th May 2005 after 106 days of testing. In general from this time onwards the pressures in all of the canister filters and hydration mats (excluding the FCT and FR901) were used to hydrate the clay. Initial attempts to raise porewater pressure in the artificial hydration arrays often resulted in the formation of preferential pathways, even at relatively modest excess water pressures, resulting in localized increases in porewater pressure and total stress. These pressure dependent features were not focused in one location within the bentonite but occurred at multiple sites at different times in the test history. These pathways were relatively short lived, closing when water pressure was reduced. The sensitivity of the system to minor increases in porewater pressure clearly indicated that both the pressure relief holes should remain open until the bentonite had generated sufficient swelling pressure to withstand the high water pressure likely to be generated in the system when these holes were closed.

Packers were installed into the pressure relief holes on 23rd March 2006 and sections in them closed off over the period to 5th July 2006. These operations caused clear effects throughout the emplacement in both the measured porewater pressures and, to a lesser extent, the total stresses. However, there was no repeat of the formation of piping through discrete channels so, on 20th November 2006, pressures to the artificial hydration filters on the canister were increased to 2350 kPa.

Pressure data from a number of sensors including FR901, RW901 and most of the porewater pressure sensors mounted on the borehole surface, seem to suggest some form of time dependent (temporal) evolution in the hydraulic characteristics of the rock mass adjacent to the Lasgit deposition hole. It is also interesting to note that hydrogeological regime in the Assembly Hall area of the HRL appears to have changed during the operation of Lasgit, with fresh discharges observed from previously dormant fractures. This hypothesis is further supported by the monitored discharge rates from the pressure relief holes which show a slow progressive reduction in value with time. These effects could be caused by a number of reasons from clogging and permeability reduction along conductive fractures near the Lasgit deposition hole, to operational activities performed at different locations within the HRL including driving new tunnel headings, sinking of new borehole/deposition holes, block sampling and the setup of new experiments.

Monitored porewater pressures within the bentonite remain low ranging from 230 kPa to 635 kPa. This is in contrast to the water pressure measured at the face of the deposition hole which ranges from 1055 kPa to 2510 kPa. Analysis of this latter data shows that as hydration progresses during the first 400 days, a small zone of increasing porewater pressure can be seen expanding from one location near the mid-plane of the canister. After the installation of the packers into the pressure relief holes this disappeared and was replaced by a high pressure zone confined to the deeper parts of one side of the deposition hole.

Suction pressures recorded at psychrometers embedded within the bentonite show that suction is declining, confirming that resaturation is progressing, although the rate of hydration does appear to be slowing. Greatest progress has been made near to the filter mats above the canister whilst the least progress occurs just below the canister.

Monitored radial stress around the clay continues to increase steadily ranging in value from 1685 kPa to 5515 kPa, with an average value of 4230 kPa. In the absence of hydraulic piping the rate at which radial stress increases appears to be insensitive to the absolute value of porewater pressure applied to the filter assemblies, confirming the modelling work described in Section 3. Analysis of the distribution in radial stress throughout the borehole clearly shows a narrow zone of elevated stress propagating vertically upwards to around 3.5m. This zone appears to be expanding as the test progresses. At this stage of the hydration history, the remaining buffer exhibits a fairly uniform distribution in stress with the exception of the upper zone, at around 5m, which has somewhat larger variations in stress. This could be explained by the close proximity of the sensors to the large filter mat located between blocks C2 and C3. Comparison of

the data from the pore pressure and radial stress analyses shows a rather poor correlation in response for a similar point in time.

Stress measurements on the canister surface indicate that radial stress varies between 4800 kPa and 5030 kPa, which is comparable with the average value of radial stress monitored on the rock face. Axial strain is significantly lower at 4380 kPa. This value is relatively low when compared to the equivalent outputs from axial stress sensors located within the bentonite above the canister and the outputs from the Glotzls cells located on three of the rock anchors. This suggests that a poor contact probably exists between the face of the stress sensor and the clay, indicating that the clay in this region of the system is poorly hydrated.

Axial stress monitored within the clay ranges from 4910 kPa to 6230 kPa (excluding sensor PB901 located directly under the canister). The data clearly shows a non-uniform distribution of axial stress across the major axis of the emplacement hole, which may explain the displacement and apparent deformation of the lid. The outputs from these devices generally exhibit only a minor sensitivity to changes in porewater. These events often correlate with other experimental activities such as changes in artificial hydration pressure or drilling and abstraction of groundwater from the pressure relief holes, however, in general, the rate at which axial stress increases seems fairly insensitive to the absolute value of water pressure applied to the canister and hydration filters.

The axial force acting on the steel lid is now greater than the initial pre-stressing value applied during the installation phase. The initial reduction in the axial force can be explained by a time dependent relaxation of forces due to compression of the bentonite blocks and the engineering void space when the hole was first sealed. Analysis of the axial force thereafter suggests that the continuum axial swelling pressure within the bentonite is now greater than the initial pre-stress applied by the lid. The slight reduction in force during the period from 200 to 400 days of the test can be explained by convex deformation of the steel lid in response to the uneven distribution in axial stress. Since the installation and closure of packers into the pressure relief holes there has been a marked rise in the axial force acting on the lid.

Displacement sensors indicated a fairly uniform drop in lid height relative to the gallery floor during the early part of the test history, mirroring the relaxation in the initial pre-stressing applied to the lid. Analysis of the subsequent displacement data indicates a cumulative drop in lid height ranging from -0.12 mm to -0.17 mm at 400 days. This data would seem to suggest a slight distortion of the lid may have occurred as it deforms to accommodate the uneven distribution in axial stress. Data from DP905 located near the centre of the lid indicates a small upward movement, supporting the concept of convexing deformation of the lid during this period. Since the installation and closure of packers into the pressure relief holes the lid has moved significantly upwards with an increasing disparity in displacements at different locations, indicating an increased distortion, probably in response to the uneven distribution of the axial forces across the section of the deposition hole.

Analysis of the volumetric flow rate data for both sets of reciprocating ISCO syringe pumps indicates that around 89% of the total flux pumped into the Lasgit system is currently through the large hydration filters. This is somewhat lower than expected from a purely hydraulic perspective, as the large filter arrays constitute over 98% of the total surface area open to flow. This suggests that the zone around the canister has a higher permeability than the rest of the clay buffer.

Volumetric flow rate into the hydration mats is decreasing with time. Analysis of the data indicates that in general the proportion of flux into the clay from the various hydration sources (i.e. mats and canister filters) remains fairly constant with time, suggesting that a reduction in clay permeability is the primary cause for the apparent reduction in volumetric flow rate.

In general the temperatures in the Gas Laboratory and canister have remained fairly constant (approximately $\pm 0.5^{\circ}\text{C}$). The ambient air temperature of the HRL has varied with an annual cycle

ranging from 11°C and 16°C. The canister also shows an annual variation, but with a much smaller range of 13.0°C to 13.8°C, and with a phase offset of about 90 days from the HRL.

Predictive models of the resaturation phase of the Lasgit experiment have been developed using the TOUGH2 code and the EOS3 equation of state module. An initial group of models was created which assumed that the bentonite buffer material could be treated as homogeneous. These models were used to assess the potential impact of the host rock treated either as a porous medium or as containing discrete fracture channels. It was found that the impact of a single flowing fracture channel could have a significant local effect but, in view of the small number of such features observed on the deposition hole wall, the effect on the overall resaturation process is likely to be limited. In contrast, flow through the general rock mass and minor fractures could give a significant contribution to the resaturation if its effective permeability is as high as 10^{-19} m^2 , a value indicated by in-situ measurements on the deposition hole wall.

A second group of models incorporated explicit representation of the individual bentonite rings and cylinders that make up the buffer around the canister. In this case, porosities and initial saturation states were specified for each block and it was found that the rings around the canister will be the most difficult to resaturate fully on the timescale of the experiment. In particular, if the gap between canister and bentonite rings seals quickly and effectively then full resaturation could take many years.

The effectiveness of the seal between canister and bentonite would seem to be a critical parameter in determining the overall time taken to resaturate the facility. In the models, this seal is represented by a zone 10mm thick around the canister. If this zone is given a permeability of 10^{-19} m^2 then zones of significant gas saturation remain after 3 yr of water injection, but if the zone is given a permeability of 10^{-18} m^2 then water saturation should be almost complete by that time. In practice, it is intended that the swelling of the bentonite will close up this zone as resaturation proceeds so that its effective permeability will change with time, an effect that cannot easily be incorporated into the models. However, it seems likely that the rate at which the swelling occurs will be critical to the progress of the resaturation process.

A preliminary set of hydraulic and gas injection tests were started on the 25th May 2007 (day 843) with the isolation of the lower canister filters FL901 to FL904 while artificial hydration continued through all other canister filters and filter mats. After a period of 27 days a constant head test was initiated on filter FL903, raising its pressure to 4.3 MPa for 28 days and then reducing it to 560 kPa for a further 19 days. Gas injection to FL903 was then begun with an initial volume of gas being compressed at a steady rate for 13 days, a period of 22 days with gas pressure held constant and then a further period of 22 days during which pressures were raised again. Compression of the gas was then halted and the pressure monitored as it decayed for a further 4 weeks. This was followed by a second hydraulic test.

Preliminary modelling of the initial hydraulic test has been carried out using a 2D axisymmetric variably saturated finite element porewater flow model. The initial saturation conditions for the hydraulic test cannot be determined *a-priori*, so it was necessary to try to model the whole hydration phase history in order to set these initial conditions. Using this approach, fits were obtained to the initial pressure decay data for the four filters that were isolated using values for hydraulic conductivity ranging from 9×10^{-14} to $1.6 \times 10^{-13} \text{ ms}^{-1}$ and specific storage values ranging from 5.5×10^{-5} to $4.4 \times 10^{-4} \text{ m}^{-1}$. The constant pressure test on filter FL903 was fitted with a hydraulic conductivity of $7.5 \times 10^{-14} \text{ ms}^{-1}$ and a specific storage of $2.5 \times 10^{-5} \text{ m}^{-1}$. The modelling done to set the initial conditions also shows that a significant zone around each of the canister filters remains unsaturated.

Analysis of the gas injection data suggest that gas starts to flow into the buffer at a pressure of about 775 kPa, which is much lower than the expected gas entry pressure for intact bentonite. It therefore seems likely that gas is flowing between the bentonite and the canister and possibly between bentonite blocks. When initial gas pressurisation stopped and the pressure was held constant at around 1.85 MPa, flow into the clay suddenly reduced by around 98.5%, indicating

that propagation of the main gas pathway(s) practically cease when the pressure stopped rising. This can be viewed as the expansion of gas pathway(s), conceptually little different to that of inflating a balloon. However, the sudden reduction in gas flux while the injection pressure was held constant is strongly indicative of pathway flow rather than visco-capillary flow within the original porosity. It would also appear that the initial network of gas pathways fails to intersect an adequate sink.

Upon restarting gas injection, the observed pressure begins to deviate from the predicted value, indicating pathway propagation continues at the onset of testing. Gas flux into the clay gradually increases as the pressure in the system rises. At a gas pressure marginally greater than the local total stress measured on the rock wall (but a little smaller than the radial and axial stresses measured on and near the canister surface respectively), flux into the clay rapidly increases. Gas pressure continues to rise reaching a peak pressure of 5.66 MPa, which is marginally greater than the axial stress measured at PB902. This is followed by a small spontaneous negative transient leading to a quasi steady state. The post peak gas flux exhibits dynamic behaviour (over and undershooting flux into the system) suggestive of unstable gas flow. This general behaviour is reminiscent of the responses observed in laboratory scale tests reported by Horseman et al. (1999) and Harrington and Horseman (2003).

Following the cessation of injection the flux declines rapidly at first but then enters an extended period of very small flows. This is reflected in the pressure response which drops rapidly initially but then decays very slowly towards an asymptotic capillary threshold pressure, which is estimated to be about 4900 kPa, close to the average radial stress measured on the canister surface of 4900 kPa.

Following peak gas pressure a well pronounced increase in radial stress occurs around the entire base of the deposition hole, with the highest increase noted in the vertical plane below the point of injection. This indicates the gas preferentially moved downwards, probably along the interface between the canister and buffer. It is notable that the radial stress immediately adjacent to FL903 actually decreases during this time.

Porewater pressure data from the deposition hole wall exhibit similar behaviour to that of radial stress, though initial results suggest that the pulse in porewater pressure dissipates at a faster rate than that of the radial stress. This may relate to the fact that significant sections of the buffer clay remain in a state of suction.

Analysis of the porewater pressure sensors located within the buffer show no obvious sensitivity to the injection of gas. In contrast, axial stress sensors located beneath and above the canister appear to register the passage of gas. Indeed, the slow and then rapid increase in PB902 immediately following the peak gas pressure is strongly indicative of the time dependent propagation of gas pathways.

A small inflection in the rate of increase in axial stress at the base of the canister occurs shortly after the peak in gas pressure. Such a reduction in stress can only be caused by the removal of load, suggesting some form of displacement has occurred as a result of gas injection. Very minor movements of the canister as gas moves along its interface with the bentonite could feasibly result in such a response.

While it is difficult to make definitive statements regarding the exact direction and number of gas flow paths, it seems highly probable that the gas moved generally downwards away from the injection filter and then along the interface between blocks C1 and R1 and/or R1 and R2. This is logical as there is a clear axial stress gradient running from high to low from the top of the deposition hole to the lowest stress sensor. Under most conditions gas would propagate along such a stress vector. The fact that the gas pressure asymptotes at a value close to the local total stress, may suggest that the small amount of gas injected during the test remained resident in the buffer/deposition hole.

However, the observed general coupling between gas, stress and porewater pressure at the repository scale is extremely important and can readily be explained through concepts of pathway dilatancy. These observations are qualitatively similar to those reported by Horseman et al. (2004).

During the hydration phase, Lasgit has yielded high quality data relating to the hydration of the bentonite and the evolution in hydrogeological properties adjacent to the deposition hole. The limited preliminary hydraulic and gas injection tests confirm the correct working of all control and data acquisition systems. Lasgit has been in successful operation for in excess of 1000 days. The decreasing rate of change in sensor outputs demonstrates that significant progress in the hydration of the bentonite has been made.

References

British Geological Survey holds most of the references listed below, and copies may be obtained via the library service subject to copyright legislation (contact libuser@bgs.ac.uk for details). The library catalogue is available at: <http://geolib.bgs.ac.uk>.

DONOHEW, A.T., HORSEMAN, S.T. AND HARRINGTON, J.F. (2000). Gas entry into unconfined clay pastes between the liquid and plastic limits. Chapter 18. In: Environmental Mineralogy - Microbial Interactions, Anthropogenic Influences, Contaminated Land and Waste Management (eds J.D. Cotter-Howells, L.S. Campbell, E. Valsami-Jones and M. Batchelder), Mineralogical Society, London, Special Publication No. 9, 369-394.

HARDENBY, C. AND LUNDIN, J. (2003). Geological mapping of the assembly hall and deposition hole. SKB report IPR-03-28.

HARRINGTON, J.F. AND HORSEMAN, S.T. (2003). Gas migration in KBS-3 buffer bentonite: Sensitivity of test parameters to experimental boundary conditions. Report TR-03-02. Svensk Kärnbränslehantering AB (SKB), Stockholm, Sweden.

HARRINGTON, J.F. AND HORSEMAN, S.T. (1999). Gas transport properties of clays and mudrocks. In: Muds And Mudstones: Physical And Fluid Flow Properties (eds A.C.Aplin, A.J. Fleet, and J.H.S. Macquaker). Geological Society of London, Special Publication No. 158, 107-124.

HORSEMAN, S.T., HARRINGTON, J.F. AND SELLIN, P. (2004). Water and gas flow in Mx80 bentonite buffer clay. In: Symposium on the Scientific Basis for Nuclear Waste Management XXVII (Kalmar), Materials Research Society, Vol. 807. 715-720.

HORSEMAN, S.T., HARRINGTON, J.F. AND SELLIN, P. (1999). Gas migration in clay barriers. Engineering Geology, Vol. 54, 139-149.

HORSEMAN, S.T., HARRINGTON, J.F. AND SELLIN, P. (1997). Gas Migration In Mx80 Buffer Bentonite. In: Proc. Scientific Basis For Nuclear Waste Management XX, Boston, 2-6 Dec., 1996 (eds W.J. Gray And I.R. Triay), MRS Symposia Proceedings, Vol. 465, Materials Research Society, Warrendale, Pennsylvania, 1003-1010.

HUME, H.B. (1999). Gas breakthrough in compacted Avonlea bentonite. MSc thesis, Department of Soil Science, University of Manitoba, Winnipeg, Canada.

JOHANNESSON, L-E. 2003. Large Scale Gas Injection Test. Manufacturing of buffer for the large scale gas injection test. SKB report TD-04-01.

NOWAK, T., FLENTJE, R. AND KÖSTER, H. (2003). Surface Packer Tests in Lasgit Borehole. BGR presentation, Nottingham.

PREUSS, K., OLDENBURG, C. AND MORIDIS, G. (1999). TOUGH2 User's Guide, Version 2.0. Lawrence Berkeley National Laboratory Report LBNL-43134.

PUSCH, R., HÖKMARK, H. AND BÖRGESSON, L. (1987). Outline of models of water and gas flow through smectite clay buffers. SKB Technical Report 87-10, Stockholm, Sweden.

PUSCH, R., RANHAGEN L. AND NILSSON, K. (1985). Gas migration through Mx-80 bentonite. Nagra Technical Report NTB 85-36, Wetztingen, Switzerland.

TANAI, K., KANNO, T. AND GALLÉ, C. (1997). Experimental study of gas permeabilities and breakthrough pressures in clays. In: Scientific Basis For Nuclear Waste Management XX, Boston (eds W.J. Gray And I.R. Triay), MRS Symposia Proceeding Vol. 465, Materials Research Society, Warrendale, Pennsylvania, 1003-1010.

VAN GENUCHTEN, M.TH. (1980). A Closed-Form Equation for Predicting the Hydraulic Conductivity of Unsaturated Soils. Soil Sci. Soc., 44, 892-898. Author, A N. 1978b. Academic or technical journal article or paper title. *Name of Academic or Technical Journal*, Vol. 12, 345-678.